Synaptic and network responses to afferent inputs in higher order cortex and their modulation by the volatile anesthetic isoflurane

By
Caitlin A. Murphy

A dissertation submitted in partial fulfillment of the requirements for the degree of

Doctor of Philosophy
Physiology

at the
UNIVERSITY OF WISCONSIN-MADISON
2020

Date of final oral examination: 5/6/2020

The dissertation is approved by the following members of the Final Oral Committee:

Matthew I. Banks, Professor, Anesthesiology
Robert A. Pearce, Professor, Anesthesiology
Gail A. Robertson, Professor, Neuroscience
Yuri B. Saalmann, Assistant Professor, Psychology
Brian A. Baldo, Associate Professor, Psychiatry

Dedication

To my shovels.

If you have to dig the dirt to build the hill you choose to die on, best not to be digging with your hands.

Acknowledgements

If you know me well, you know that I believe strongly that the expression of gratitude – and a lot of other things, frankly – should be delivered frequently, candidly, and authentically[1]. You also know that I don't prescribe to ceremonial motivations for such expressions – nor ceremonial anything, really[2]. So, if you're included in the paragraphs below, I hope my gratitude isn't news to you and that previously I've expressed my appreciation directly if not in so many words; this section is not to express my gratitude to you *per se*.

My motivations for writing this monologue are three-fold:

1. Upon reading this thesis from beginning to end, I don't want a multitude of strangers thinking I'm an unappreciative heathen for omitting an acknowledgements section "on principle".
2. I welcome opportunities to reflect on the things and people I appreciate, especially in cases where informality and candor are marginally less unacceptable with respect to the rest of the document.
3. I want the people I appreciate to understand the contributions of all the others. The world is unfathomably connected.

I'd like to be able to say that this "wouldn't have been possible without the following", but that notion is saccharine and cliché (at best) and in most cases patently untrue[1]. I can say, though, that without each contribution described herein, this process was at risk being unequivocally dreadful and most certainly not worth it.

These acknowledgements are roughly arranged into four contiguous sections.

First, people without whom I *couldn't* have done this. These are people without whom the very completion of this thesis and the experiments described within are impossible. I'm also fortunate that their contributions to my experience have transcended the bare necessities multiple times over.

Second, people without whom I *wouldn't* have done this. This list is difficult to accurately compile. As such, it is certainly not exhaustive - but is there really any way of knowing?

Third, the people without whom I *shouldn't* have done this. I might not have known it at the beginning, but I'd have been foolish to go at this without you.

And, lastly, the custodian who cleans my office every day, my friend who fixed the thermostat, and FH.

[1]Of course, to some of us, "candidly" and "authentically" are synonymous.
[2] Truthfully, if there is anything so unceremonious as writing and defending a thesis during a global pandemic, I'll swallow my words.

First and foremost, a loving thank you to Donata Oertel, the matriarch and chair of my program. I remember vividly the day she called me to tell me I'd be a welcome addition to the Physiology Graduate Training Program. Donata constantly and fiercely supported both my teaching and research. She was the one to suggest I reach out to Matt for a rotation and is a big reason I chose his lab. Besides Matt, she was the first to provide feedback on my first first-author manuscript. She passed away on the day I finished this thesis. I'm grateful to have gotten to witness her candor, passion, and enthusiasm for science, teaching, and service. And her cookies.

To my advisor Matt Banks, thank you. I could not have conceived of, conducted, and written up these experiments without his mentorship – there is no one to whom I attribute my success in graduate school more. When I first interviewed with Matt before my rotation, he asked if I had ever taken a neuroscience course or a signal processing course. No, not really, not officially. Had I any computer programming experience? No. Did I even take calculus in college? Technically, no. He asked me what I *had* taken and what I had to contribute. I said I believed in education and I was willing to work really hard, given the proper guidance. Apparently that was enough for him – he has supported me unconditionally ever since. Matt has never (and will never) lower his standards for excellent science and has mentored me every step of the way in upholding the same standards for my own work. He has been present, responsive, and attentive to the minutiae of my experiments, data, and writing – often down to the very last control group, data point, and comma (literally). Matt has also unconditionally supported my other priorities – from teaching to my extracurricular activities (namely ultimate frisbee). I owe nearly all of my scientific training, as well as myriad other opportunities and experiences during graduate school to Matt, and I'm forever grateful.

To my committee. Many people who know me would question how I would justify having more white men named Robert on my committee than women. I chose my committee very intentionally – each of them has served very specific training purposes. They're some of the most brilliant, empathetic, and invested people I have ever met. Special thanks to Dr. Gail Robertson for listening, empowering, and encouraging me, even though (and especially because) my work is multiple sigma away from being relevant to her own work. For the letters of support, excellent questions, rigorous standards, career advice, and even great lunch conversations from my committee – thank you.

To my labmates. Thank you to Sean Grady, who conducted almost every single channelrhodopsin virus injection upon which each data point in these chapters relies. To Bryan Krause, not only for his amazing attention to statistical details and standards for rigorous analysis, but for his patience, mentorship, and friendship for more than five years. To Aeyal Raz, who trained me on many of the technically challenging methods of my work, provided clear and concise feedback to my science and writing, and whose kindness has been more meaningful than I can express. To Zarmeen Zahid and Ziyad Sultan, who have been amazing friends in the last months of writing my thesis and who instill immense optimism in me for the future of science – both for their potential as scientists and for the culture of empathy they create in all the spaces they occupy. To other current lab members – Chris Endemann, Jens Mellby, Hazel Bastien, Declan

Campbell, Graham Berger, and Sebastian Piedra – and past Banks lab members – Payge Barnard, Graham Findlay, Rachel Greenberg, Liz Jaeckel, Jeremiah Kakes, Sahibnoor Kaur, Rick Lennertz, Eric Lonergan, Rong Mao, Will Mayner, Nick Moran, Arel Otles, Anand Ramamoorthy, Avery Sipe, Tyler Stilp, Paulo Vianney, and Sam Wright – I really believe that independent of the amount of time we spent together in the Banks lab, each of you made a unique impact on my experience; thank you!

To the Department of Kinesiology and the Anatomy and Physiology teaching teams. I am indebted to this group for their profound influence on me as a scientist and educator. To my A&P 235 TAs – Jess Muer, Justin Lopez, Andrew Pearson, and Aaron Ward. To Morgan Shields, my co-lecturer and mentor in my first semesters with Physiology 235. To the A&P 335 and 435 teaching teams – Drew Lokuta, Kevin Strang, Beth Altschafl, and Grace Lee, as well as my fellow TAs. Kevin wrote my letters of recommendation for graduate school; the 335 teaching team has infallibly encouraged me from my undergraduate years to the day of my thesis defense. Thank you for showing me what world-class physiology education looks like, for constant support for my teaching and research, and for giving invaluable life and career advice.

Thank you, especially, to Janet Branchaw, the Leslie Knope to my April Ludgate (a reference she might not know, but aptly describes her superpower capabilities with regard to her work). Janet has been a mentor to me in science, in education, and (of course) a mentor in mentorship. Thank you for not only being my dissertation's biggest cheerleader, but for assuming responsibility for the overwhelming majority of the work involved in transitioning online this semester, and for going above and beyond what any of our students could have asked for with incredible grace and dedication. Thank you for showing me how to advocate for myself, to exercise my philosophies through my work, and to put my whole heart into everything I do. Thank you for embodying everything I know research and science education can be: thorough, thoughtful, and empirically-driven. And, most importantly, thank you for being the perfect example of how excellence and kindness can (and should) thrive together.

To my family, both immediate and otherwise. My family is quirky, candid, kind, and curious about the world – qualities I strive to exude. PhDs are just interest compounded from a lifetime of previous investments, and I absolutely would not have been here without theirs. No one – including me – is more proud of me than my family.

To Nate. Thank you for the adventures, for so rationally fielding my existential crises, for your unwavering practicality and your love, and for being my most steadfast supporter (both logistical and emotional). I can name only one person in the world I can spend more than a handful of hours in a car with alone and still keep driving, let alone with such beguiled resolution. A PhD is a pretty long car ride, and I'd do it all again as long as I was with you.

To my parents, Tim and Kathy Murphy. As a kid, I didn't really understand what they meant when they said "books can take you anywhere", as I was (am) a pretty literal person and instantaneous transport through time and space is not yet possible. I owe

the core of who I am as a scientist and person – my work ethic, value of education and literacy, diligence for precision in writing, and sense of personal responsibility – to them. I also have my parents to thank for the intensity and heart I bring to everything I do. My parents love it *all,* and because of them, so do I. They taught me to love, to empathize, and to express gratitude. To question everything. To grind. That wealth isn't measured in dollars. That "prior planning prevents piss poor performance". That you can't go wrong with a "PMA" (positive mental attitude). To me, science is meaningless without all of these things. I wouldn't be here – literally and figuratively – without them.

To Randy and Susie, Nate's parents. That they haven't questioned why their son's 28-year-old partner has never not been in school is a true miracle. Thank you to them, to Nate's sister Anna, and the rest of the Kleinhans and Schueler families, for welcoming me so lovingly into the family, for blissful weekends away from work or around Camp Randall, for constant affirmation, and for never failing to remind Nate and me of their love, pride, and gratitude. Their thoughtfulness and warmth – expressed in cards, texts, words, and time spent – mean more to me than a lifetime in the lab.

To my sisters, Meghan and Brianna. Thank you for challenging me, humoring me, and empowering me. All of the things I cared about growing up I did because of my sisters – even gymnastics (yikes) or soldering a circuit board on a Friday night. My sisters are both smarter than I am; one is an engineer and the other a soon-to-be-physician (yet by the grace of middle child's luck, I get the "Dr." title first!). They are also more thoughtful than I am, and it's from them that I'm learning the delicate balance of patience and vigor when demanding excellence from the world. I'm inspired to change the world with both of them. And, of course, thank you in advance for making a lot more money than I ever will to support our loving parents in their later years.

To my Uncle Dennis and Aunt Kathleen, for inspiring the academic in me. No one in the world can make a better book recommendation than Dennis and Kathleen. For Christmas one year, they gave me a sketchbook and charcoal pencils. For my 16th birthday, a subscription to Anesthesia & Analgesia, one of the handful of journals specific to anesthesia research. Just this year, a copy of *Why Are So Many Incompetent Men Leaders and How to Fix It* arrived in my mailbox. Because of them, I know that scientists are multifaceted and unique and expressive and warm; I am a scientist, artist, and activist (and dozens of other "ist"s) thanks to them.

To my loving grandparents, Shirlie and Don Deery, Marcie and Tom Murphy (in memory). I wrote my entire thesis wrapped in my Grandma Deery's quilt she made me in 1996, taking breaks to do crosswords sent from my Grandpa Deery. My Grammy and Grampy Murphy are the reason all the moments of my life are riddled with instances of Murphy's Law (and Murphy's Luck). For the cards, letters, jokes, cookies, reminders to vote (and disdain for corruption in politics), character, and most of all, for the joy, optimism, and gratitude you breed – thank you.

To my PGTP friends, especially Joe Sepe and Steven Wiesner, with whom I spent many long hours of studying, working, teaching, and grading. They are the truest of

colleagues and friends; I am grateful to have had such smart and kind-hearted humans with whom to go through graduate school in solidarity. More than these collegial experiences, though, Joe and Steven have been a relentless source of positivity and affirmation and have never hesitated to drop everything to lend an ear or shoulder. To Lin, Julie, and Thejas, my fellow PGTP friends. I look back fondly on my early memories of struggling (successfully!) together through our coursework in the first year(s) of our program, which manifested lifelong friendships for which I'll always be grateful.

To my "non-frisbee" friends, especially Tracy, Karina, Kurt, Jess, Brandon, Anna, Melissa, Kevin, and Renee. From board games, vacations, and football games to coffee, living room visits, and sailboat cruises with Ruby – despite the paucity (and brevity) of the times I see them, those times are always some of the richest and whole.

Penultimately, and certainly not least – neither by quality nor by quantity – to the possibly hundreds of incredible friends I have through ultimate frisbee. It's hard to express to ultimate muggles how deeply intertwined ultimate is with the various facets of my identity; suffice it to say that the people and ideas I've found through ultimate are not mutually exclusive from my priorities as a scientist.

To my Boomtown, Bella Donna, Heist, BFFs, and NOISE families and to the MUFA and Madison Youth Ultimate communities. I'm completely overwhelmed by the love and support they have shown me both in the past several weeks, and always.

Special thanks to Sara, for inspiring, supporting, and loving me, and for showing me how to be everything I hope I can be. To Glenn, for Thursday morning breakfast, for challenging me, listening to me, and knowing me arguably better than me. To Robyn, for championing leadership with heart and compassion; our friendship has long-since transcended the bounds of ultimate and is even richer for it. To Ben, Jessie, Claire, and Toby, for their ubiquitous love and support of everything I've ever done; I leave their company feeling like the luckiest person in the world. To Forty, it's bizarre it took almost 8 years on campus to get there, but I have so much gratitude for our friendship; you have been there for the highest highs and lowest lows of my time in graduate school, and your words and actions have meant everything to me. To Pete and Lindsay, for providing opportunities to play such a beautiful game, but also for our times in Washington, which are some of my fondest memories of my entire time in graduate school. And to my grad student ultimate friends and/or the women who wine – Laura, Mila, Charlotte, Chris, Evie, Cassie, Gordon, Sab, Karen, Rachel, April, Laurel, and Rose – there is no group in the world made up of people who are so unique from each other, yet with whom I have so much in common. Words cannot express how much I love and appreciate you.

And lastly, to the often-invisible, unnamed contributors to who peppered my time in the lab with hundreds of seemingly meaningless interactions. You made me smile, laugh, and reminded me – sometimes multiple times per day – that as long as I have something I care about and people who support me, I have reason to be grateful every single day.

Table of Contents

Abstract

Conscious sensory perception requires integration of incoming signals with internal processes, such as attention, expectation, and motivation. The neocortex is hierarchically organized and highly specialized, allowing it to perform these relevant computations. How the integration of diverse sources of information contributes to spiking activity in the column and to sensory perception is an area of active research. Evidence suggests that higher order thalamocortical (TC) inputs to layer 1 enhance responses to sensory stimuli and promote cortical arousal, whereas feedback corticocortical (CC) inputs to layer 1 modulate signal integration and promote accurate sensory perception. Afferent inputs to cortical layer 1 terminate on both excitatory and inhibitory cells, but key features of these circuits as well as how their properties are altered during loss of consciousness are unclear.

Interestingly, feedback CC synaptic responses are preferentially sensitive to clinically relevant doses of isoflurane in vivo and in vitro, while TC afferents are preserved. Given the overlap of the terminal fields of CC feedback and TC afferents in cortical layer 1, the preferential suppression of feedback CC responses is particularly notable. Some studies have suggested differential roles of superficial and deep cortical layers in processing information, and that the balance of synaptic excitation and inhibition in cortical networks may be crucial for sensory perception. What are the mesocircuit-level implications of this differential sensitivity to isoflurane, and how does it contribute to loss of consciousness under isoflurane?

In this thesis, I will describe brain slices experiments I conducted to further explore the cell type-specific targets of feedback CC and TC projections to layer 1 in

higher order sensory association areas, as well as the effects of the volatile anesthetic isoflurane on inputs to excitatory and inhibitory targets in the cortical column. I show that TC and CC inputs to layer 1 evoke responses with different properties at both the cellular and network levels. TC inputs evoke spikes in parvalbumin-positive interneurons and in some pyramidal cells, and the magnitude of their inputs is correlated with spike output in the infragranular layers. CC inputs rarely evoke spikes in pyramidal cells, activate somatostatin-positive interneurons, and induce low-amplitude spike outputs in local networks. Isoflurane anesthesia suppressed both TC and CC inputs to layer 4 pyramidal cells and leaves parvalbumin-positive interneurons unaffected, suggesting a shift in the balance of excitation and inhibition during isoflurane, particularly in the feedforward circuits in which layer 4 pyramidal cells are involved. Integration of feedback inputs may also be disrupted by anesthesia; CC inputs to somatostatin-positive interneurons – which modulate inputs to dendrites of local pyramidal cells – were also suppressed by isoflurane.

As one of the hallmark features of consciousness is sensory awareness, investigating anesthetic-induced loss of consciousness helps to elucidate the neural basis of consciousness. In addition, this research has broad implications for potential treatments of pathologies with sensory features, including sensory association disorders and schizophrenia, and for improvement of perioperative patient safety through more reliable anesthetic monitoring and development of more specific anesthetic agents.

Chapter 1

Introduction

Responding to external stimuli to maintain physiological homeostasis is paramount for the survival of individuals and species. Organisms engage with their external environments via the transduction of sensory information from the peripheral nervous system to the central nervous system. Here, sensory information enters the black box that is the brain - a dynamic, complex computational machine that integrates sensory information into its own pre-existing schemes to generate the conscious experience.

Feedforward signals carry information about specific features of the external environment, with varying levels of abstraction at higher levels of the cortical hierarchy. Conversely, higher order areas generate outputs in the feedback direction, providing contextual information to lower order areas based on internally generated predictions and expectations. Conscious perception occurs by way of functional integration and iterative processing of each of these signals (Friston, 2005; Dehaene and Changeux, 2011).

Numerous studies conducted during wakeful, sleep, anesthetic, and vegetative states have suggested that thalamocortical and intracortical networks are particularly relevant for studies of conscious perception (Llinas et al., 1998; Crick and Koch, 2003; Koch et al., 2016). Physiological and anatomical characteristics of these networks give rise to their functional significance and the role they play in mediating consciousness. Messages are passed between levels of the cortical hierarchy via direct corticocortical

connections, or indirectly via cortico-thalamo-cortical loops (Sherman and Guillery, 2011). Studies that have focused on the effects of anesthetics on the contents of consciousness have focused on these networks in particular (Mashour and Hudetz, 2017). Still, the degree to which anesthetic effects on individual thalamic, cortical, feedback, and feedforward pathways contribute to changes in conscious perception remains unclear.

In the chapters that follow, I will outline a series of investigations of higher order thalamocortical circuits in brain slices. In Chapter 2, I describe in detail the methods by which each of the experiments in Chapters 2-5 is conducted. In Chapter 3, I outline a series of experiments in which I compared the cell type- and pathway-specific responses of two distinct afferent inputs to layer 1 of higher order neocortex. In the remaining chapters, I describe the changes I observed in these evoked responses during isoflurane anesthesia.

Thalamocortical networks and the organization of the cortical hierarchy

The neocortex exhibits highly sophisticated organization. Though imperfect, the multi-dimensional classification of various cell populations delineates a set of rules upon which to scaffold functional properties. Information from individual sensory receptors must be amalgamated to form object-based representations of the world. This occurs by way of integration of signals from converging inputs. Simple stimulus features are extracted and recomposed in increasingly complex representations as they ascend the cortical hierarchy in the “feedforward” direction (Cappe et al., 2012). However, that cortex is a serial processor of information is an increasingly outdated notion; at nearly

every iteration of processing, feedforward signals are modulated both by horizontal connections and by “feedback” signals.

Stereotyped, lamina-specific connectivity patterns across sensory modalities have been described with varying fidelity to classical models, though these patterns are less distinct in rodents. Ascending corticocortical feedforward projections originate in the superficial layers and terminate in layer 4; descending projections originate in layer 5 and terminate in all layers except for layer 4 (Felleman and Van Essen, 1991; Binzegger et al., 2004; Markov et al., 2014). Sensory thalamic nuclei can be broadly categorized as either specific (primary) or non-specific (higher order) (Jones, 2001). Specific thalamic nuclei are considered information-bearing “driver” or “core” projections; in primary cortical areas, “core” projections target cortical layer 5, while in higher order cortices, core thalamocortical projections terminate in cortical layer 4. In contrast, nonspecific thalamic nuclei extend “matrix” projections to layer 1, terminating on apical dendrites of cortical pyramidal cells or layer 1 interneurons. Anatomical data show that higher order projections to layer 1 diffuse (Jones, 2001; Rubio-Garrido et al., 2009) and thus well-positioned to synchronize multiple cortical areas (Saalmann et al., 2012).

Populations of inhibitory interneurons in cortex

As I will demonstrate in chapter 4 of this thesis, the long-range cortical afferents I described in the previous section are excitatory, glutamatergic connections. However, inhibitory interneurons make up a notable fraction of the targets of these excitatory inputs and are a major contributor to encoding of sensory information (Murayama et al., 2009; Haider et al., 2013). Inhibitory neurons are a minority of all cortical neurons (10-

15% in rodents), and have been characterized using a variety of cytological, electrophysiological, and morphological features (Rudy et al., 2011; Kubota, 2014; Tremblay et al., 2016). Nearly all inhibitory neurons in neocortex fall into one of three non-overlapping populations of interneurons, marked by the expression of unique peptide or proteins markers: parvalbumin, somatostatin, or 5HT3a receptors. In chapters 4 and 5 of this thesis, I will describe experiments during which I recorded from either somatostatin- or parvalbumin-expressing interneurons in non-primary neocortex and evaluated responses following activation of higher order thalamocortical and corticocortical afferents. I will also show findings that suggest a cell type-specific effect of isoflurane on the response properties of parvalbumin- and somatostatin-expressing interneurons.

Parvalbumin-positive interneurons make up approximately 40% of GABAergic cells in neocortex. The cell bodies of parvalbumin-positive cells are found primarily in layer 2/3 and layer 5, extend dendrites into layer 1, and target the proximal dendrites, soma, and initial axon segments of excitatory pyramidal cells (Tremblay et al., 2016). Several studies have demonstrated the role of parvalbumin-positive interneurons in providing fast, precisely-timed feedforward inhibition to their targets (Pouille and Scanziani, 2001; Sun et al., 2006; Cruikshank et al., 2010; Audette et al., 2018), likely restricting spike windows of pyramidal cells (Pouille and Scanziani, 2001). Investigations in our lab have demonstrated the role in fast-spiking parvalbumin-positive cells in regulating precision of spike timing of pyramidal cells in the context of coordinated network events in mouse auditory cortex (Krause, 2017).

Another 30% of inhibitory interneurons in neocortex are somatostatin-positive. Somatostatin-positive interneurons are a more heterogenous group than parvalbumin-positive interneurons. The mostly frequently studied and morphologically distinct type of somatostatin cell is the Martinotti cell, a distinctive type of somatostatin-positive cell found in layers 2-6. Martinotti cells send extensive axonal projections to layer 1, where they provide feedforward inhibition to the distal dendritic tufts of pyramidal cells (Xu et al., 2013; Kubota, 2014; Tremblay et al., 2016), likely modulating inputs to these cells. Dendritic calcium spikes, which are important for gain control of input/output function of the pyramidal cells, are particularly sensitive to inhibition by somatostatin-expressing interneurons (Murayama et al., 2009). Somatostatin-positive cells also connect extensively with other inhibitory interneuron populations (Cottam et al., 2013) (but not with each other), sending and receiving GABAergic inputs to and from 5HT3 receptor-expressing and parvalbumin-positive cells, resulting in net disinhibition of local networks (Pfeffer et al., 2013).

Reports describing corticocortical and thalamcortical inputs to inhibitory interneurons demonstrate differential activation of somatostatin- and parvalbumin-positive interneurons. Primary thalamocortical inputs to somatostatin cells in primary cortex are either weak or non-existent (Beierlein et al., 2003; Cruikshank et al., 2010; Audette et al., 2018). Similarly, somatostatin-positive cells in barrel cortex also did not receive any direct input from higher order thalamus (Audette et al., 2018), though in some cases thalamcortically-evoked, 5HT3a receptor-mediated silencing of somatostatin-positive cells was observed. Indeed, somatostatin-positive cells are more likely to be tonically active than other cell types, and several studies have demonstrated

that they are silenced during sensory-activated network activity (Gentet et al., 2012; Urban-Ciecko et al., 2015; Audette et al., 2018). Conversely, corticocortical connections to somatostatin-positive interneurons have been observed ubiquitously. Local and distant cortical inputs to somatostatin-positive cells exhibit robust facilitation (Beierlein et al., 2003; Cruikshank et al., 2010; Urban-Ciecko et al., 2015), a feature that, given their high input resistance, frequently results in somatostatin cell action potentials (Urban-Ciecko et al., 2015).

Properties of thalamocortical and corticocortical synapses

In addition to the distinct connectivity patterns, cytoarchitecture, and functional features of thalamocortical networks, the properties of thalamocortical and corticocortical synapses contribute to the mechanisms by which signals are integrated and propagated in cortical networks. For example, short-term plasticity (Stevens and Wang, 1995) influences the summation of incoming signals over consecutive inputs and plays an important role in information processing (Fortune and Rose, 2000; Rotman et al., 2011) with varying spatiotemporal dynamics (Motanis et al., 2018). The influence of short-term plasticity upon cortical networks is highly complicated by the variability among different cell types (Cruikshank et al., 2012), layers (Viaene et al., 2011b, a), and brain areas (Sherman and Guillery, 2011; Viaene et al., 2011c). The same is true for other synaptic features such as post-synaptic receptors, response amplitudes, or convergence onto post-synaptic targets (Sherman and Guillery, 2013).

Still, upon examining the properties of synapses in thalamocortical networks, patterns emerge. Led by the efforts of Murray Sherman and colleagues at the University

of Chicago, the response properties at thalamocortical, corticocortical, and corticothalamic synapses have been well-characterized. By grouping certain synaptic properties based on putative functional roles, Sherman and colleagues outline a principled classification system for synapses in thalamocortical networks and describe how these synaptic influences may confer unique functional properties to the networks in which they operate. This classification system was first proposed for inputs to thalamus (Sherman and Guillery, 1998) and has since been extended and modified for cortex (Reichova and Sherman, 2004; Lee and Sherman, 2008; Lee and Sherman, 2010; Theyel et al., 2010; Covic and Sherman, 2011; De Pasquale and Sherman, 2011; Lee and Sherman, 2011; Petrof et al., 2011; Viaene et al., 2011b, a; Viaene et al., 2011c; Sherman and Guillery, 2013). Relevant for the experiments I describe herein are thalamocortical and corticocortical synapses. These include synapses between primary thalamic nuclei and their primary cortical targets, as well as those between higher order thalamic nuclei and primary or higher order cortical targets.

Primary sensory thalamic nuclei convey feature-specific sensory information to primary sensory cortices with high fidelity, and their Class 1 (‘driver’) synaptic properties have been well-described across sensory modalities (Lee and Sherman, 2008; Viaene et al., 2011a, b). Generally speaking, Class 1 synapses exhibit paired pulse depression and large EPSPs, consistent with driver-type properties one might expect at synapses tasked with conveying unequivocally time-locked sensory information from the external environment (Lee and Sherman, 2008). Class 1 synapses can be further delineated into Class 1A, 1B, and 1C inputs; all of these are considered to be “drivers”, and only vary in the level of convergence (lower levels of convergence in Class 1A) and frequency-

dependence of synaptic plasticity (Class 1C) (Viaene et al., 2011b). Class 2 (’modulator’) synapses exhibit paired pulse facilitation, high levels of convergence, and small EPSPs (Sherman and Guillery, 2013). Class 2 synapses also recruit metabotropic glutamate receptors, which contribute to their “modulator” properties to high frequency stimuli especially (Lee and Sherman, 2008).

One might expect driving and modulating synapses to be neatly distributed among feedforward or “bottom-up” and feedback “top-down” pathways, respectively. Feedforward pathways are considered to carry stimulus-specific information from external sources, while feedback pathways are often discussed in the context of “modulating” these external inputs. Surprisingly, this is not the case. Intracortical feedback afferents elicit Class 1 responses as often as they do Class 2 responses (Covic and Sherman, 2011; De Pasquale and Sherman, 2011). Meanwhile, certain thalamocortical synapses – such as those from higher order thalamus to primary cortex – exhibit Class 2 properties (Viaene et al., 2011c).

Despite the thorough characterization of many synapses in thalamus and cortex, most – especially those investigating intracortical projections – have involved at least one primary area. Moreover, only recently has optogenetics enabled the disentangling of inputs that overlap in specific cortical layers. For example, higher order thalamocortical and intracortical feedback projections overlap in layer 1 (Rockland and Virga, 1989; Shipp, 2007; Rubio-Garrido et al., 2009), yet their synaptic properties have not been examined in isolation nor have they been compared. In the experiments I describe in this thesis, especially those in Chapter 3, I show that some thalamocortical and corticocortical synapses exhibit characteristics consistent with previously described

synapses, and some do not. My results suggest that especially among higher order cortical areas, the properties of afferent synapses may diverge from previously described classifications and their implied roles for cortical function.

The role of thalamocortical and corticocortical connections in mediating consciousness

Previous investigations implicate thalamic nuclei as gates of bottom-up information flow, suppressed upon loss of consciousness (Llinas et al., 1998; Alkire et al., 2000). Thalamic metabolism and blood flow are consistently reduced under several different anesthetic agents during unconsciousness (White and Alkire, 2003; Alkire and Miller, 2005). Yet, the reduction of thalamic activity may not correlate with loss of consciousness. Changes in thalamic metabolism occur at sub-hypnotic doses of sevoflurane (Alkire et al., 2007) and propofol (Kaisti et al., 2002), but further suppression of the thalamus is not observed during hypnotic doses.

Fewer studies have evaluated the effect of anesthetics on nonspecific thalamic nuclei. Intralaminar and medial thalamic nuclei are nonspecific thalamic nuclei that receive relatively little direct sensory input (Saalmann, 2014) but connect extensively within corticothalamocortical networks. Their anatomical and physiological properties suggest these projections may be an apt candidate for anesthetic-induced LOC. Indeed, Hudetz et al. (2012) show that functional connectivity of nonspecific thalamic nuclei is preferentially reduced by propofol compared to specific thalamic centers (Hudetz, 2012). As yet, however, the direct effects of anesthetics on synaptic responses to

activation of nonspecific thalamo-cortical afferents in higher order cortical areas has yet to be tested.

Converging evidence highlights the importance of cortex in mediating consciousness and, therefore, anesthetic-induced LOC (Llinas et al., 1998; Crick and Koch, 2003; Koch et al., 2016). Previously described effects of anesthetics on thalamic metabolism are eliminated upon removal of the cortex (Angel, 1993), despite the cortical EEG remaining activated following removal of the thalamus (Villablanca and Salinas-Zeballos, 1972)**.** Evoked responses in primary sensory cortex, the target of specific thalamic nuclei, do not correlate with stimulus percept (Grunewald et al., 2002; Wilke et al., 2006; Panagiotaropoulos et al., 2014); likewise, responses to sensory stimuli in primary cortical areas are relatively unaffected during sleep (Issa and Wang, 2008), anesthetic (Hubel and Wiesel, 1959; Sellers et al., 2015), or vegetative states (Laureys et al., 2002). However, deactivation or disconnection of non-primary cortical areas is closely associated with anesthetic-mediated unconsciousness (Alkire, 2008; Schrouff et al., 2011; Mashour, 2014). Processes such as expectation and attention are carried out in higher cortical areas, and information is carried via feedback connections to be integrated and compared to sensory input (Todorovic et al., 2011; Chennu et al., 2013; Kok et al., 2013). Across an abundance of anesthetics and recording schemes, corticocortical feedback connectivity is preferentially suppressed upon loss of consciousness (Imas et al., 2005; Peltier et al., 2005; Alkire, 2008; Lee et al., 2009; Ku et al., 2011; Schrouff et al., 2011; Boly et al., 2012; Liu et al., 2012; Raz et al., 2014).

Despite suggesting in the previous paragraphs that the true nature of the neural correlates of consciousness may be settled by an either-or debate between thalamus

and cortex, it is more accurate to articulate that both thalamus and cortex (in addition to lower centers, such as the brainstem and hypothalamus) contribute to the conscious experience. Some have suggested, for example, that thalamocortical and corticocortical mechanisms contribute to different dimensions of consciousness, whereby bottom-up inputs mediate arousal or “level” of consciousness and top-down afferents contribute context or “contents” of consciousness (Mashour and Hudetz, 2017). Or, in an alternative (though not mutually exclusive) paradigm, thalamic centers enable consciousness by mediating intracortical interactions and synchronizing activity in distant cortical areas (Saalmann, 2014). Indeed, Redinbaugh et al. (2020) recently show that activity in both thalamus and cortex are correlated with consciousness level, and that stimulation of a higher order thalamic nucleus induces arousal in macaques by facilitating synchronization between hierarchically distinct cortical areas (Redinbaugh et al., 2020).

The enigmatic cortical layer 1

Compared to cortical layers 2-6, cortical layer 1 is characterized by dense neuropil and a relative paucity of cell bodies belonging to a subset of GABAergic interneurons (Winer and Larue, 1989). The sparse population of cell bodies that occupies layer 1 can be characterized almost entirely by their expression of serotonin 5HT3a receptors (Rudy et al., 2011). Importantly, layer 1 also contains the dendrites of cells occupying the layers below(Binzegger et al., 2004; Muralidhar et al., 2014). Inputs to layer 1 arise from higher order thalamic nuclei (Jones, 1998; Rubio-Garrido et al., 2009), higher order cortical areas (Yang et al., 2013; D'Souza et al., 2016), and in some cases from lower order

cortical areas (Coogan and Burkhalter, 1993; D'Souza et al., 2016). Despite a relatively thorough understanding of the underlying anatomical and cellular features of layer 1, its functional properties remain relatively enigmatic.

Most studies describing functional roles of thalamocortical, corticocortical, feedforward, or feedback projections in thalamocortical networks do not separate inputs to layer 1 from those targeting other layers, nor do they distinguish between thalamocortical and cortical afferents in layer 1. First, especially for investigations of the function of intact systems, this strategy is appropriate – connections within (and beyond) thalamocortical networks operate concurrently, if not independently. As such, afferents originating from the same area but targeting different laminae, or overlapping inputs within a single layer function simultaneously and perhaps even synergistically. Moreover, until recently, methodological constraints have precluded study of synaptic and circuit properties of distinct long-range inputs in brain slices (Petreanu et al., 2009; Cruikshank et al., 2010); the tortuous path of thalamocortical fiber tracts made activation of independent afferent pathways all but impossible by electrical stimulation, even for a careful geometer.

Still, inputs may elicit lamina- or pathway-dependent responses, perhaps due to the cytoarchitecture and intrinsic physiology of their targets or differences in synaptic physiology. For example, synaptic responses of higher order thalamocortical inputs to layer 1 have significantly longer half-widths compared to inputs to layer 4 originating from the same thalamic nucleus (Murphy et al., 2019) (see Chapter 4), which may differentially affect the spatiotemporal dynamics of information integration. Furthermore, previous studies have demonstrated that properties of intracortical synaptic responses

are highly dependent upon the layer of both the source and target layer (Covic and Sherman, 2011; De Pasquale and Sherman, 2011), and synapses by afferents originating in unique areas vary at the molecular level despite overlapping terminal fields (Fremeau et al., 2004). Thus, because of the potential pathway- and layer-specific effects of cortical afferents, investigations of their discrete contributions to cortical processing are essential.

Preface to Chapters 2-6

In the chapters that follow, I will describe experiments in which I use optogenetics in cortical brain slices to disentangle properties of distinct thalamocortical and corticocortical afferents. In Chapter 2, I will thoroughly outline the methods by which the data in Chapters 3-5 were collected. The steps I describe in this chapter include: expression of the excitatory light-activated opsin protein channelrhodopsin, breeding of transgenic animals for the targeting of select interneuron populations, preparation of cortical brain slices, multichannel and whole cell patch-clamp recording, activation of distinct afferent axons to higher order cortex, and modulation of synaptic responses by isoflurane delivered via artificial cerebral spinal fluid. In Chapter 3, I will describe the properties of synaptic responses to distinct afferent pathways to cortical layer 1. I provide evidence that suggests differing roles of thalamocortical and corticocortical inputs, given the relationship between inputs and outputs to the cortical column. Because the underlying architecture of the cortical network subserves its function, I also describe pathway- and cell type-specific differences in synaptic responses. In Chapter 4, I explore the effects of isoflurane on extracellularly recorded synaptic responses to

activation of layer 1 afferents from Chapter 3, as well as those of two additional pathways reciprocal to the pathways described in Chapter 3. I demonstrate that the effects of isoflurane are pathway-specific, where feedback corticocortical afferents are preferentially suppressed by isoflurane compared to feedforward corticocortical afferents and thalamocortical afferents to layers 1 and 4. Lastly, in Chapter 5, I expand upon results from Chapter 4 by showing that in addition to pathway-specific effects, isoflurane preferentially suppressed synaptic responses in a cell type-specific manner.

The results shown and conclusions drawn from these chapters will provide insight to both past and future investigations of thalamocortical networks, sensory processing, and anesthetic-induced loss of consciousness. They may also inform the design of future experiments, upon which I elaborate in the final Chapter 6.

References

Alkire MT (2008) Loss of effective connectivity during general anesthesia. IntAnesthesiolClin 46:55-73.

Alkire MT, Miller J (2005) General anesthesia and the neural correlates of consciousness. ProgBrain Res 150:229-244.

Alkire MT, Haier RJ, Fallon JH (2000) Toward a unified theory of narcosis: brain imaging evidence for a thalamocortical switch as the neurophysiologic basis of anesthetic- induced unconsciousness. Conscious Cogn 9:370-386.

Alkire MT, McReynolds JR, Hahn EL, Trivedi AN (2007) Thalamic microinjection of nicotine reverses sevoflurane-induced loss of righting reflex in the rat. Anesthesiology 107:264-272.

Angel A (1993) Central neuronal pathways and the process of anaesthesia. British Journal of Anaesthesia 71:148-163.

Audette NJ, Urban-Ciecko J, Matsushita M, Barth AL (2018) POm Thalamocortical Input Drives Layer-Specific Microcircuits in Somatosensory Cortex. Cereb Cortex 28:1312-1328.

Beierlein M, Gibson JR, Connors BW (2003) Two dynamically distinct inhibitory networks in layer 4 of the neocortex. Journal of Neurophysiology 90:2987-3000.

Binzegger T, Douglas RJ, Martin KA (2004) A quantitative map of the circuit of cat primary visual cortex. JNeurosci 24:8441-8453.

Boly M, Moran R, Murphy M, Boveroux P, Bruno MA, Noirhomme Q, Ledoux D, Bonhomme V, Brichant JF, Tononi G, Laureys S, Friston K (2012) Connectivity changes underlying spectral EEG changes during propofol-induced loss of consciousness. J Neurosci 32:7082-7090.

Cappe C, Rouiller EM, Barone P (2012) Cortical and Thalamic Pathways for Multisensory and Sensorimotor Interplay. In: The Neural Bases of Multisensory Processes (Murray MM, Wallace MT, eds). Boca Raton, FL: CRC Press/Taylor & Francis.

Chennu S, Noreika V, Gueorguiev D, Blenkmann A, Kochen S, Ibanez A, Owen AM, Bekinschtein TA (2013) Expectation and attention in hierarchical auditory prediction. J Neurosci 33:11194-11205.

Coogan TA, Burkhalter A (1993) Hierarchical organization of areas in rat visual cortex. JNeurosci 13:3749-3772.

Cottam JC, Smith SL, Häusser M (2013) Target-specific effects of somatostatin-expressing interneurons on neocortical visual processing. Journal of Neuroscience 33:19567-19578.

Covic EN, Sherman SM (2011) Synaptic properties of connections between the primary and secondary auditory cortices in mice. CerebCortex 21:2425-2441.

Crick F, Koch C (2003) A framework for consciousness. Nat Neurosci 6:119-126.

Cruikshank SJ, Urabe H, Nurmikko AV, Connors BW (2010) Pathway-Specific Feedforward Circuits between Thalamus and Neocortex Revealed by Selective Optical Stimulation of Axons. Neuron 65:230-245.

Cruikshank SJ, Ahmed OJ, Stevens TR, Patrick SL, Gonzalez AN, Elmaleh M, Connors BW (2012) Thalamic Control of Layer 1 Circuits in Prefrontal Cortex. The Journal of Neuroscience 32:17813-17823.

D'Souza RD, Meier AM, Bista P, Wang Q, Burkhalter A (2016) Recruitment of inhibition and excitation across mouse visual cortex depends on the hierarchy of interconnecting areas. eLife 5:e19332.

De Pasquale R, Sherman SM (2011) Synaptic properties of corticocortical connections between the primary and secondary visual cortical areas in the mouse. JNeurosci 31:16494-16506.

Dehaene S, Changeux JP (2011) Experimental and theoretical approaches to conscious processing. Neuron 70:200-227.

Felleman DJ, Van Essen DC (1991) Distributed hierarchical processing in the primate cerebral cortex. CerebCortex 1:1-47.

Fortune ES, Rose GJ (2000) Short-Term Synaptic Plasticity Contributes to the Temporal Filtering of Electrosensory Information. The Journal of Neuroscience 20:7122.

Fremeau RT, Voglmaier S, Seal RP, Edwards RH (2004) VGLUTs define subsets of excitatory neurons and suggest novel roles for glutamate. Trends in Neurosciences 27:98-103.

Friston K (2005) A theory of cortical responses. Philos Trans R Soc Lond B Biol Sci 360:815-836.

Gentet LJ, Kremer Y, Taniguchi H, Huang ZJ, Staiger JF, Petersen CC (2012) Unique functional properties of somatostatin-expressing GABAergic neurons in mouse barrel cortex. Nat Neurosci 15:607-612.

Grunewald A, Bradley DC, Andersen RA (2002) Neural Correlates of Structure-from-Motion Perception in Macaque V1 and MT. The Journal of Neuroscience 22:6195.

Haider B, Häusser M, Carandini M (2013) Inhibition dominates sensory responses in the awake cortex. Nature 493:97-100.

Hubel DH, Wiesel TN (1959) Receptive fields of single neurones in the cat's striate cortex. J Physiol 148:574-591.

Hudetz AG (2012) General anesthesia and human brain connectivity. Brain Connect 2:291-302.

Imas OA, Ropella KM, Ward BD, Wood JD, Hudetz AG (2005) Volatile anesthetics enhance flash-induced gamma oscillations in rat visual cortex. Anesthesiology 102:937-947.

Issa EB, Wang X (2008) Sensory responses during sleep in primate primary and secondary auditory cortex. J Neurosci 28:14467-14480.

Jones EG (1998) Viewpoint: the core and matrix of thalamic organization. Neuroscience 85:331-345.

Jones EG (2001) The thalamic matrix and thalamocortical synchrony. Trends in neurosciences 24:595-601.

Kaisti KK, Metsahonkala L, Teras M, Oikonen V, Aalto S, Jaaskelainen S, Hinkka S, Scheinin H (2002) Effects of surgical levels of propofol and sevoflurane anesthesia on cerebral blood flow in healthy subjects studied with positron emission tomography. Anesthesiology 96:1358-1370.

Koch C, Massimini M, Boly M, Tononi G (2016) Neural correlates of consciousness: progress and problems. Nat Rev Neurosci 17:307-321.

Kok P, Brouwer GJ, van Gerven MA, de Lange FP (2013) Prior expectations bias sensory representations in visual cortex. J Neurosci 33:16275-16284.

Krause BMM, C. A.; Uhlrich, D. J.; Banks, M. I. (2017) Evidence that PV+ cells enhance temporal population codes but not stimulus-related timing in auditory cortex. bioRxiv 213249.

Ku SW, Lee U, Noh GJ, Jun IG, Mashour GA (2011) Preferential inhibition of frontal-to-parietal feedback connectivity is a neurophysiologic correlate of general anesthesia in surgical patients. PLoSOne 6:e25155.

Kubota Y (2014) Untangling GABAergic wiring in the cortical microcircuit. Current opinion in neurobiology 26:7-14.

Laureys S, Faymonville ME, Peigneux P, Damas P, Lambermont B, Del Fiore G, Degueldre C, Aerts J, Luxen A, Franck G, Lamy M, Moonen G, Maquet P (2002) Cortical processing of noxious somatosensory stimuli in the persistent vegetative state. Neuroimage 17:732-741.

Lee CC, Sherman SM (2008) Synaptic Properties of Thalamic and Intracortical Inputs to Layer 4 of the First- and Higher-Order Cortical Areas in the Auditory and Somatosensory Systems. Journal of Neurophysiology 100:317-326.

Lee CC, Sherman SM (2010) Drivers and modulators in the central auditory pathways. Front Neurosci 4:79.

Lee CC, Sherman SM (2011) On the classification of pathways in the auditory midbrain, thalamus, and cortex. HearRes 276:79-87.

Lee U, Kim S, Noh GJ, Choi BM, Hwang E, Mashour GA (2009) The directionality and functional organization of frontoparietal connectivity during consciousness and anesthesia in humans. ConsciousCogn 18:1069-1078.

Liu X, Lauer KK, Ward BD, Rao SM, Li SJ, Hudetz AG (2012) Propofol disrupts functional interactions between sensory and high-order processing of auditory verbal memory. Hum Brain Mapp 33:2487-2498.

Llinas R, Ribary U, Contreras D, Pedroarena C (1998) The neuronal basis for consciousness. Philos Trans R Soc Lond B Biol Sci 353:1841-1849.

Markov NT, Vezoli J, Chameau P, Falchier A, Quilodran R, Huissoud C, Lamy C, Misery P, Giroud P, Ullman S, Barone P, Dehay C, Knoblauch K, Kennedy H (2014) Anatomy of hierarchy: feedforward and feedback pathways in macaque visual cortex. J Comp Neurol 522:225-259.

Mashour GA (2014) Top-down mechanisms of anesthetic-induced unconsciousness. Front Syst Neurosci 8:115.

Mashour GA, Hudetz AG (2017) Bottom-Up and Top-Down Mechanisms of General Anesthetics Modulate Different Dimensions of Consciousness. Front Neural Circuits 11:44.

Motanis H, Seay MJ, Buonomano DV (2018) Short-Term Synaptic Plasticity as a Mechanism for Sensory Timing. Trends in neurosciences 41:701-711.

Muralidhar S, Wang Y, Markram H (2014) Synaptic and cellular organization of layer 1 of the developing rat somatosensory cortex. Frontiers in Neuroanatomy 7.

Murayama M, Pérez-Garci E, Nevian T, Bock T, Senn W, Larkum ME (2009) Dendritic encoding of sensory stimuli controlled by deep cortical interneurons. Nature 457:1137-1141.

Murphy C, Krause B, Banks M (2019) Selective effects of isoflurane on cortico-cortical feedback afferent responses in murine non-primary neocortex. Br J Anaesth 123:488-496.

Panagiotaropoulos TI, Kapoor V, Logothetis NK (2014) Subjective visual perception: from local processing to emergent phenomena of brain activity. Philos Trans R Soc Lond B Biol Sci 369:20130534.

Peltier SJ, Kerssens C, Hamann SB, Sebel PS, Byas-Smith M, Hu X (2005) Functional connectivity changes with concentration of sevoflurane anesthesia. Neuroreport 16:285-288.

Petreanu L, Mao T, Sternson SM, Svoboda K (2009) The subcellular organization of neocortical excitatory connections. Nature 457:1142-1145.

Petrof I, Viaene AN, Sherman SM (2011) Two populations of corticothalamic and interareal corticocortical cells in the subgranular layers of the mouse primary sensory cortices. JComp Neurol.

Pfeffer CK, Xue M, He M, Huang ZJ, Scanziani M (2013) Inhibition of inhibition in visual cortex: the logic of connections between molecularly distinct interneurons. Nature Neuroscience 16:1068-1076.

Pouille F, Scanziani M (2001) Enforcement of temporal fidelity in pyramidal cells by somatic feed- forward inhibition. Science 293:1159-1163.

Raz A, Grady SM, Krause BM, Uhlrich DJ, Manning KA, Banks MI (2014) Preferential effect of isoflurane on top-down versus bottom-up pathways in sensory cortex. Front Syst Neurosci 8.

Redinbaugh MJ, Phillips JM, Kambi NA, Mohanta S, Andryk S, Dooley G, Afrasiabi M, Raz A, Saalmann Y (2020) Thalamus Modulates Consciousness Via Layer-Specific Control of Cortex. Neuron 105.

Reichova I, Sherman SM (2004) Somatosensory corticothalamic projections: distinguishing drivers from modulators. J Neurophysiol 92:2185-2197.

Rockland KS, Virga A (1989) Terminal arbors of individual "feedback" axons projecting from area V2 to V1 in the macaque monkey: a study using immunohistochemistry of anterogradely transported Phaseolus vulgaris-leucoagglutinin. J Comp Neurol 285:54-72.

Rotman Z, Deng P-Y, Klyachko VA (2011) Short-Term Plasticity Optimizes Synaptic Information Transmission. The Journal of Neuroscience 31:14800.

Rubio-Garrido P, Pérez-de-Manzo F, Porrero C, Galazo MJ, Clascá F (2009) Thalamic input to distal apical dendrites in neocortical layer 1 is massive and highly convergent. Cerebral Cortex 19:2380-2395.

Rudy B, Fishell G, Lee S, Hjerling-Leffler J (2011) Three groups of interneurons account for nearly 100% of neocortical GABAergic neurons. Developmental neurobiology 71:45-61.

Saalmann YB (2014) Intralaminar and medial thalamic influence on cortical synchrony, information transmission and cognition. Front Syst Neurosci 8:83.

Saalmann YB, Pinsk MA, Wang L, Li X, Kastner S (2012) The pulvinar regulates information transmission between cortical areas based on attention demands. Science 337:753-756.

Schrouff J, Perlbarg V, Boly M, Marrelec G, Boveroux P, Vanhaudenhuyse A, Bruno MA, Laureys S, Phillips C, Pelegrini-Issac M, Maquet P, Benali H (2011) Brain functional integration decreases during propofol-induced loss of consciousness. Neuroimage 57:198-205.

Sellers KK, Bennett DV, Hutt A, Williams JH, Frohlich F (2015) Awake vs. anesthetized: layer-specific sensory processing in visual cortex and functional connectivity between cortical areas. J Neurophysiol 113:3798-3815.

Sherman SM, Guillery RW (1998) On the actions that one nerve cell can have on another: distinguishing "drivers" from "modulators". Proc Natl Acad Sci USA 95:7121-7126.

Sherman SM, Guillery RW (2011) Distinct functions for direct and transthalamic corticocortical connections. J Neurophysiol 106:1068-1077.

Sherman SM, Guillery RW (2013) Functional Connections of Cortical Areas: A New View from the Thalamus. Cambridge, MA: MIT Press.

Shipp S (2007) Structure and function of the cerebral cortex. Curr Biol 17:R443-449.

Stevens CF, Wang Y (1995) Facilitation and depression at single central synapses. Neuron 14:795-802.

Sun QQ, Huguenard JR, Prince DA (2006) Barrel Cortex Microcircuits: Thalamocortical Feedforward Inhibition in Spiny Stellate Cells Is Mediated by a Small Number of Fast-Spiking Interneurons. Journal of Neuroscience 26:1219-1230.

Theyel BB, Llano DA, Sherman SM (2010) The corticothalamocortical circuit drives higher-order cortex in the mouse. Nat Neurosci 13:84-88.

Todorovic A, van Ede F, Maris E, de Lange FP (2011) Prior expectation mediates neural adaptation to repeated sounds in the auditory cortex: an MEG study. J Neurosci 31:9118-9123.

Tremblay R, Lee S, Rudy B (2016) GABAergic Interneurons in the Neocortex: From Cellular Properties to Circuits. Neuron 91:260-292.

Urban-Ciecko J, Fanselow EE, Barth AL (2015) Neocortical somatostatin neurons reversibly silence excitatory transmission via GABAB receptors. Current Biology 25:722-731.

Viaene AN, Petrof I, Sherman SM (2011a) Synaptic properties of thalamic input to layers 2/3 and 4 of primary somatosensory and auditory cortices. JNeurophysiol 105:279-292.

Viaene AN, Petrof I, Sherman SM (2011b) Synaptic properties of thalamic input to the subgranular layers of primary somatosensory and auditory cortices in the mouse. JNeurosci 31:12738-12747.

Viaene AN, Petrof I, Sherman SM (2011c) Properties of the thalamic projection from the posterior medial nucleus to primary and secondary somatosensory cortices in the mouse. Proc Natl Acad Sci USA 108:18156-18161.

Villablanca J, Salinas-Zeballos ME (1972) Sleep-wakefulness, EEG and behavioral studies of chronic cats without the thalamus: the 'athalamic' cat. Arch Ital Biol 110:383-411.

White NS, Alkire MT (2003) Impaired thalamocortical connectivity in humans during general-anesthetic-induced unconsciousness. Neuroimage 19:402-411.

Wilke M, Logothetis NK, Leopold DA (2006) Local field potential reflects perceptual suppression in monkey visual cortex. Proc Natl Acad Sci USA 103:17507.

Winer JA, Larue DT (1989) Populations of GABAergic neurons and axons in layer I of rat auditory cortex. Neuroscience 33:499-515.

Xu H, Jeong HY, Tremblay R, Rudy B (2013) Neocortical Somatostatin-Expressing GABAergic Interneurons Disinhibit the Thalamorecipient Layer 4. Neuron 77:155-167.

Yang W, Carrasquillo Y, Hooks BM, Nerbonne JM, Burkhalter A (2013) Distinct Balance of Excitation and Inhibition in an Interareal Feedforward and Feedback Circuit of Mouse Visual Cortex. The Journal of Neuroscience 33:17373.

Chapter 2

Optogenetic activation of afferent pathways in brain slices and modulation of responses by volatile anesthetics.

This chapter was accepted for publication as:

Murphy CM, Raz A, Grady, SM, Banks MI (in press). Optogenetic activation of afferent pathways in brain slices and modulation of responses by volatile anesthetics. Journal of Visualized Experiments.

Caitlin A. Murphy[1], Aeyal Raz[1,2], Sean M. Grady[1], Matthew I. Banks[1]

[1]Department of Anesthesiology, University of Wisconsin, Madison, Wisconsin
[2]Department of Anesthesiology, Rambam Health Care Campus, the Ruth and Bruce Rappaport Faculty of Medicine, Technion - Israel Institute of Technology, Haifa, Israel

Keywords

channelrhodopsins, optogenetics, thalamus, neocortex, isoflurane, anesthesia, inhalation, electrophysiology, patch-clamp techniques, interneurons

Summary

Ex vivo brain slices can be used to study the effects of volatile anesthetics on evoked responses to afferent inputs. Optogenetics are employed to independently activate thalamocortical and corticocortical afferents to non-primary neocortex, and synaptic and

network responses are modulated with isoflurane.

Abstract

Anesthetics influence consciousness in part via their actions on thalamocortical circuits. However, the extent to which volatile anesthetics affect distinct cellular and network components of these circuits remains unclear. Ex vivo brain slices provide a means by which investigators may probe discrete components of complex networks and disentangle potential mechanisms underlying the effects of volatile anesthetics on evoked responses. To isolate potential cell type- and pathway-specific drug effects in brain slices, investigators must be able to independently activate afferent fiber pathways, identify non-overlapping populations of cells, and apply volatile anesthetics to the tissue in aqueous solution. In this protocol, methods to measure optogenetically-evoked responses to two independent afferent pathways to neocortex in ex vivo brain slices are described. Extracellular responses are recorded to assay network activity, and targeted whole-cell patch clamp recordings are conducted in somatostatin- and parvalbumin-positive interneurons. Delivery of physiologically relevant concentrations of isoflurane via artificial cerebral spinal fluid to modulate cellular and network responses is described.

Introduction

Volatile anesthetics have been used ubiquitously in a variety of clinical and academic settings for more than a century. Distinct classes of anesthetics have unique, often non-overlapping molecular targets(Herring et al., 2009; Xie et al., 2013; Baumgart et al., 2015), yet nearly all of them produce unconsciousness. While their behavioral effects are

quite predictable, the mechanisms by which anesthetics induce loss of consciousness are largely unknown. Anesthetics may ultimately influence both the level and contents of consciousness via actions on corticothalamic circuits, disrupting integration of information throughout the cortical hierarchy(Crick and Koch, 2003; Friston, 2005; Dehaene and Changeux, 2011; Koch et al., 2016; Mashour and Hudetz, 2017; Voss et al., 2019). More broadly, modulation of corticothalamic circuits may play a role in experimentally(Redinbaugh et al., 2020) or pharmacologically(Carhart-Harris and Friston, 2019) altered states of consciousness, and may also be implicated in sleep(Mak-McCully et al., 2017) and in pathophysiological disorders of consciousness(Alkire et al., 2008; Sanders and Maze, 2012).

The elusiveness of the mechanisms underlying loss and return of consciousness during anesthesia may be attributed partially to non-linear, synergistic actions of anesthetics at the cellular, network, and systems levels(Hemmings et al., 2019). Isoflurane, for example, suppresses activity within the selected brain regions(Liu et al., 2012; Hentschke et al., 2017; Nourski et al., 2018), impairs connectivity between distant brain regions(Ferrarelli et al., 2010; Ku et al., 2011; Murphy et al., 2011; Lee et al., 2013; Lee et al., 2017), and diminishes synaptic responses in a pathway-specific manner(Raz et al., 2014; Murphy et al., 2019). Which effects of anesthetics, from the molecular to the systems level, are necessary or sufficient to effect loss of consciousness remains unclear. In addition to substantive clinical investigations of consciousness using non-invasive techniques(Ferrarelli et al., 2010; Schrouff et al., 2011; Lee et al., 2013), it is important that experimentalists seek to disentangle the distinct cellular and network interactions that

subserve the conscious experience.

By simplifying the complex interactions found in the intact brain, ex vivo brain slices allow the study of isolated components of the brain's dynamic systems (Voss et al., 2019). A reduced slice preparation combines the benefits of relatively intact anatomical structures of local neural circuits with the versatility of in vitro manipulations. However, until recently, methodological constraints have precluded the study of synaptic and circuit properties of long-range inputs in brain slices(Petreanu et al., 2009; Cruikshank et al., 2010); the tortuous path of corticothalamic fiber tracts made activation of independent afferent pathways all but impossible by electrical stimulation.

Investigating the effects of anesthetic agents on the brain slice preparations presents additional challenges. Absent an intact respiratory and circulatory system, anesthetic agents must be bath-applied, and concentrations carefully matched to estimated effect site concentrations. For many intravenous anesthetic agents, the slow rate of equilibration in the tissue renders traditional pharmacological investigations laborious(Gredell et al., 2004; Benkwitz et al., 2007). Investigating the effects volatile gas anesthetics in ex vivo preparations is more tractable, but also presents challenges. These include converting inhaled partial pressure doses to aqueous concentrations, and the need for a modified delivery system of the drug to the tissue via artificial cerebral spinal fluid(Franks and Lieb, 1993).

Here, methods are described by which investigators may capitalize on the well-

documented physicochemical properties of the volatile anesthetic isoflurane for drug delivery to ex vivo brain slices, activate pathway- and layer-specific inputs to a cortical area of interest with high spatiotemporal resolution, and conduct simultaneous laminar recordings and targeted patch clamp recordings from select populations of neurons. Combined, these procedures allow investigators to measure volatile anesthetic-induced changes in several observable electrophysiological response properties, from the synaptic to local network level.

Protocol

All procedures involving animals described in this protocol were approved by the University of Wisconsin-Madison School of Medicine and Public Health Animal Care and Use Committee.

1. Breeding mice to express fluorescent reporter protein in interneuron subpopulations

1.1. Pair homozyogous, Cre-dependent tdTomato male mouse with either homozygous SOM-Cre female or homozygous PV-Cre female mouse.

NOTE: Other specific neuronal populations may be targeted by using the appropriate Cre lines.

1.2. Allow heterozygous offspring to mature to at least 3 weeks of age before proceeding. For experiments described here, genotyping is not necessary, as homozygous parents produce offspring that are all heterozygous for both cell type-specific Cre recombinase and Cre-dependent reporter alleles.

2. Performing unilateral stereotaxic injection of viral construct

2.1. Adjust settings of the micropipette puller for injection pipettes as indicated in the instrument user manual (see **Table 1** for recommended settings). Pull the glass micropipette.

2.2. Break the tip of the sharp end of the pipette such that the tip diameter is approximately 30 µm with minimal taper over several millimeters.

2.3. Using previously documented procedures, decide on the appropriate titer and volume of virus to be injected. In the experiments described here, 1.0 µL (titer: 3.1-5.7 TU/mL) injected unilaterally produced good results.

2.4. Backfill the full volume of the pipette with mineral oil. Load the pipette onto the microsyringe and flow a small amount of mineral oil through the tip to ensure the tip is not clogged.

2.5. Frontfill at least 1.0 µL of viral construct. The recombinant adeno-associated viral

vector used in these experiments was AAV2-hSyn-hChR2(H134R)-EYFP.

2.6. Arrange sterile drape in a surgical area. Sterilize tools for stereotaxic procedure and place them on the drape.

2.7. Anesthetize SOM-tdTomato or PV-tdTomato heterozygous animal using isoflurane (3% for induction, 1.5-2% for maintenance) and oxygen mixture. Periodically confirm surgical level of anesthesia with toe pinch throughout surgery. Ensure animal does not move beyond the surgical plan of anesthesia by monitoring respirations every 10-15 min.

2.8. Shave the top of the animal's head. Apply 70% isopropyl alcohol and iodine-based solution liberally to surgical area and ophthalmic ointment to eye sockets to prevent drying of the membrane. Administer bupivacaine/lidocaine (1:1 ratio, 1.0 mg/kg) subcutaneously to surgical site for local anesthetic.

2.9. Fit the animal into stereotaxic frame.

2.10. Use scalpel to make incision along sagittal axis of skin overlying the dorsal surface of the skull. Retract skin using forceps. Hydrate skull with 0.9% saline as necessary.

2.11. On the surface of the skull, lightly mark the intersection of anterior and lateral coordinates with a cross in pencil. Drill a hole at the appropriate coordinates in the transverse plane (in mm relative to Bregma, for cingulate cortex (Cg) injection: anterior

0.2, lateral 0.3; for posterior thalamus (Po) injection: posterior 2.25, lateral 3.4).

NOTE: Markings should extend beyond the boundaries of the burr hole to provide guidance for accurate placement of pipette.

2.12. Turn on and balance the air table.

2.13. Reposition the electrode manipulator of the stereotaxic frame at 0° for injections into Cg, or 45° in the coronal plane for injections into Po.

2.14. Attach the syringe pump to the electrode manipulator. Attach the microsyringe pump controller to the syringe pump.

2.15. Navigate the pipette tip near (but not touching) the surface of the brain, at the intersection of markings created in Step 2.11. Advance the pipette at approximately 1 mm/s along its longitudinal axis into the brain either 0.9 mm (injection in Cg) or 3.1 mm (injection in Po). Wait for 10 min before proceeding.

2.16. Inject 1.0 µL of viral construct over a period of 10 min (100 nL/min). If welling of virus from pipette insertion site is observed, slow the injection rate to 50 nL/min.

2.17. After injection, wait for 10 min before slowly retracting the injection pipette.

2.18. Suture to close the scalp incision and administer 2-5 mg/kg meloxicam subcutaneously.

2.19. Discontinue isoflurane and monitor animal during emergence from anesthesia. Allow to recover according to procedures described by Institution's Animal Care and Use Committee, including further administration of analgesics.

3. Preparation of acute brain slices

3.1. Allow at least 3 weeks for the expression of viral construct before harvesting tissue.

3.2. Prepare 1 L of artificial cerebral spinal fluid for slicing procedure (slicing artificial cerebral spinal fluid, sACSF). See **Table 2** for ingredients.

3.3. Throughout the slicing procedure, supply sACSF with dissolved 95% O_2/5% CO_2 mixture, delivered via gas dispersion tube.

3.5. Prepare ice cold bath for vibrating blade microtome. Mount ice-cold specimen stage onto microtome and fix sapphire blade in place for tissue sectioning.

3.4. Anesthetize mouse with 3% isoflurane and oxygen until loss of righting reflex.

3.5. Decapitate the mouse using guillotine and immediately submerge head in 4°C

sACSF. To preserve the health of the tissue, complete the following steps as swiftly as possible.

3.6. Open skull cavity by making a small incision at the base of the skull and gently removing each skull plate. Gently remove underlying dura mater.

3.7. While the brain is still in the skull cavity, use the razor blade to remove the cerebellum. Make a second vertical cut along the sagittal plane in the left hemisphere, just lateral to the midline.

3.8. Prepare tissue block for sectioning.

3.8.1. Gently lift the brain from the skull cavity. Place the brain on the filter paper with the flat, sagittal plane down. Guide the filter paper over the blocking template and align the brain to the underlying template outline (**Supplementary Figure 1**).

3.8.2. Make two parallel cuts in the coronal plane as indicated by the lines on the template. Add a small drop of sACSF to keep filter paper wet, if necessary.

3.8.3. Place the tissue block in 4°C sACSF briefly while step 3.8.4 is conducted.

3.8.4. Apply a small amount of super glue to the ice-cold specimen stage.

3.8.5. Lift the tissue block from cold sACSF. Use the corner of an absorbent towel to wick away excess sACSF. Glue the posterior coronal plane of the tissue block to the specimen stage, with the dorsal surface of the brain facing the sapphire blade.

3.9. Collect 500 µm thick coronal brain slices. Place slices of interest on nylon mesh (**Supplementary Figure 2**) in 34 °C sACSF and allow the container to reach room temperature.

NOTE: For experiments described here, electrophysiological recordings were collected from a coronal section centered approximately 2.25 mm posterior to bregma to study a non-primary sensory area, medial secondary visual cortex (V2MM).

4. Preparation of experimental artificial cerebral spinal fluid (eACSF) bags, one with and one without dissolved volatile anesthetic isoflurane

4.1. Prepare 300 mL of a stock mixture of 3.0% isoflurane.

4.1.1. In a sealed polytetrafluoroethylene gas bag, add ~100 mL of 95% O_2/5% CO_2 gas mixture to 20-30 mL of liquid isoflurane and a small amount of 0.9% saline. Wait at least for 30 min to allow equilibration of isoflurane between liquid and gas phases.

4.1.2. Determine the amount of saturated isoflurane gas, V_{sat}, to add to the stock bag using the following equation:

$$V_{sat} = \frac{P\%_{stock} * V_{stock}}{\left(\frac{P_{isoflurane}}{P_{total}}\right) * 100} \quad (1)$$

where $P\%_{stock}$ is the target composition of the stock gas (3% in this case), V_{stock} is the final volume of the stock gas bag, $P_{isoflurane}$ is the partial pressure of isoflurane at room temperature (~240 mmHg), and P_{total} is the atmospheric pressure (~760 mmHg).

4.1.3. Add the calculated amount of saturated gas to an empty gas bag and fill the bag with a volume of 95% O_2/5% CO_2 gas mixture to bring the total volume of stock bag to 300 mL.

4.2. Prepare 2 L of artificial cerebral spinal fluid for perfusion of the slice during the experiment (experimental ACSF, eACSF). See **Table 2** for ingredients. Dissolve 95% O_2/5% CO_2 gas mixture into solution.

4.3. Prepare two separate bags of Control and Isoflurane solutions.

4.3.1. To an empty polytetrafluoroethylene gas bag, add 600 mL eACSF and 600 mL of 95% O_2/5% CO_2 gas mixture. Label this bag as Control.

4.3.2. To another empty polytetrafluoroethylene gas bag, add 300 mL of eACSF. Label this bag as Isoflurane.

4.3.3. Choose a physiologically relevant equilibrated gas phase concentration of isoflurane. Experiments were conducted using gas concentrations equivalent to 1.3% isoflurane. Mice lose righting reflex, and presumably consciousness, at 0.9% inhaled isoflurane.

4.3.4. Use the following equation to calculate the equivalent gas phase concentration at room temperature, $P\%(T_{room})$ (Franks and Lieb, 1993):

$$P\%(T_{room}) = P\%(T_{body}) * e^{\frac{-20.2(T_{body}-T_{room})}{273.15+T_{room}}} \quad (2)$$

where $P\%(T_{body})$ is the physiologically relevant gas phase concentration chosen in Step 4.3.3, T_{room} is 25 °C, and T_{body} is 37 °C.

4.3.5. Use the following equation to determine volume of gas from stock gas bag, V_{stock}, to add to the Isoflurane solution.

$$V_{stock} = \frac{V_{solution} * P\%(T_{room}) * (1+\lambda)}{P\%_{stock}} \quad (3)$$

where $V_{solution}$ is the volume of eACSF in ISOFLURANE bag (300 mL), $P\%(T_{room})$ is entered from equation (2), λ is the saline/gas Ostwald partition coefficient of isoflurane (λ = 1.2(Honemann et al., 1998)), and $P\%_{stock}$ is the gas phase concentration of the stock gas bag ($P\%_{stock}$ = 3.0%).

4.3.6. To the Isoflurane solution bag, add the volume of gas from the stock gas bag, V_{stock}, calculated in Step 4.3.5.

4.3.7. To the Isoflurane solution bag, add a volume of 95% O_2/5% CO_2 gas mixture to bring the total volume of gas in the Isoflurane solution bag to 300 mL.

4.4. Shake both Control and Isoflurane bags on shaker for at least 1 h to allow isoflurane phase equilibration.

4.5. After all data has been collected, the correct concentration may be verified by using an anesthetic gas monitor to measure equilibrated gas concentration of isoflurane above the remaining solution in bag.

4.6. Report experimental concentrations of volatile gases in aqueous units, as millimolar concentrations are more robust to changes in temperature. Use the following equation to convert room temperature gas phase concentration, $P\%(T_{room})$, to equivalent aqueous concentration ($C_{aqueous}$, in mM) (Franks and Lieb, 1993):

$$C_{aqueous} = 0.44614 * \alpha * P\%(T_{room}) \quad (4)$$

where α is the saline/gas Bunsen partition coefficient for isoflurane at 25°C(Honemann et al., 1998).

5. Preparation of hardware and software for multi-channel recordings

5.1. Set up 16-channel data acquisition system according to manufacturer instructions.

NOTE: Several commercially available amplifiers and data acquisition systems can be used to collect multi-channel recordings. In the experiments described here, analog signals are delivered via an electrode reference panel to two amplifiers, where they are amplified (2000x) and filtered (0.1-10kHz). Analog inputs to the data acquisition system are digitized at 40kHz.

5.2. Fasten the appropriate 16-channel headstage adaptor to a microscope micromanipulator. Orient the adaptor such that the female connector ports are facing downward.

5.3. Adjust the angle of operation of this micromanipulator such that it is oriented downward toward the recording chamber, at an angle approximately 70° relative to horizontal.

5.4. Connect the headstage input to a 16 x 1 probe for in vitro electrophysiology via the headstage adaptor anchored to the micromanipulator.

5.5. Connect the headstage output connector to the data acquisition system.

5.6. Install appropriate software for data acquisition. Configure 15 input channels to correspond to input signals from the first 15 multi-channel probe contacts. Configure the remaining channel to receive input from the intracellular electrode.

NOTE: Take care to consider electrode and adaptor maps when collecting and analyzing data, to ensure the appropriate signal corresponds to the electrode contact from which it was collected.

6. Configure light stimulation protocols

6.1. Set up light delivery system and install the accompanying software.

6.2. Open the software. Choose hardware wiring configuration in which a Trigger Source (Digital/TTL Out) provides Trigger In signal to the light delivery system, and the light delivery system provides Trigger Out signal to a 470 nm LED.

6.3. Mount high-power objective lens. Using digital camera, calibrate high-power objective for use with light delivery system.

6.4. Create new profile sequence of light stimulation profiles.

6.4.1. Create a pattern of choice. In the experiments described here, a circle of diameter 150 µm is used to allow layer-specific activation of axon terminals.

6.4.2. To construct a profile sequence, copy and paste this profile for each of any number of trials.

6.4.3. Create a waveform list that contains waveforms of any light intensity, pulse duration, or pulse number.

6.4.4. Randomly assign waveforms to each profile. Each profile with its assigned waveform corresponds to one trigger pulse from a Digital TTL input, or one trial.

6.4.5. Save the profile sequence.

6.5. In the data acquisition software, create a new protocol.

6.5.1. Set the number of trials to equal the number of profiles in the profile sequence just created.

6.5.2. Choose signal inputs to match those configured in Step 5.6. Configure a protocol that provides a single digital TTL output, recording from these 16 input channels for an appropriate amount of time before and after the digital trigger.

7. Placing multi-channel probe in ex vivo brain tissue slice

7.1. Perfuse bubbled eACSF (not in sealed bags) at 3-6 mL/min.

7.2. Transfer the brain slice containing area of interest onto mesh grid in microscope perfusion chamber. Anchor with platinum harp (see **Supplementary Figure 3**).

7.3. Rotate mesh grid such that the line of electrode contacts on the distal end of the multi-channel probe is approximately perpendicular to the pial surface.

7.4. Under broadfield illumination and under fine control of the micromanipulator, lower the multi-channel probe toward the surface of the slice.

7.5. Rotate the filter cube turret to engage the appropriate filter cube for visualization of the fluorescent reporter protein expressed in axon terminals of cortical afferents. If necessary, rotate the slice to more precisely align the probe with the pial surface.

7.6. Position the probe just above the plane of the slice, □200 µm short of the final target position along the x-axis, leaving at least one channel outside the boundary of the area of tissue being recorded

7.7. Slowly insert the probe into the slice by moving the manipulator along its longitudinal axis. To minimize damage to the tissue, only advance the probe to the extent that the sharp tips are just visible below the tissue surface. This will minimize damage to the tissue while still ensuring the electrode contacts are in contact with the tissue.

8. Patch clamping targeted neurons and obtaining whole-cell configuration

8.1. Switch eACSF source to bagged Control solution.

8.2. Identify fluorescently labeled cell for targeted patch clamp recording.

8.2.1. Restrict the aperture iris diaphragm to the smallest diameter. Engage a low-power objective lens and bring the tissue into focus.

8.2.2. Center the light over an area of tissue adjacent to (but not overlapping) the multi-channel probe.

8.2.3. Engage the high-power (40x or 60x) water immersion objective, using caution to avoid contact between the multi-channel probe and objective lens.

8.2.4. Rotate the filter cube turret to engage the appropriate filter set to allow imaging of cells expressing Cre-dependent fluorescent marker.

8.2.5. Identify a fluorescently labeled cell as a target for patch clamp recording. Raise the objective lens to create ample space to lower a patch pipette.

8.3. Load a patch pipette (see **Table 1**) with internal solution (**Table 2**) and mount pipette

into electrode holder. Using 1 mL syringe, apply positive pressure corresponding to ~0.1mL air.

8.4. Lower patch pipette into the solution. Bring the pipette tip into focus under visual guidance.

8.5. Obtain whole-cell recording from the targeted cell using the steps previously demonstrated(Au - Segev et al., 2016).

8.6. If planning to assess changes to intrinsic properties of the cell (e.g., input resistance, action potential firing rate in response to current steps), conduct these recordings. Otherwise, move to axon stimulation protocol in below.

9. Layer-specific optogenetic activation of axon terminals

9.1. Manipulate field of view in the x-y plane to align light stimulation profile with desired location on slice.

9.2. Load light stimulus protocol and prepare the light delivery system to receive a digital TTL pulse.

9.3. Optogenetically activate axon terminals while simultaneously recording extracellular field potentials and intracellular membrane fluctuations.

9.4. Switch eACSF source to Isoflurane solution and wash drug in for 15 min. If necessary, collect spontaneous recordings during the wash-in.

9.5. Repeat step 9.2-9.3.

9.6. Switch eACSF source to Control solution and wash drug out for 20 min. If necessary, collect spontaneous recordings during wash-out.

9.7. Repeat step 9.2-9.3.

Representative Results

A timeline of steps described in the protocol is shown in **Figure 1**. Cortical inputs arriving from higher order cortical areas or from non-primary thalamic nuclei have partially overlapping terminal fields in layer 1 of non-primary visual cortex(Murphy et al., 2019). To isolate independent thalamocortical or corticocortical afferent pathways, a viral vector containing ChR2 and an eYFP fluorescent reporter was injected into either Po or Cg. Cells within the injection radius take up the viral vector and, after 2-4 weeks, express the non-specific cation channel ChR2 and the reporter in both the soma and projecting axons (**Figure 2A**). Coronal slices were collected. With the appropriate filter cube engaged, axons expressing the viral construct were imaged (**Figure 2B**). The use of ChR2 to activate axon terminals allows for activation of afferents without the prerequisite for an attached soma.

The animals used in the experiments described here were SOM-tdTomato or PV-tdTomato hybrid animals, which express the fluorescent reporter protein tdTomato in either somatostatin- (SOM+) or parvalbumin-positive (PV+) interneurons, respectively. SOM+ or PV+ interneurons in layer 2/3 were targeted for patch clamping under visual guidance with the appropriate filter cube engaged (Layer 1C). These interneurons have dendrites in layer 1 and are targets of corticocortical inputs (**Figure 3A**).

Addition of 125 mL of 3.0% isoflurane gas and 175 mL of 95% O_2/5% CO_2 to a sealed bag resulted in a pre-equilibrium concentration of gas of 1.3%. Gas dissolved into eACSF according to its partition coefficient; the predicted gas phase equilibrium concentration of isoflurane at room temperature was 0.6% (**Figure 2D**). This was confirmed via gas monitor.

The tissue slice was transferred to the recording chamber and the 16 x 1 multi-channel recording probe was placed orthogonally to the cortical laminae (**Figure 2E**). A 150 µm circle of 470 nm light centered over cortical layer 1 was delivered via the objective light path, while extracellular field potentials were collected using the 16 x 1 multi-channel probe and targeted whole-cell patch clamp recordings were conducted in interneurons. A schematic of the recording set-up is shown in **Figure 2F**.

Post-synaptic potentials (PSPs) were observed in interneurons in response to a train of four 2 ms pulses of light (10 Hz; **Figure 3A**). Local field potentials were also recorded

(**Figure 3B**). Current source density (CSD; **Figure 3C**) and multi-unit activity (MUA; **Figure 3D**) were extracted from local field potentials. Ten trials at several different light intensities were used to conduct post hoc analyses. The amplitude of current sinks extracted from the CSD increased as a function of light intensity (**Figure 4A**). A three-parameter nonlinear logistic equation was fit to the data for comparisons across pathways. PSP amplitude also increased with current sink amplitude (**Figure 4B**).

Synaptic responses to thalamocortical and corticocortical inputs were measured during control, isoflurane (0.28 mM), and recovery conditions. Post-synaptic responses of somatostatin- (**Figure 5A**) to corticocortical stimuli were suppressed during isoflurane, as were evoked current sinks (**Figure 5B**).

Discussion

In this manuscript, a protocol for evaluating intra- and extracellular responses to selectively activated afferent pathways in ex vivo brain slices is described.

The use of optogenetic tools and parallel recording schemes allows investigators to probe responses of local populations to afferent inputs from distant brain regions, while recording simultaneously from targeted populations of interneurons. The use of optogenetic technology allows for axon terminals of afferent projections to be preserved and activated even though their cell bodies are no longer attached. This relieves geometric restrictions previously imposed upon *ex vivo* slices, as preservation of long-range electrical connections is no longer paramount. Still, care should be taken to prepare

slices in a geometrical plane that preserves any remaining connections of interest. For example, pyramidal cells are oriented vertically along the cortical column, and evoked network activity measured by the multichannel probes in these experiments requires such local connections to be preserved as much as possible. Thus, coronal slices were prepared to keep local connectivity intact.

When choosing optogenetic constructs and relevant fluorescent reporter proteins, properties of their excitation/emission spectra and microscopic optics must be considered. Persistent light stimulation may result in partial inactivation of many channelrhodopsin variants(Lin et al., 2009), which can be avoided by choosing reporter proteins whose excitation spectra do not overlap with that of the opsin. Alternative variants with different kinetics or light sensitivities may also be chosen depending on the experimental paradigm(Lin, 2011), including manipulations using alternative excitatory or inhibitory opsins. Filter cubes must also be appropriately aligned with the chosen fluorescent reporters, such that afferent axon terminals or interneurons may be imaged independently and without activating expressed opsins. To account for the variability in virus expression, it may also be pertinent for investigators to normalize any optogenetically-induced activity to the expression level of the viral construct, measured by the fluorescent output of the reporter protein.

Delivery of pre-calculated concentrations of volatile anesthetics to slice tissue is also possible using the methods outlined here. When choosing appropriate physiologically relevant gas equilibrium percentages, investigators should account for 10-15% loss of

dissolved isoflurane gas between the perfusion line and tissue(Banks and Pearce, 1999). The methods applicable to isoflurane have been presented, but other drugs such as halothane, sevoflurane, or desflurane can be handled similarly using the appropriate Ostwald and Bunsen coefficients (**Supplementary Table 1**). The partitioning properties of volatile anesthetics assure that they will predictably dissolve into ACSF. However, because partial pressures are more sensitive to changes in temperature than aqueous EC_{50} concentrations(Hagan et al., 1998), gas equilibrium volume percentages of volatile anesthetics must be converted to predicted room temperature millimolar concentrations to compare observed effects to physiologically relevant doses *in vivo*. If opting to study intravenous anesthetics such as etomidate or propofol in brain slices, investigators must consider diffusion profiles of the drugs under study, as equilibration times and physiologically relevant concentrations may vary greatly(Benkwitz et al., 2007).

In this manuscript, a protocol is described for testing the effects of volatile anesthetics on distinct components of thalamocortical circuits in ex vivo brain slices. Many of the variables and parameters in the methods described may be manipulated for further investigations. For example, different brain areas, afferent pathways, cell targets, or volatile anesthetics may be studied by adapting the outlined methods to answer novel questions. Combined with other theoretical and experimental methods, study of unique cellular and network components using ex vivo brain slices will advance our understanding of the dynamic brain, and the changes it undergoes during pharmacological and pathophysiological changes in consciousness.

Acknowledgements

The authors thank Bryan Krause for technical support and guidance on this project.

This work was supported by the International Anesthesia Research Society (IMRA to AR), National Institutes of Health (R01 GM109086 to MIB), and the Department of Anesthesiology, School of Medicine and Public Health, University of Wisconsin, Madison, WI, USA.

Disclosures

The authors have nothing to disclose.

References

Alkire MT, Hudetz AG, Tononi G (2008) Consciousness and anesthesia. Science 322:876-880.

Au - Segev A, Au - Garcia-Oscos F, Au - Kourrich S (2016) Whole-cell Patch-clamp Recordings in Brain Slices. JoVE:e54024.

Banks MI, Pearce RA (1999) Dual actions of volatile anesthetics on $GABA_A$ IPSCs: dissociation of blocking and prolonging effects. Anesthesiology 90:120-134.

Baumgart JP, Zhou ZY, Hara M, Cook DC, Hoppa MB, Ryan TA, Hemmings HC, Jr. (2015) Isoflurane inhibits synaptic vesicle exocytosis through reduced Ca2+ influx, not Ca2+-exocytosis coupling. Proc Natl Acad Sci U S A 112:11959-11964.

Benkwitz C, Liao M, Laster MJ, Sonner JM, Eger EI, 2nd, Pearce RA (2007) Determination of the EC50 amnesic concentration of etomidate and its diffusion profile in brain tissue: implications for in vitro studies. Anesthesiology 106:114-123.

Carhart-Harris RL, Friston KJ (2019) REBUS and the Anarchic Brain: Toward a Unified Model of the Brain Action of Psychedelics. Pharmacological Reviews 71:316.

Crick F, Koch C (2003) A framework for consciousness. Nat Neurosci 6:119-126.

Cruikshank SJ, Urabe H, Nurmikko AV, Connors BW (2010) Pathway-Specific Feedforward Circuits between Thalamus and Neocortex Revealed by Selective

Optical Stimulation of Axons. Neuron 65:230-245.

Dehaene S, Changeux JP (2011) Experimental and theoretical approaches to conscious processing. Neuron 70:200-227.

Ferrarelli F, Massimini M, Sarasso S, Casali A, Riedner BA, Angelini G, Tononi G, Pearce RA (2010) Breakdown in cortical effective connectivity during midazolam-induced loss of consciousness. Proc Natl Acad Sci USA 107:2681-2686.

Franks NP, Lieb WR (1993) Selective actions of volatile general anaesthetics at molecular and cellular levels. British Journal of Anaesthesia 71:65-76.

Friston K (2005) A theory of cortical responses. Philos Trans R Soc Lond B Biol Sci 360:815-836.

Gredell JA, Turnquist PA, MacIver MB, Pearce RA (2004) Determination of diffusion and partition coefficients of propofol in rat brain tissue: implications for studies of drug action in vitro. BJA: British Journal of Anaesthesia 93:810-817.

Hagan CE, Pearce RA, Trudell JR, MacIver MB (1998) Concentration measures of volatile anesthetics in the aqueous phase using calcium sensitive electrodes. J Neurosci Meth 81:177-184.

Hemmings HC, Riegelhaupt PM, Kelz MB, Solt K, Eckenhoff RG, Orser BA, Goldstein PA (2019) Towards a Comprehensive Understanding of Anesthetic Mechanisms of Action: A Decade of Discovery. Trends in Pharmacological Sciences 40:464-481.

Hentschke H, Raz A, Krause BM, Murphy CA, Banks MI (2017) Disruption of cortical network activity by the general anesthetic isoflurane. Br J Anaesth 119:685-696.

Herring BE, Xie Z, Marks J, Fox AP (2009) Isoflurane inhibits the neurotransmitter release machinery. J Neurophysiol 102:1265-1273.

Honemann CW, Washington J, Honemann MC, Nietgen GW, Durieux ME (1998) Partition coefficients of volatile anesthetics in aqueous electrolyte solutions at various temperatures. Anesthesiology 89:1032-1035.

Koch C, Massimini M, Boly M, Tononi G (2016) Neural correlates of consciousness: progress and problems. Nat Rev Neurosci 17:307-321.

Ku SW, Lee U, Noh GJ, Jun IG, Mashour GA (2011) Preferential inhibition of frontal-to-parietal feedback connectivity is a neurophysiologic correlate of general anesthesia in surgical patients. PLoSOne 6:e25155.

Lee M, Sanders RD, Yeom S-K, Won D-O, Seo K-S, Kim HJ, Tononi G, Lee S-W (2017) Network Properties in Transitions of Consciousness during Propofol-induced

Sedation. Scientific Reports 7:16791.

Lee U, Ku S, Noh G, Baek S, Choi B, Mashour GA (2013) Disruption of frontal-parietal communication by ketamine, propofol, and sevoflurane. Anesthesiology 118:1264-1275.

Lin JY (2011) A user's guide to channelrhodopsin variants: features, limitations and future developments. Exp Physiol 96:19-25.

Lin JY, Lin MZ, Steinbach P, Tsien RY (2009) Characterization of engineered channelrhodopsin variants with improved properties and kinetics. Biophys J 96:1803-1814.

Liu X, Lauer KK, Ward BD, Rao SM, Li SJ, Hudetz AG (2012) Propofol disrupts functional interactions between sensory and high-order processing of auditory verbal memory. Hum Brain Mapp 33:2487-2498.

Mak-McCully RA, Rolland M, Sargsyan A, Gonzalez C, Magnin M, Chauvel P, Rey M, Bastuji H, Halgren E (2017) Coordination of cortical and thalamic activity during non-REM sleep in humans. Nature Communications 8:15499.

Mashour GA, Hudetz AG (2017) Bottom-Up and Top-Down Mechanisms of General Anesthetics Modulate Different Dimensions of Consciousness. Front Neural Circuits 11:44.

Murphy C, Krause B, Banks M (2019) Selective effects of isoflurane on cortico-cortical feedback afferent responses in murine non-primary neocortex. Br J Anaesth 123:488-496.

Murphy M, Bruno MA, Riedner BA, Boveroux P, Noirhomme Q, Landsness EC, Brichant JF, Phillips C, Massimini M, Laureys S, Tononi G, Boly M (2011) Propofol anesthesia and sleep: a high-density EEG study. Sleep 34:283-291A.

Nourski KV, Steinschneider M, Rhone AE, Kawasaki H, Howard MA, 3rd, Banks MI (2018) Auditory Predictive Coding across Awareness States under Anesthesia: An Intracranial Electrophysiology Study. J Neurosci 38:8441-8452.

Petreanu L, Mao T, Sternson SM, Svoboda K (2009) The subcellular organization of neocortical excitatory connections. Nature 457:1142-1145.

Raz A, Grady SM, Krause BM, Uhlrich DJ, Manning KA, Banks MI (2014) Preferential effect of isoflurane on top-down versus bottom-up pathways in sensory cortex. Front Syst Neurosci 8.

Redinbaugh MJ, Phillips JM, Kambi NA, Mohanta S, Andryk S, Dooley G, Afrasiabi M, Raz A, Saalmann Y (2020) Thalamus Modulates Consciousness Via Layer-

Specific Control of Cortex. Neuron 105.

Sanders RD, Maze M (2012) Noradrenergic trespass in anesthetic and sedative states. Anesthesiology 117:945-947.

Schrouff J, Perlbarg V, Boly M, Marrelec G, Boveroux P, Vanhaudenhuyse A, Bruno MA, Laureys S, Phillips C, Pelegrini-Issac M, Maquet P, Benali H (2011) Brain functional integration decreases during propofol-induced loss of consciousness. Neuroimage 57:198-205.

Voss LJ, Garcia PS, Hentschke H, Banks MI (2019) Understanding the Effects of General Anesthetics on Cortical Network Activity Using Ex Vivo Preparations. Anesthesiology 130:1049-1063.

Xie Z, McMillan K, Pike CM, Cahill AL, Herring BE, Wang Q, Fox AP (2013) Interaction of anesthetics with neurotransmitter release machinery proteins. Journal of neurophysiology 109:758-767.

Figure 1

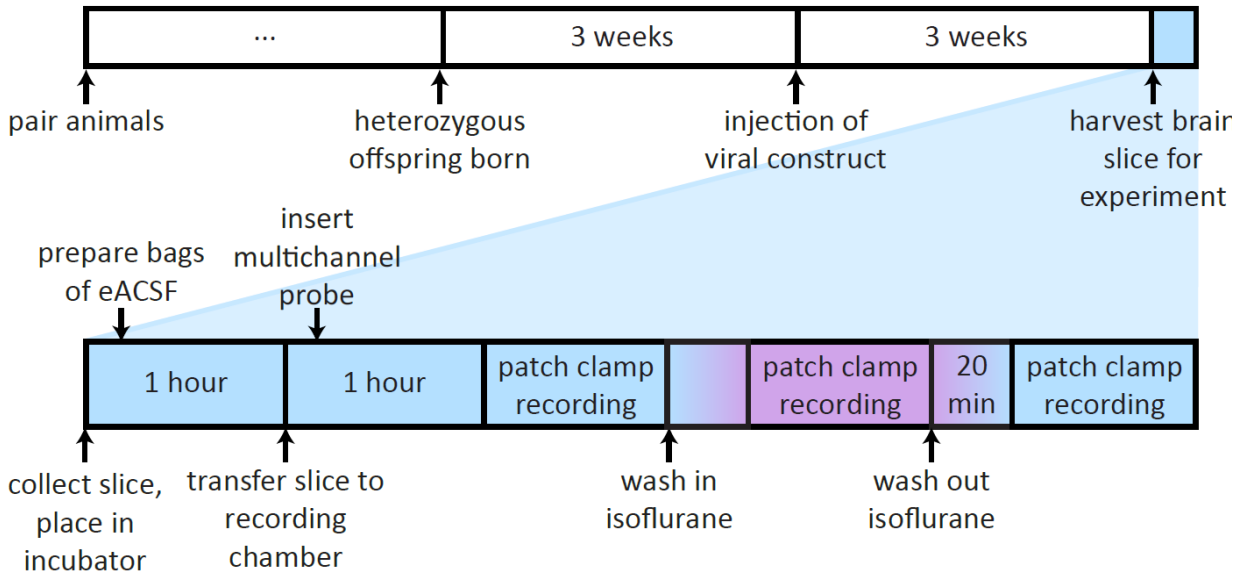

Figure 1: A schematic outlining timeline of important steps in protocol. Top: Describes timeline of steps necessary for breeding of transgenic animals and expression of viral vector. **Bottom:** Depicts steps and timeline for preparing materials and conducting experiment on the day of slice preparation.

Figure 2

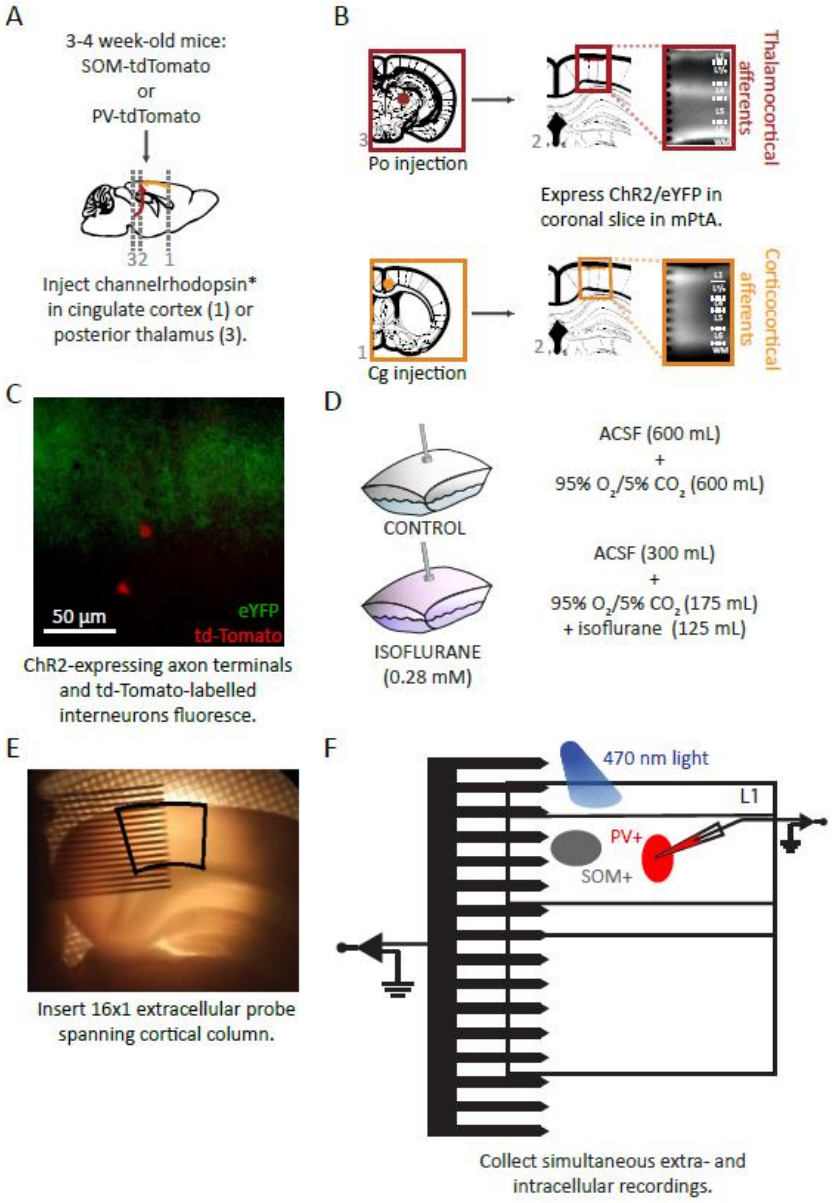

Figure 2: Injection of viral vector and preparation ex vivo coronal brain slices. (**A**) Schematic representation of injection of viral vector into SOM-tdTomato or PV-tdTomato hybrid mice. (**B**) Coronal slices of the medial parietal association area (mPtA) were harvested, and thalamocortical (top) or corticocortical (bottom) afferent fibers were identified by their eYFP reporter in layer 1. This figure is modified with permission from (Murphy et al., 2019). (**C**) Overlay of eYFP-labeled axon terminals in layer 1 (green) and tdTomato-labelled SOM+ interneurons (red) in superficial layer 2/3. (**D**)

Sealed bags were prepared with a 50:50 solution-to-gas mixture. (**E**) Placement of a 16 x 1 probe into mPtA (black outline). (**F**) Schematic of the recording set-up in the cortical slice.

Figure 3

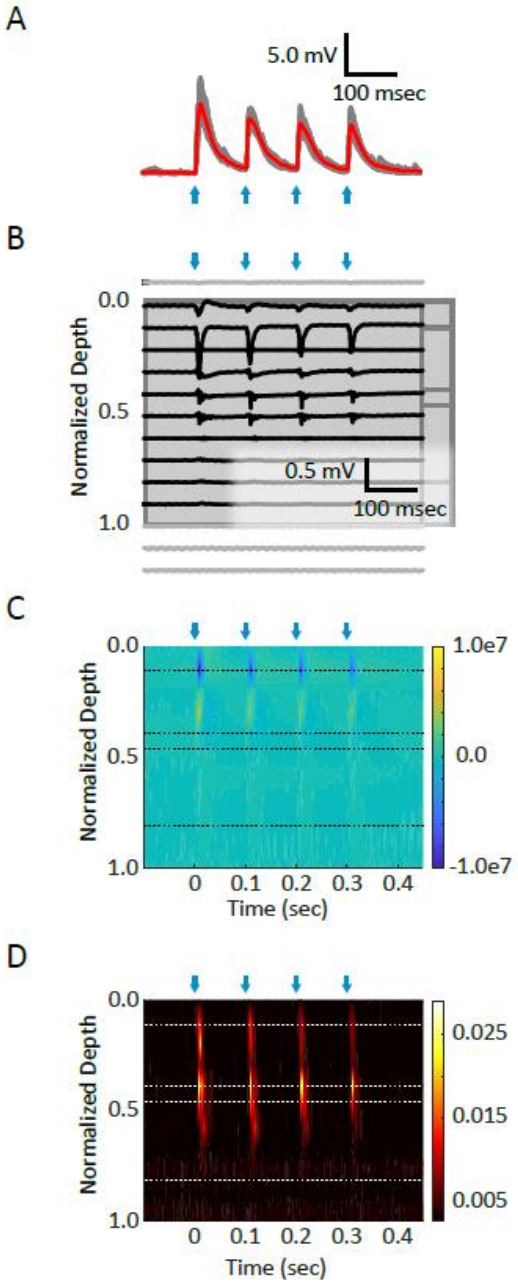

Figure 3: Simultaneous intracellular and multi-channel extracellular recordings in cortical slice. (**A**) Whole-cell current clamp patch recording from the soma of a layer 2/3 PV+ interneuron. Four pulses (2 ms each, blue arrows) of blue light (2.2 mW) at 10 Hz were delivered to corticocortical axon terminals in L1. Average (red trace) of ten trials (grey traces) are shown. (**B**) Raw data from 16 channels of extracellular 16 x 1 probe. Channels placed in cortical tissue are shown in black, and those lying outside of

cortex in grey. (**C**) A current source density diagram, extracted from the local field potential signal, shows synaptic current sinks (blue) in layer 1. (**D**) Multi-unit activity, generated by applying a high-pass filter to the local field potential signal, isolates spiking activity evoked in lower layers.

Figure 4

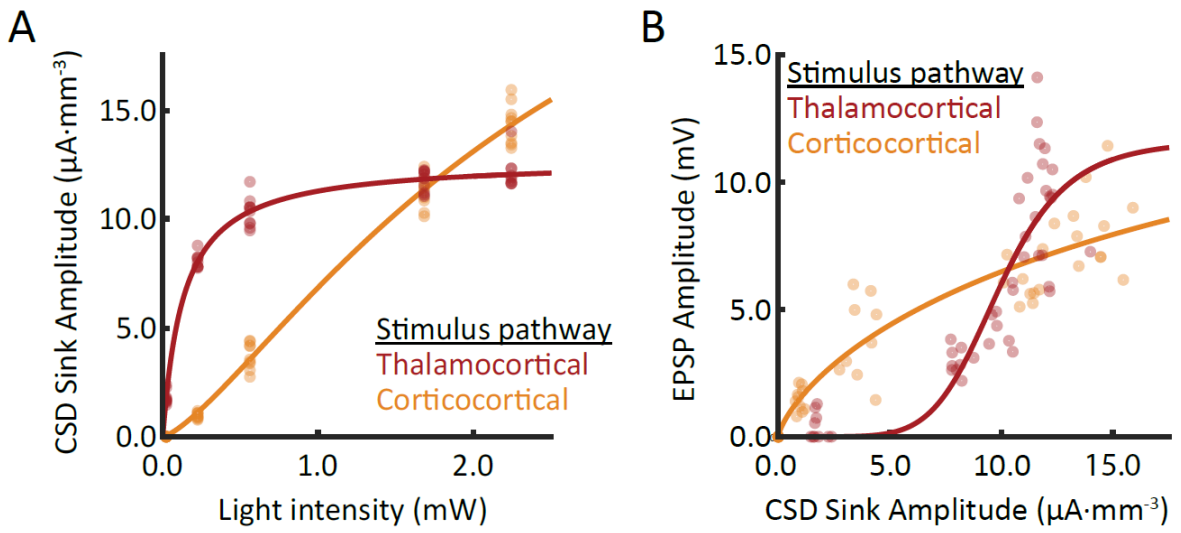

Figure 4: Comparison of responses from recordings in two different slices. Multiple light intensities were used to evoke synaptic responses in cortical layer 1. For each trial, the peak amplitude of the evoked response was extracted from the layer 1 extracellular current sink and EPSPs in layer 2/3 PV+ interneurons. (**A**) Extracellular response profiles of thalamocortical and corticocortical afferents are compared as a function of light intensity. (**B**) The relationship between current sink amplitude and EPSP amplitude is pathway dependent. Within each stimulus pathway, data from (A) and (B) were collected simultaneously.

Figure 5

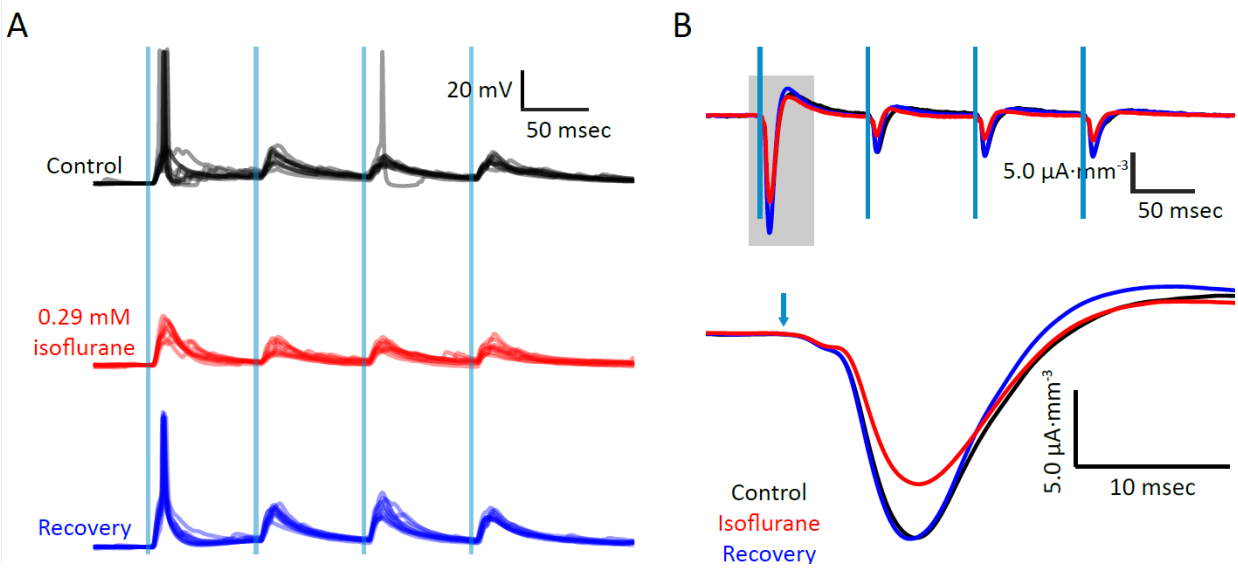

Figure 5: Bath application of isoflurane dissolved in eACSF during simultaneous recordings. (**A**) Intracellular whole-cell current clamp recording from layer 2/3 SOM+ interneuron upon activation of corticocortical afferents during control, isoflurane, and wash conditions. Vertical blue lines indicate light stimuli (2 ms; 1.65 mW). (**B**) Current source density trace extracted from electrode in layer 1. Data were collected simultaneously with those collected in (A). Recovery of responses upon wash demonstrates depression of synaptic responses by isoflurane.

Table 1

Micropipette for virus injection				
Glass	ID: 0.05 mm, OD: 0.11 mm			
Loops	1			
Heat	**Pull**	**Vel**	**Time**	**Pressure**
Ramp + 10	20	40	200	300
Micropipette for whole-cell patch clamp recordings				
Glass	ID: 1.1 mm, OD: 1.7 mm			
Loops	4			
Heat	**Pull**	**Vel**	**Time**	**Pressure**
Ramp	0	25	250	500

Table 1: Recommended glass and parameters for pulling micropipettes for viral injections and whole-cell patch clamp recordings. Glass used for viral injections and whole-cell patch clamp recordings is described, as well as the parameters for pulling micropipettes using the micropipette puller. Consult instruction manuals for micropipette puller for further recommendations or fine-tuning of settings.

Table 2

	Slicing ACSF, sACSF (in mM)	Experiment ACSF, eACSF (in mM)
NaCl	111	111
$NaHCO_3$	35	35
HEPES	20	20
KCl	1.8	1.8
$CaCl_2$	1.05	2.1
$MgSO_4$	2.8	1.4
KH_2PO_4	1.2	1.2
glucose	10	10
	Internal Solution	
K-gluconate	140	
NaCl	10	
HEPES	10	
EGTA	0.1	
MgATP	4	
NaGTP	0.3	
	pH = 7.2	

Table 2: Composition of artificial cerebral spinal fluid and intracellular solution. Reagents and concentrations for sACSF, eACSF, and intracellular pipette solution for patch clamp recordings are listed.

Supplementary Figure 1

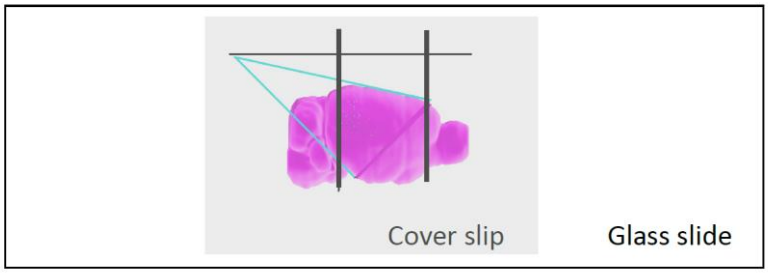

Supplementary Figure 1: Template for preparing block of tissue to collect brain slices. The template is adjusted to the appropriate size, printed, and glued to a microscope slide. A cover slip is glued over the template to prolong its use. The tissue block is placed on a piece of filter paper with the sagittal plane down, aligned to the pink background, and a vertical cut is made in the coronal plane along the black line.

Supplementary Figure 2

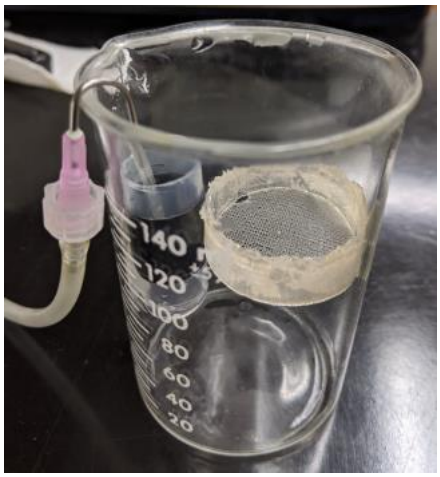

Supplementary Figure 2: Incubation chamber for harvested brain slices. The chamber is filled with sACSF and bubbled with 95% O_2/5% CO_2 gas mixture via a bent needle attached to tubing. Incubation platform is made of nylon stretched over a plastic circular fitting.

Supplementary Figure 3

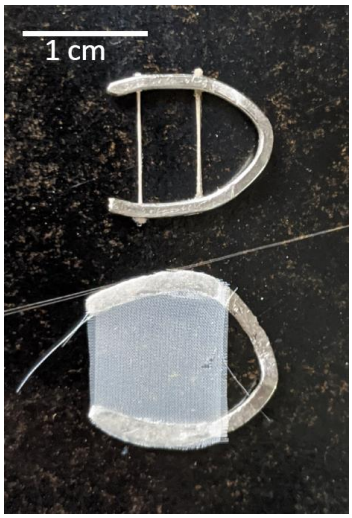

Supplementary Figure 3: Platinum structures for slice in recording chamber. Brain slice is transferred to recording chamber via pipette and placed on top of nylon mesh, which is stretched over a horseshoe-shaped piece of flattened platinum wire and super glued in place. Platinum harp is placed over brain slice to anchor it in place during recording.

Supplementary Table 1

	λ	α
Halothane	1.45	1.34
Sevoflurane	0.45	0.42
Desflurane	0.32	0.30

Supplementary Table 1: Ostwald (λ) and Bunsen (α) coefficients for other volatile anesthetics. Adapt this protocol for study of other volatile gas anesthetics, such as halothane, sevoflurane, or desflurane. Substitute the equations described in the protocol with the appropriate coefficients as listed in this table.

Chapter 3

Characterization of synaptic and network responses to distinct thalamocortical and corticocortical inputs to cortical layer 1.

This chapter will be submitted for publication as:

Murphy CA, Banks MI (2020). Characterization of synaptic and network responses to distinct thalamocortical and corticocortical inputs to cortical layer 1.

Abstract

Afferent projections to cortical layer 1 are traditionally considered to be modulatory. However, most descriptions of the thalamic and cortical areas from which they originate have not investigated layer 1 inputs isolation from those to other layers, nor have thalamocortical and corticocortical afferents been directly compared. In these experiments, we optogenetically activate two distinct thalamocortical (TC) and corticocortical (CC) afferent pathways to layer 1 of higher order cortex. We record extracellular synaptic and network responses to activation of these inputs, and we conduct intracellular recordings from distinct populations of pyramidal cells as well as somatostatin-positive (SOM+) and parvalbumin-positive (PV+) interneurons. We show that inputs originating in the posterior medial nucleus of the thalamus (POm) or cingulate cortex (Cg) elicit synaptic responses with varying characteristics depending on the identity of the post-synaptic target. In addition, we demonstrate that the relationship

between inputs to layer 1 and spike output of the cortical column is pathway- and layer-dependent. Our results suggest that afferent inputs to layer 1 may play different functional roles in integration and propagation of information, subserved by unique underlying circuit dynamics.

Introduction

Excitatory afferents to layer 1 of neocortex most often originate in higher order thalamic nuclei and higher order cortical areas, and play an important role in sensory processing (Gilbert and Li, 2013; Manita et al., 2015; Mease et al., 2016; D'Souza and Burkhalter, 2017; Zhang and Bruno, 2019) and in conscious experiences (Mashour and Hudetz, 2017; Redinbaugh et al., 2020). In classical descriptions of the cortical microcircuit, these afferents are postulated to play a modulatory role. Cortical layer 1 contains only a small population of GABAergic interneurons and the distal dendrites of cells in lower layers (Binzegger et al., 2004; Muralidhar et al., 2014), ostensibly limiting the influence of layer 1 afferents over excitatory output of the cortical column. Projections to cortical layer 1 are anatomically diffuse (Rockland and Virga, 1989; Rubio-Garrido et al., 2009), connecting multiple cortical columns, and in some cases, multiple levels of the cortical hierarchy, which positions them well to synchronize activity in multiple cortical areas (Saalmann et al., 2012; Redinbaugh et al., 2020). Many higher order thalamocortical and feedback corticocortical synapses exhibit characteristics often associated with modulatory roles, such as low amplitude post-synaptic potentials (PSPs), paired pulse facilitation, and graded responses with respect to changes in stimulus intensity (Covic

and Sherman, 2011; De Pasquale and Sherman, 2011; Viaene et al., 2011c). Functionally, several investigations *in vivo* have implicated higher order thalamic and cortical areas in modulating or enhancing responses to sensory stimuli (Manita et al., 2015; Mease et al., 2016; Roth et al., 2016; Takahashi et al., 2016; Zhang and Bruno, 2019), despite receiving very little direct sensory input themselves.

Most descriptions of the functional roles of higher order thalamic and cortical areas have not discriminated between influences of inputs to layer 1 and those to other layers. Even so, some findings challenge the notion that layer 1 afferents are exclusively modulatory. Electrical activation of intracortical feedback projections *in vivo* drives robust spiking in primary sensory cortex, which is abolished by blocking inputs to layer 1 specifically (Manita et al., 2015). TC and CC inputs to layer 1 of prefrontal cortex drive spiking in some post-synaptic cells *in vitro* (Cruikshank et al., 2012). For example, activation of higher order thalamus, from which a large number of layer 1 inputs originate, synchronizes cortical areas and restores consciousness in anesthetized animals (Redinbaugh et al., 2020), suggesting more than simply a modulatory role. Some intracortical and higher order thalamocortical synapses are modulatory, while others exhibit robust responses with high temporal precision, similar to information-bearing projections in lower areas (Covic and Sherman, 2011; De Pasquale and Sherman, 2011; Cruikshank et al., 2012; Delevich et al., 2015; Mo and Sherman, 2019). Indeed, physiological properties of higher order thalamocortical and feedback corticocortical signals may depend on layer-specific termination patterns of afferents (Lee and Sherman, 2008), the hierarchical relationship between the connected areas

(Viaene et al., 2011c; D'Souza et al., 2016), or the identities of post-synaptic cells (Cruikshank et al., 2012; Audette et al., 2018).

Dedicated investigations of afferent inputs to layer 1 are limited. Studies characterizing the physiological and functional properties of these afferents have primarily been conducted in primary cortex (though, see D'Souza et al., 2016) and only rarely isolate and compare distinct layer 1 inputs (e.g. (Cruikshank et al., 2012)). Moreover, the relationship between layer 1 input and resulting output of the cortical column has not been explicitly described. Input and output of the cortical column rely heavily on the involvement of specialized interneuron populations. For example, SOM+ interneurons target the distal dendrites of pyramidal cells and control inputs, while PV+ interneurons target axosomatic regions of pyramidal cells and regulate their outputs. But, to what extent TC and CC inputs to layer 1 recruit subpopulations of interneurons to integrate signals and generate output is not clear, leaving open the question of whether the roles of overlapping afferents are functionally distinct.

By expressing channelrhodopsin in afferents from posterior medial thalamus and from cingulate cortex, we independently activate two distinct inputs to cortical layer 1 and assay evoked cellular and network responses. We demonstrate that thalamocortical and corticocortical inputs differentially engage post-synaptic pyramidal cell and interneuron targets and evoke distinct, layer-dependent spiking activity.

Methods

Expression of channelrhodopsin in distinct POm and Cg afferents

To independently activate higher order thalamocortical or corticocortical feedback afferents, viral constructs containing channelrhodopsin-2 (ChR2) and fluorescent reporter YFP (AAV2-hSyn-hChR2(H134R)-eYFP; generously provided by K. Deisseroth, Stanford University via University of North Carolina Vector Core) were injected into either posterior medial thalamus (AP: -2.25 mm, ML: 1.25 mm, DV: -3.35 mm; volume: 1 µL) or cingulate cortex (AP: 0.2 mm, ML: 0.3 mm, DV: 0.9 mm; volume: 1 µL), respectively. Coronal brain slices (500 µm thick) were prepared from anteromedial visual cortex (AM), a secondary visual area.

Electrophysiological recordings and activation of afferents

Multichannel extracellular recordings were collected in AM using a 16x1 multichannel silicon probe with evenly spaced contacts (100 µm) spanning the cortical laminae. Whole-cell patch clamp recordings were conducted in current clamp mode from four different populations of cells. Layer 2/3 (L2/3) or L5 (L5) pyramidal cells were targeted based on morphology under DIC microscopy (Olympus BX51); td-Tomato-labelled somatostatin-positive (SOM+) or parvalbumin-positive (PV+) interneurons were visualized using combined DIC and fluorescence (filter cube 49008; Chroma, Bellows Falls, VT). After whole-cell configuration was achieved and a series of 600 msec-long current steps were delivered to further characterize cell identity.

POm or Cg afferents were activated with four brief pulses of 470 nm light at 10 Hz (2 msec pulses, diameter: 150 µm) at a range of intensities (0.022-2.2 mW). At least 5 different stimulus intensities were used for each cell, and 8-10 trials of each intensity were randomly interleaved and delivered every 10 seconds. In a subset of experiments,

APV (20 μM) and APV + CNQX (20 μM + 50 μM, respectively) were bath applied and evoked responses compared to baseline recordings.

Isolation and analysis of extracellular synaptic and network responses

To control for the possibility that observed physiological differences between pathways were not due to levels of viral expression, eYFP fluorescence was compared between Po- and Cg-injected animals. Using a standardized light intensity, the maximum value of fluorescence adjacent to the recording probe in layer 1 (less the background fluorescence) was measured for each slice and normalized to the maximum value across all slices. Mean fluorescence values between POm- and Cg-injected slices were compared using an independent t-test.

Signals from each channel were averaged across trials of the same light intensity. Current source density (Mitzdorf, 1985) (CSD) was calculated from local field potential signals using the spline inverse CSD method (Pettersen et al., 2006), where negative-going currents indicate current sinks, or inward transmembrane currents. Further analysis of the CSD was conducted on the earliest onset current sink, which was in layer 1 in all cases. Peak amplitudes were multiplied by -1 for ease of interpretation and statistical analysis. Multiunit activity (MUA) was isolated by high pass filtering (1-3kHz), rectifying, and smoothing (low-pass filter, 600Hz) extracellular signals. Further analysis of MUA signals was conducted on the largest amplitude peak for both the superficial and deep layers. Integral of the MUA was calculated from the area under the curve from the first threshold crossing (2.5 times the geometric mean) to the point at which the signal returned to and remained below threshold for at least 5 msec.

Analysis of evoked responses in pyramidal cells and interneurons

Intracellular recordings were bandpass filtered at 0.1-2000Hz. Paired-pulse ratio was calculated using responses from the lowest stimulus intensity that evoked non-zero amplitudes on at least 50% of trials and had a latency jitter of <1 msec. Cells that did not exhibit responses within these criteria at any stimulus intensity or which exhibited latencies >10 msec were considered to be non-responders and were not used for further analysis (Table 1).

For each experiment, either layer 1 current sink or post-synaptic potential amplitudes, y, at each recorded stimulus intensity, x, were fit to a logistic equation

$$y(x) = (A_{max} \cdot x^h)/(ES_{50}^h + x^h)$$

where A_{max} is the asymptotic maximum amplitude, ES_{50} is the stimulus intensity at which the response amplitude is 50% of the maximum, and h represents the degree of cooperativity exhibited among individual units within the synaptic machinery with increases in stimulus intensity. Functionally, we interpret maximum amplitude (A_{max}) as the maximum possible response for a given experiment given unlimited illumination power, which we used to quantify and compare magnitude of current sinks and PSPs. We use ES_{50} as a proxy for gradedness of responses, where the more linear (graded) increases in amplitude are with increases in stimulus intensity, the higher the expected ES_{50}. Previous studies have suggested that graded response profiles represent activation of additional axons with increasing stimulus intensities, and therefore higher levels of convergence (see Sherman et al., 2013 for summary (Sherman and Guillery, 2013)). The *h* coefficient mathematically represents the analog of the unitless Hill

coefficient used to quantify biochemical properties of proteins. Hill coefficients greater than or less than 1 reflect deviations from hyperbolicity that might be expected if the components of the process being modeled are independent of each other. If some level of competition or cooperativity exists during the activation of afferent fibers or synaptic transmission, for example, we would expect the *h* coefficient to deviate from 1.

Cells for which the curve fit ultimately failed to converge were excluded from analysis (10 of 112 cells). By fitting each cell to this model, synaptic parameters could be compared independently of one another, and in a manner that is putatively more robust than direct comparison of amplitudes to subtle variations between slices that might interact with pathway effects (e.g., viral expression).

It should be noted that analysis of post-synaptic potentials did not include trials on which action potentials were evoked, which may ostensibly lead to erroneous estimations of fit parameters (e.g., underestimation of A_{max}). To evaluate whether exclusion of spike data significantly altered pathway or cell type effects, the analysis described above was re-run with spike trials included, where the difference between baseline membrane potentials and spike threshold was used for PSP amplitudes on spike trials. Conclusions based on estimates of pathway and cell type effects were not significantly different when spike trials were included (data not shown).

Statistical Models

Responses variables from intracellular recordings were analyzed using a linear mixed effects model. All models included a dependent response variable from the whole cell current clamp recording (e.g., A_{max}), fixed effects of afferent pathway (POm or Cg)

and cell type (L2/3 PYR, L5 PYR, SOM+, PV+), and an interaction between afferent pathway and cell type. Random effect was slice experiment, with random slopes by cell type.

$$Response_{cpe} \sim \beta_0 + \beta_{1c} + \beta_{2p} + \beta_{3cp} + b_{0e} + b_{1ce} + \varepsilon_{cpe}$$

For each response measure, a likelihood ratio test was used to determine whether the interaction of fixed effects was significant. The full model was compared to a restricted model from which the fixed effect was omitted, and results of log likelihood ratios are reported using chi-squared values. For each pathway-cell type combination, estimated values of each response measure are reported as a sum of individual fixed effects coefficients. For select comparisons of interest across pathways or cell types, the significance of individual coefficients was tested, and differences are reported. Residuals were visually inspected for homoscedasticity. Heteroscedasticity was corrected by log transforming the response variables and coefficients reported in their exponentiated form for ES_{50}.

Response variables from POm- and Cg-evoked CSD signals in layer 1 were compared using an independent t-test unless normality was rejected by visual inspection, in which case a Mann Whitney U test was used. For analysis of APV and CNQX results, a linear mixed effects model was used to compare effects on layer 1 current sink amplitude of fixed effects drug and afferent pathway, using slice experiment as a random effect with random slopes by drug. Significance of the interaction term was evaluated using a likelihood ratio test as described above. The significance of individual coefficients was tested and estimates of the individual coefficients (i.e., drug effects for each pathway) are reported with 95% confidence intervals.

To investigate the relationship between input and output of the cortical column, MUA integral in either superficial or deep layers was modeled as a function of layer 1 current sink amplitude, and slopes were compared by pathway and layer. The full model of the response variable MUA integral included individual fixed effects of layer 1 sink amplitude, pathway, and layer as well as interaction terms between and among fixed effects and random effect of slice experiment. This model was significantly improved compared to a restricted model from which the three-way interaction term was omitted (χ^2 (1)= 6.29, P = 0.012).

Results

Optogenetic activation of POm and Cg inputs to AM elicits distinct responses in layer 1

Injection of viral vector in POm (Figure 1A) or Cg (Figure 1B) resulted in expression of eYFP reporter in axon terminals in layer 1 of AM. Mean eYFP fluorescence ($Fluor_{YFP}$) was not significantly different for POm (n_{TC} = 17, $Fluor_{YFP,TC}$ = 0.41) compared to Cg (n_{CC} = 20, $Fluor_{YFP,CC}$ = 0.38) inputs to layer 1 (t(35) = 0.4193, P = 0.68; Figure 1G). Expression of the eYFP reporter was also observed in L4 of Po-injected slices and in the infragranular layers of Cg-injected slices, but light delivery for the experiments described here was restricted to layer 1.

Activation of POm and Cg inputs to AM elicited short-latency synaptic current sinks in layer 1 (Figure 1C and 1D, respectively). To elucidate the nature of these responses, APV (20 μM, n = 15) and APV + CNQX (50 μM, n = 5) were applied to a subset of slices. Application of APV alone had no effect on sink amplitude for either pathway (POm = -5.1%, 95% CI [-21.6 15.0], P = 0.58; Cg = -9.4% [-22.6 5.9], P =

0.21), while POm- and Cg-evoked responses were abolished by APV + CNQX compared to control (POm = -80.3% [-90.0 -61.0], P < 0.0001; Cg = -90.3% [-94.1 -84.0], P < 0.0001; Figure 1H). The interaction term between fixed effects of drug and pathway was not significant (χ^2 (2) = 2.7971, P = 0.24696), indicating that effects of APV and CNQX were not different between pathways.

To quantify the relationship between stimulus intensity and response magnitude in layer 1, current sink amplitudes were fit to a three-parameter nonlinear logistic equation as a function of stimulus intensity (Figure 2), with parameters describing maximum predicted amplitude (A_{max}), effective stimulus intensity to evoke 50% of the maximum amplitude (ES_{50}), and cooperativity coefficient *h* (see Methods). A_{max} was not significantly different for POm (mean $A_{max,POm}$ ± SEM = 12.4 ± 2.0 $\mu A \cdot mm^{-3}$) versus Cg (mean $A_{max,Cg}$ ± SEM, = 14.2 ± 2.0 $\mu A \cdot mm^{-3}$) inputs (t(35) = 0.64, P = 0.53; Figure 2E), nor was the h value (mean h_{POm} ± SEM = 1.28 ± 0.11, mean h_{Cg} ± SEM = 1.19 ± 0.04, t(35) = 0.84, P = 0.41; Figure 2G). However, the stimulus intensity required to evoke a current sink with an amplitude 50% of the maximum (ES_{50}) was significantly greater for Cg inputs compared to POm inputs (Cg vs. POm medians 1.02 vs. 0.14 mW, Mann Whitney U test, z = 4.7695, P <0.0001; Figure 2F). Thus, further increasing the stimulus intensity beyond the threshold for minimal response resulted in a much larger increase in the amplitude of the response for Cg inputs compared to POm inputs.

Short-term synaptic plasticity describes temporary changes in synaptic strength during sustained activity. For example, synapses with high release probabilities exhibit paired pulse depression, transmitting signals with high fidelity, but only transiently. Both

Pom and Cg inputs exhibited short-term paired pulse depression (PPR_{POm} ± SEM = 0.80 ± 0.03; PPR_{Cg} ± SEM = 0.70 ± 0.04; Figure 2H).

Properties of post-synaptic responses are pathway- and cell type-dependent

CSD assume a uniform, vertical dendritic compartment and reflect sums of all currents across synapses and cell types. The properties of synapses and synaptic currents flowing into specific cell types may diverge significantly from this average depending on their relative density and their exact location relative to the recording electrode array. In addition, inward membrane currents that arise in compartments not oriented orthogonally to the pia – for example, horizontally-oriented dendritic arbors of pyramidal cells or interneurons – may contribute less to the CSD signal. Thus, to further characterize thalamocortical and corticocortical inputs to layer 1, we conducted intracellular recordings in distinct subpopulations of pyramidal cells and interneurons and compared responses across cell types and between pathways.

Post-synaptic responses to activation of layer 1 afferents were recorded in L2/3 and L5 pyramidal cells and in PV+ and SOM+ interneurons using whole-cell patch clamp recordings. POm and Cg inputs to layer 1 evoked short latency post-synaptic potentials in all cell types, though with varying efficacy. In some cells, these EPSPs drove action potentials as well (Table 1). For example, POm inputs evoked early responses in every L2/3 and almost every L5 pyramidal cell recorded, and in every PV+ cell, but only 5 of 12 SOM+ cells. This is consistent with previous reports that suggest that both primary and higher order thalamocortical activation of SOM+ cells is either weak or non-existent (Beierlein et al., 2003; Cruikshank et al., 2010; Audette et al.,

2018); yet, that the SOM+ cells that were activated by POm inputs tended to spike diverges from expectations.

Spike probability was both pathway- and cell type-dependent (Table 1, Supplementary Figure 1), though no significant interaction between pathway and cell type was observed ($\beta_{3;}$ $\chi(3) = 2.482$, $P = 0.48$). Spikes were rarely evoked in L2/3 pyramidal cells by either afferent pathway. Spikes were similarly rare for Cg inputs to L5 pyramidal cells, though slightly more common for POm inputs. Conversely, both afferent inputs elicited spikes in SOM+ cells, with approximately 50% spike probability at the highest stimulus intensity. POm inputs were significantly more likely than Cg inputs to evoke spikes in PV+_interneurons; at the highest stimulus intensity, half of all PV+ cells recorded in POm-injected slices spiked on every trial, while only 2 of 15 PV+ cells spiked at all in response to Cg input.

Amplitudes of PSPs were fit to a logistic equation as a function of stimulus intensity, as described for extracellular responses in the previous section. A significant effect of pathway was observed for A_{max} values ($\chi(1) = 10.6$, $P = 0.0011$), but no pathway effect was observed for ES_{50} ($\chi(1) = 0.70$, $P = 0.40$) nor for *h* coefficient ($\chi(1) = 2.42$, $P = 0.12$). That pathway effects vary between intracellular versus extracellular recordings suggests that CSD results do not necessarily represent the behavior of individual cells. Indeed, we observed a significant effect of the interaction between pathway and cell type on both A_{max} ($\chi(3) = 8.26$, $P = 0.041$) and ES_{50} ($\chi(3) = 11.6$, $P = 0.0087$), demonstrating that pathway-dependent differences in responses manifest at the level of cell type.

POm inputs to L5 pyramidal cells elicited large post-synaptic potentials at high stimulus intensities, reflected in high A_{max} values (>10 mV) for nearly all L5 pyramidal cells sampled in POm-injected slices (Figure 3I). A_{max} values for inputs to L5 pyramidal cells were significantly greater for POm inputs compared to Cg inputs (Table 2). A_{max} values for inputs to L2/3 pyramidal cells were highly variable, ranging from less than 2 mV to more than 45 mV. Cg inputs elicited comparatively low amplitude post-synaptic potentials in pyramidal cells in both L2/3 and L5 (Figure 3I, Table).

POm inputs to L2/3 pyramidal cells tended to elicit all-or-none responses, where the amplitudes of synaptic potentials changed very little with increases in stimulus intensity beyond ~0.2 mW (Figure 3I; Supplementary Table 3). In contrast, compared to POm inputs, the ES_{50} for Cg inputs to L2/3 cells was significantly higher, suggesting a more graded response profile for cortical afferents compared to thalamocortical afferents (Figure 3I; Table 3). Indeed, of the nine L2/3 pyramidal cells fit from POm-injected slices, only one had an ES_{50} higher than 0.2 mW, while only 4 of the remaining 49 cells from any other pathway-cell type combination had an ES_{50} *lower* than 0.2 mW. This suggests that POm activation of L2/3 pyramidal cells is relatively independent of stimulus intensity, and that even at low intensities thalamocortical inputs to the superficial layers can be recruited. No effects of pathway or cell type were observed for *h* coefficients (Supplementary Table 4).

Synaptic plasticity was also analyzed for each afferent input to each cell type (Figure 3G-H, Figure 4E-H, Supplementary Table 5). Cg inputs to SOM+ interneurons exhibited robust paired pulse facilitation (Figure 4E). Notably, Cg inputs to SOM+ cells exhibited significantly higher paired pulse ratios than PV+ cells (Figure 4E,F;

Supplementary Table 5), suggesting distinct functional roles for afferent inputs to the two populations of interneurons. Interestingly, this difference in synaptic plasticity between inhibitory cell types was not observed for POm inputs (Table 5; Figure 4G,H). POm inputs to L5 pyramidal cells and Cg inputs to L2/3 pyramidal cells exhibited paired pulse depression, while POm inputs to L2/3 pyramidal cells and Cg inputs to L5 pyramidal cells exhibited a mixture of facilitation and depression (Supplementary Figure 2; Supplementary Table 5).

MUA response profiles demonstrate pathway- and layer-dependence of column output

We have demonstrated from intracellular recordings that thalamocortical and corticocortical inputs to layer 1 evoke distinct responses in post-synaptic cells. Cg inputs elicited responses with modulatory characteristics, activating low amplitude, graded responses in both superficial and deep layers and rarely evoking action potentials. POm inputs to the excitatory cells in the superficial layers also rarely elicited spikes, instead activating PSPs with variable amplitude and intensity-independent responses. POm inputs to L5 pyramidal cells exhibited responses with large amplitudes (and occasionally action potentials) at high stimulus intensities. The pathway-, cell type- and layer-specificty of these afferent responses are likely to have implications for spiking responses on the cortical column. Superficial and deep layers occupy distinct functional domains *in vivo*. Superficial layers participate in intracortical transmission, integrating modulatory intracortical and higher order thalamocortical inputs (Zhang and Bruno, 2019) with sensory-specific inputs to provide output to higher cortical areas (Shipp, 2007). Cells in the deep layers also receive input from multiple cortical and thalamic

areas but with pathway-dependent characteristics, and activity in deep layers likely represents local recurrent processing and interplay with subcortical targets (Maier et al., 2010; Buffalo et al., 2011). Consistent with this paradigm, we hypothesized that pathway- and layer-dependent differences we observed in inputs to the column would manifest as well in the output of the cortical column, i.e. that multiunit activity in L5 would exceed that of L2/3 for increasing POm but not Cg input.

To examine the relationship between inputs and outputs to the cortical column, we recorded multiunit activity across the cortical laminae and compared responses to POm and Cg inputs between superficial and deep layers. Activation of layer 1 afferents evoked polysynaptic spiking activity in superficial and deep layers (Figure 5). For POm inputs, layer 1 current sink amplitude was strongly correlated with MUA integral in L5, but this correlation was not significant for L2/3 (Figure 5G). The slope of this function was significantly different between layers, i.e. increasing input from POm had a greater effect on spiking in L5 than L2/3. By contrast, increasing input from Cg had the same effect on spiking in L2/3 and L5 (Figure 5H). In other words, as the magnitude of POm input to layer 1 increased, a bias favoring L5 MUA was observed, but for Cg inputs MUA integral was similar between layers. Thus, with increasing activation, higher order thalamus shifts the output of the cortical column to the deep layers, suggesting that with sufficient input from higher order thalamus, the cortical column ultimately returns to thalamus and lower order cortex a processed iteration of the original input.

Discussion

In this study, we characterized response properties of distinct thalamocortical and corticocortical inputs to layer 1 in non-primary sensory cortex. Within cortical layer 1, long-range projecting axons from higher cortical areas and from thalamus target a select few GABAergic cells residing in layer 1, as well as the distal dendrites of cells with somata in the layers below. Activity in these distal dendrites is particularly relevant for integration of sensory information against a background of internally-generated input (Gilbert and Sigman, 2007; Bastos et al., 2012; Muckli and Petro, 2013), and is highly correlated with sensory perception (Takahashi et al., 2016). Inputs to layer 1 have historically been characterized as modulatory due to their diffuse axonal arbors and the regulatory functional properties they impose upon their targets. This study is the first to investigate how layer 1 inputs differentially engage discrete cell populations in higher areas and to compare thalamocortical versus corticocortical inputs directly. We find that despite their overlapping terminal fields, activation of afferents originating in either posterior medial thalamus or cingulate cortex evoke pathway-dependent responses at both the cellular and population level. We show that layer 1 afferents can in some cases effect strong spiking responses with high efficacy, and we propose that distinct cell type- and layer-specific response characteristics underlie pathway-specific columnar output.

Role of feedback corticocortical inputs to layer 1

We show that Cg inputs to pyramidal cells elicit low amplitude PSPs, even at high stimulus intensities, and exhibit synaptic depression. However, Cg afferents elicit strong paired pulse facilitation and drive spikes in inhibitory SOM+ interneurons. This suggests that while intracortical feedback afferents to layer 1 may not strongly activate excitatory

populations, they drive a subpopulation of inhibitory cells without attenuation during persistent activation. That Cg inputs disproportionately activate SOM+ cells may provide insight into our finding that even with high amplitude currents sinks in layer 1, we observed only modest increases in spike output within the cortical column. Our findings provide evidence that intracortical feedback afferents to layer 1 may contribute to SOM+ cell-mediated modulatory control over local pyramidal cells, without strongly influencing excitatory cell populations themselves, consistent with experimental (Murayama et al., 2009; Manita et al., 2015; Takahashi et al., 2016) and theoretical (Rao and Ballard, 1999; Bastos et al., 2012) models of sensory processing. Layer 1 inputs increase the gain of the input/output relationship of cortical pyramidal cells and are highly correlated with sensory perception (Manita et al., 2015; Takahashi et al., 2016). This process is tightly regulated by powerful disynaptic inhibition from SOM+ interneurons (Murayama et al., 2009). The inhibitory influence of SOM+ cells is impressive. Most SOM+ cells in the superficial layers target the distal dendrites of pyramidal cells (Gentet et al., 2012; Kubota, 2014) with remarkable horizontal reach (Ma et al., 2006; Riedemann et al., 2018) and provide disynaptic inhibition to many pyramidal cells that persists during sustained activity (Silberberg and Markram, 2007). Activation of even a single L2/3 pyramidal cell can recruit widespread SOM+-mediated inhibition that strongly influences the sensitivity and range of the local circuit (Kapfer et al., 2007).

Intracortical feedback inputs provide contextual information to lower order areas based on internally-generated phenomena such as attention, prediction, or expectation (Gilbert and Sigman, 2007; Muckli and Petro, 2013). Our results are consistent with the notion that these signals are mediated by inhibitory connections (Bastos et al., 2012),

though in our experiments afferents were activated in isolation and without additional signals upon which to apply computations. In activating afferents that effect modulatory control over signals *in absentia*, we expect that we did not maximize the regulatory potential of feedback connections.

Characterization of layer 1 inputs under previously described classes of cortical synapses

Properties of synapses and laminar organization of inputs subserve the integration and propagation of information throughout thalamocortical networks. Previous studies have described the synaptic dynamics of different thalamocortical (Lee and Sherman, 2008; Viaene et al., 2011b, a; Viaene et al., 2011c), corticocortical (Covic and Sherman, 2011; De Pasquale and Sherman, 2011), and corticothalamic (Petrof et al., 2011; Mo and Sherman, 2019) projections, and suggest that synaptic influences may confer unique functional properties to individual pathways. Primary sensory thalamic nuclei convey feature-specific sensory information to primary sensory cortices with high fidelity, and their Class 1 (‘driver’) synaptic properties have been well-described across sensory modalities (Lee and Sherman, 2008; Viaene et al., 2011a, b). For example, Class 1 synapses exhibit paired pulse depression and large EPSPs; Class 2 (’modulator’) synapses exhibit paired pulse facilitation, graded responses to increasing stimulus intensities, and small EPSPs (Sherman and Guillery, 2013).

Class 1A and 1B synapses, subclasses of the ‘driver’ class, differ only in the gradedness of their responses to stimulus intensity, where Class 1A responses exhibit all-or-none profiles compared to graded profiles for Class 1B synapses (Viaene et al.,

2011b). POm inputs to L5 pyramidal cells tended to elicit graded responses with large amplitudes (Figure 3B,F,I) and paired pulse depression (Figure 3H), consistent with driving Class 1B responses. Previous investigations ascribed Class 1A characteristics to POm inputs to layer 4 of secondary somatosensory cortex (Viaene et al., 2011c), suggesting that in non-primary cortical areas, layer 1 and 4 thalamocortical inputs to L5 cells differ only in the level of convergence onto their post-synaptic targets. POm inputs to L2/3 pyramidal cells, on the other hand, activated all-or-none responses with relatively low amplitudes (Figure 3B,E,I) and a mixture of facilitation and depression (Figure 3G). These properties suggest a more modulatory role for thalamocortical inputs to L2/3 pyramidal cells compared to L5 pyramidal cells, mediated by a limited number of afferents. Similar reports of mixed responses have been observed for thalamocortical inputs to the superficial layers (Viaene et al., 2011a). Viaene et al. (2011a) show that at least in primary areas, modulatory thalamocortical synapses were three times more common in L2/3 than were driver-type synapses. The layer dependence we find in our data and by others indicates potentially diverging roles for higher order thalamocortical inputs to superficial versus deep layers, subserved by the synaptic dynamics of layer 1 afferents.

Contrary to our findings for POm inputs, we did not observe notable differences between layers for Cg inputs to pyramidal cells. In both superficial and deep layers, nearly all pyramidal cells exhibited small EPSPs, synaptic depression, and graded activation profiles (Figure 3G,I). These properties share qualities of both driving and modulating synapses, but are not consistent with any previously classified response profiles. Previous investigations of corticocortical feedback connections to primary

cortex have shown an even distribution of driving and modulatory synapses (Covic and Sherman, 2011; De Pasquale and Sherman, 2011), a conclusion that was contradictory to expectations that feedback projections would be mostly modulatory.

Comparison of extracellular and intracellular responses

We show that extracellularly recorded current sinks in layer 1 are similar for POm versus Cg inputs, except for the gradedness with which response amplitudes change as a function of stimulus intensity (Figure 2). Both POm and Cg inputs elicit paired pulse depression (Figure 2H) and approximately the same amplitude synaptic responses. POm-evoked current sinks demonstrated very low ES_{50} values, with only marginal changes in amplitude with further increases in intensity beyond 0.2 mW. This “all-or-none” type of response is in stark contrast to the graded nature of current sink amplitudes exhibited by Cg inputs.

Properties of evoked responses recorded extracellularly diverge greatly from those recorded from some populations of cells. For example, Cg inputs elicited spikes in many SOM+ cells, which might suggest their signals would be manifest in the extracellular signal; yet, the strong paired pulse facilitation we find in SOM+ cells is not observed in the CSD signal. Instead, the extracellular response profile of layer 1 inputs most closely resembles that of inputs to L2/3 pyramidal cells, which suggests that these cells may dominate the CSD signal. Whether this phenomenon has biological or experimental underpinnings is not clear. For example, it may be the case that evoked currents are truly dominated by synapses with L2/3 cells and relatively small for other cell types. Then, differences between extracellular and intracellular recordings would

putatively arise due to cell type-specific variability of intrinsic dynamics of post-synaptic targets. Conversely, dendrites of L2/3 pyramidal cells are oriented orthogonally to the pia and branch less in the horizontal direction than do inhibitory cells or tufted L5 pyramidal cells (Radnikow and Feldmeyer, 2018) and may therefore contribute more to the CSD signal.

Recruitment of a greater number of afferent axons with increasing stimulus intensity manifests as a graded activation profile, represented in our experiments by a higher ES_{50}. Graded response profiles are thought to reflect high levels of convergence characteristic of modulatory cortical synaptic inputs (Covic and Sherman, 2011; De Pasquale and Sherman, 2011). This principle assumes, of course, that the contribution of any single axon to the synaptic response is independent of stimulus intensity. Responses evoked optogenetically may be sensitive to artificially high release probability (Jackman et al., 2014; Anastasiades et al., 2018), which could result in a leftward shift of fitted curves in our experiments. However, given the relative low light intensities and pulse frequency used here, we do not expect this to be the case in our experiments, especially not in a pathway-dependent manner.

Differential activation of superficial and deep layers by POm suggests diverging functional roles

We show that activating POm inputs to L5 pyramidal cells elicits intensity-dependent responses in a wide range of amplitudes (Figure 3B,I) and occasional spiking (Table 1, Supplementary Figure 1), while POm inputs to L2/3 pyramidal cells activated all-or-none responses with relatively low amplitudes (Figure 3B,I) and rare spiking (Table 1,

Supplementary Figure 1). This suggests that POm is capable of transmitting information with high fidelity to L5 cells, but only after requisite recruitment of inputs has been achieved. Yet, for L2/3 cells, further depolarization beyond their maximum amplitude - as would be required to trigger spike output and so propagate information through the ascending cortical hierarchy - would require input from additional sources beyond POm, such as concurrent stimulus-evoked input to basal dendrites or local recurrent activity.

Layer-specific differences in synaptic responses to POm input likely drive layer-specific multiunit spiking activity. POm inputs evoked robust spike output in L5 that was correlated with the magnitude of inputs, while spike output was weak in L2/3 and insensitive to differences in the size of layer 1 inputs (Figure 5). The relative insensitivity of L2/3 cells observed here is consistent with observations *in vivo* showing that activity in L2/3 is sparse upon optogenetic activation of POm (Zhang and Bruno, 2019) and during simple sensing tasks (Sakata and Harris, 2009). Similar observations have also been made *in vitro*; brief activation of POm afferents (Audette et al., 2018) or direct activation of pyramidal cells (Beltramo et al., 2013) results in large synaptic responses and recurrent spiking in L5, but not in L2/3.

This layer dependence of the input-output relationship we and others have reported is further evidence of unique functional roles for each layer. Deep cortical layers participate in local processing of signals and engage lower cortical areas and subcortical centers, such as the thalamus (Guillery and Sherman, 2002; Theyel et al., 2010; Sherman and Guillery, 2011). Cells in L5, for example, send feedback projections to lower cortical areas as well as input to higher order thalamic nuclei involved in corticothalamocortical circuits (Theyel et al., 2010) (see Usrey & Sherman, 2019 for

summary). Cells in L6 project both to the thalamic area that returns reciprocal thalamocortical projections to the same cortical area and to other areas of cortex that receive thalamic input. Cells in L2/3 participate in intracortical message passing, especially in the feedforward direction (Bastos et al., 2012; Markov et al., 2014), and horizontal intracortical connections are reciprocally exchanged within L2/3 of hierarchically equivalent areas (Felleman and Van Essen, 1991; Markov et al., 2014). In addition to facilitating intracortical communication, L2/3 may exert modulatory control over feedback circuits; during active sensing tasks, activity in L2/3 suppresses L5 via recruitment of local inhibitory populations (Pluta et al., 2019).

It is possible that POm inputs serve to enhance – but not drive – activity in L2/3 pyramidal cells and may do so independently of the degree of POm activation. However, the utility of POm inputs to L2/3 cells may be brought to bear only in the presence of other stimuli. Indeed, Zhang et al. (2019) demonstrate that despite relatively low maximum amplitudes of POm-evoked post-synaptic potentials alone, POm activation enhanced responses in L2/3 pyramidal cells to whisker stimulation in primary somatosensory cortex in a supralinear manner, and POm inputs were required for sustained depolarization of L2/3 pyramidal cells. Together, these results suggest that POm acts as an on-off switch in L2/3, providing “facultative modulation” of sensory-evoked activity at any level of POm activation. Interestingly, the diffuse nature of higher order thalamocortical projections would imply that this modulatory control would be simultaneously imposed upon any connected cortical areas, synchronizing sensory responses and coordinating activity across multiple cortical areas.

Conversely, activity of the deep layers was sensitive to the level of POm input (Figure 3, Figure 5). We show that increasing POm input enhanced output of L5 without changing that of L2/3. This asymmetry implies that while the superficial layers may be naïve to the activity of POm, the deep layers can precisely sample the number of inputs activated and provide output in the feedback direction to lower cortical areas and subcortical structures accordingly. Of course, the integration of inputs to generate meaningful output from L5 relies on the contributions of local cell populations to amplify network responses and coordinate spike timing (Pouille and Scanziani, 2001). For example, fast-spiking PV+ interneurons have been shown to provide feedforward inhibition to L5 pyramidal cells especially (Audette et al., 2018), restricting the window of opportunity for output(Cruikshank et al., 2010) and improving spike timing of pyramidal cells (Pouille and Scanziani, 2001; Krause et al., 2017). We demonstrate that POm inputs strongly activate PV+ cells, which we expect would help to synchronize local excitation and output of L5 pyramidal cells.

Future directions

We demonstrate that higher order corticocortical and thalamocortical inputs to non-primary neocortex activate excitatory and inhibitory populations in a pathway- and cell type-specific manner. We artificially activated layer 1 inputs to simulate activity generated in higher cortical or thalamic areas to explore the unique dynamics of each input on distinct cell types. Of course, the effects of layer 1-mediated modulation of responses are likely relevant in the context of other inputs. We propose distinct functional roles for each pathway and provide evidence that the nature of inputs to layer

1 may be more nuanced than previously considered. Still, neither Cg nor POm afferents are likely to be active in the absence of sensory inputs in vivo, and given their overlapping terminal fields, corticocortical and thalamocortical inputs to layer 1 are likely to have interacting, multiplicative effects on cortical dynamics. As the development of opsins evolves, kinetically similar variants may be used *in vivo* to test the effects of thalamocortical and corticocortical inputs to layer 1 independently and simultaneously. Moreover, it is not clear how either TC or CC inputs activate dendritic spikes. Electrical activation of layer 1 elicits large plateau potentials in dendrites of pyramidal cells, which, when concurrently activated with “typical” axonal spikes can produce robust bursts of action potentials (Larkum et al., 1999; Larkum et al., 2004; Larkum, 2013). This amplification of input signals is tightly regulated by local inhibitory interneuron populations (Pérez-Garci et al., 2006; Palmer et al., 2012). Future investigations of dendritic amplification of sensory signals by layer 1 afferents will provide insight into the specialized roles of TC and CC inputs in sensory processing.

Acknowledgements

The authors are grateful for the technical support provided by Sean Grady, and the insight and expertise provided by Bryan Krause to the statistical analysis of data in this manuscript.

References

Anastasiades PG, Marques-Smith A, Butt SJB (2018) Studies of cortical connectivity using optical circuit mapping methods. The Journal of physiology 596:145-162.

Audette NJ, Urban-Ciecko J, Matsushita M, Barth AL (2018) POm Thalamocortical Input Drives Layer-Specific Microcircuits in Somatosensory Cortex. Cereb Cortex 28:1312-1328.

Bastos AM, Usrey WM, Adams RA, Mangun GR, Fries P, Friston KJ (2012) Canonical microcircuits for predictive coding. Neuron 76:695-711.

Beierlein M, Gibson JR, Connors BW (2003) Two dynamically distinct inhibitory networks in layer 4 of the neocortex. Journal of Neurophysiology 90:2987-3000.

Beltramo R, D'Urso G, Dal Maschio M, Farisello P, Bovetti S, Clovis Y, Lassi G, Tucci V, De Pietri Tonelli D, Fellin T (2013) Layer-specific excitatory circuits differentially control recurrent network dynamics in the neocortex. Nature Neuroscience 16:227-234.

Binzegger T, Douglas RJ, Martin KA (2004) A quantitative map of the circuit of cat primary visual cortex. JNeurosci 24:8441-8453.

Buffalo EA, Fries P, Landman R, Buschman TJ, Desimone R (2011) Laminar differences in gamma and alpha coherence in the ventral stream. Proc Natl Acad Sci USA 108:11262-11267.

Covic EN, Sherman SM (2011) Synaptic properties of connections between the primary and secondary auditory cortices in mice. CerebCortex 21:2425-2441.

Cruikshank SJ, Urabe H, Nurmikko AV, Connors BW (2010) Pathway-Specific Feedforward Circuits between Thalamus and Neocortex Revealed by Selective Optical Stimulation of Axons. Neuron 65:230-245.

Cruikshank SJ, Ahmed OJ, Stevens TR, Patrick SL, Gonzalez AN, Elmaleh M, Connors BW (2012) Thalamic Control of Layer 1 Circuits in Prefrontal Cortex. The Journal of Neuroscience 32:17813-17823.

D'Souza RD, Burkhalter A (2017) A Laminar Organization for Selective Cortico-Cortical Communication. Front Neuroanat 11:71.

D'Souza RD, Meier AM, Bista P, Wang Q, Burkhalter A (2016) Recruitment of inhibition and excitation across mouse visual cortex depends on the hierarchy of interconnecting areas. eLife 5:e19332.

De Pasquale R, Sherman SM (2011) Synaptic properties of corticocortical connections between the primary and secondary visual cortical areas in the mouse. JNeurosci 31:16494-16506.

Delevich K, Tucciarone J, Huang ZJ, Li B (2015) The Mediodorsal Thalamus Drives Feedforward Inhibition in the Anterior Cingulate Cortex via Parvalbumin Interneurons. The Journal of Neuroscience 35:5743.

Felleman DJ, Van Essen DC (1991) Distributed hierarchical processing in the primate cerebral cortex. CerebCortex 1:1-47.

Gentet LJ, Kremer Y, Taniguchi H, Huang ZJ, Staiger JF, Petersen CC (2012) Unique functional properties of somatostatin-expressing GABAergic neurons in mouse barrel cortex. Nat Neurosci 15:607-612.

Gilbert CD, Sigman M (2007) Brain states: top-down influences in sensory processing. Neuron 54:677-696.

Gilbert CD, Li W (2013) Top-down influences on visual processing. Nat Rev Neurosci 14:350-363.

Guillery RW, Sherman SM (2002) Thalamic Relay Functions and Their Role in Corticocortical Communication: Generalizations from the Visual System. Neuron 33:163-175.

Jackman SL, Beneduce BM, Drew IR, Regehr WG (2014) Achieving High-Frequency Optical Control of Synaptic Transmission. The Journal of Neuroscience 34:7704.

Kapfer C, Glickfeld LL, Atallah BV, Scanziani M (2007) Supralinear increase of recurrent inhibition during sparse activity in the somatosensory cortex. Nature Neuroscience 10:743-753.

Krause BM, Murphy CA, Uhlrich DJ, Banks MI (2017) PV+ Cells Enhance Temporal Population Codes but not Stimulus-Related Timing in Auditory Cortex. Cereb Cortex.

Kubota Y (2014) Untangling GABAergic wiring in the cortical microcircuit. Current opinion in neurobiology 26:7-14.

Larkum M (2013) A cellular mechanism for cortical associations: an organizing principle for the cerebral cortex. Trends Neurosci 36:141-151.

Larkum ME, Zhu JJ, Sakmann B (1999) A new cellular mechanism for coupling inputs arriving at different cortical layers. Nature 398:338-341.

Larkum ME, Senn W, Luscher HR (2004) Top-down Dendritic Input Increases the Gain of Layer 5 Pyramidal Neurons. Cerebral Cortex 14:1059-1070.

Lee CC, Sherman SM (2008) Synaptic Properties of Thalamic and Intracortical Inputs to Layer 4 of the First- and Higher-Order Cortical Areas in the Auditory and Somatosensory Systems. Journal of Neurophysiology 100:317-326.

Ma Y, Hu H, Berrebi AS, Mathers PH, Agmon A (2006) Distinct subtypes of somatostatin-containing neocortical interneurons revealed in transgenic mice. J Neurosci 26:5069-5082.

Maier A, Adams GK, Aura C, Leopold DA (2010) Distinct superficial and deep laminar domains of activity in the visual cortex during rest and stimulation. Frontiers in Systems Neuroscience 4.

Manita S, Suzuki T, Homma C, Matsumoto T, Odagawa M, Yamada K, Ota K, Matsubara C, Inutsuka A, Sato M, Ohkura M, Yamanaka A, Yanagawa Y, Nakai J, Hayashi Y, Larkum ME, Murayama M (2015) A Top-Down Cortical Circuit for Accurate Sensory Perception. Neuron 86:1304-1316.

Markov NT, Vezoli J, Chameau P, Falchier A, Quilodran R, Huissoud C, Lamy C, Misery P, Giroud P, Ullman S, Barone P, Dehay C, Knoblauch K, Kennedy H (2014) Anatomy of hierarchy: feedforward and feedback pathways in macaque visual cortex. J Comp Neurol 522:225-259.

Mashour GA, Hudetz AG (2017) Bottom-Up and Top-Down Mechanisms of General Anesthetics Modulate Different Dimensions of Consciousness. Front Neural Circuits 11:44.

Mease RA, Metz M, Groh A (2016) Cortical Sensory Responses Are Enhanced by the Higher-Order Thalamus. Cell Rep 14:208-215.

Mitzdorf U (1985) Current source-density method and application in cat cerebral cortex: investigation of evoked potentials and EEG phenomena. Physiol Rev 65:37-100.

Mo C, Sherman SM (2019) A Sensorimotor Pathway via Higher-Order Thalamus. The Journal of Neuroscience 39:692.

Muckli L, Petro LS (2013) Network interactions: non-geniculate input to V1. Current Opinion in Neurobiology 23:195-201.

Muralidhar S, Wang Y, Markram H (2014) Synaptic and cellular organization of layer 1 of the developing rat somatosensory cortex. Frontiers in Neuroanatomy 7.

Murayama M, Pérez-Garci E, Nevian T, Bock T, Senn W, Larkum ME (2009) Dendritic encoding of sensory stimuli controlled by deep cortical interneurons. Nature 457:1137-1141.

Palmer L, Murayama M, Larkum M (2012) Inhibitory Regulation of Dendritic Activity in vivo. Front Neural Circuits 6:26.

Pérez-Garci E, Gassmann M, Bettler B, Larkum ME (2006) The GABA-B1b Isoform Mediates Long-Lasting Inhibition of Dendritic Ca2+ Spikes in Layer 5 Somatosensory Pyramidal Neurons. Neuron 50:603-616.

Petrof I, Viaene AN, Sherman SM (2011) Two populations of corticothalamic and interareal corticocortical cells in the subgranular layers of the mouse primary sensory cortices. JComp Neurol.

Pettersen KH, Devor A, Ulbert I, Dale AM, Einevoll GT (2006) Current-source density estimation based on inversion of electrostatic forward solution: effects of finite extent of neuronal activity and conductivity discontinuities. JNeurosciMethods 154:116-133.

Pluta SR, Telian GI, Naka A, Adesnik H (2019) Superficial Layers Suppress the Deep Layers to Fine-tune Cortical Coding. The Journal of Neuroscience 39:2052.

Pouille F, Scanziani M (2001) Enforcement of temporal fidelity in pyramidal cells by somatic feed- forward inhibition. Science 293:1159-1163.

Radnikow G, Feldmeyer D (2018) Layer- and Cell Type-Specific Modulation of Excitatory Neuronal Activity in the Neocortex. Frontiers in Neuroanatomy 12.

Rao RP, Ballard DH (1999) Predictive coding in the visual cortex: a functional interpretation of some extra-classical receptive-field effects. Nat Neurosci 2:79-87.

Redinbaugh MJ, Phillips JM, Kambi NA, Mohanta S, Andryk S, Dooley G, Afrasiabi M, Raz A, Saalmann Y (2020) Thalamus Modulates Consciousness Via Layer-Specific Control of Cortex. Neuron 105.

Riedemann T, Straub T, Sutor B (2018) Two types of somatostatin-expressing GABAergic interneurons in the superficial layers of the mouse cingulate cortex. PLoS One 13:e0200567.

Rockland KS, Virga A (1989) Terminal arbors of individual "feedback" axons projecting from area V2 to V1 in the macaque monkey: a study using immunohistochemistry of anterogradely transported Phaseolus vulgaris-leucoagglutinin. J Comp Neurol 285:54-72.

Roth MM, Dahmen JC, Muir DR, Imhof F, Martini FJ, Hofer SB (2016) Thalamic nuclei convey diverse contextual information to layer 1 of visual cortex. Nat Neurosci 19:299-307.

Rubio-Garrido P, Pérez-de-Manzo F, Porrero C, Galazo MJ, Clascá F (2009) Thalamic input to distal apical dendrites in neocortical layer 1 is massive and highly convergent. Cerebral Cortex 19:2380-2395.

Saalmann YB, Pinsk MA, Wang L, Li X, Kastner S (2012) The pulvinar regulates information transmission between cortical areas based on attention demands. Science 337:753-756.

Sakata S, Harris KD (2009) Laminar structure of spontaneous and sensory-evoked population activity in auditory cortex. Neuron 64:404-418.

Sherman SM, Guillery RW (2011) Distinct functions for direct and transthalamic corticocortical connections. J Neurophysiol 106:1068-1077.

Sherman SM, Guillery RW (2013) Functional Connections of Cortical Areas: A New View from the Thalamus. Cambridge, MA: MIT Press.

Shipp S (2007) Structure and function of the cerebral cortex. Curr Biol 17:R443-449.

Silberberg G, Markram H (2007) Disynaptic inhibition between neocortical pyramidal cells mediated by Martinotti cells. Neuron 53:735-746.

Takahashi N, Oertner TG, Hegemann P, Larkum ME (2016) Active cortical dendrites modulate perception. Science 354:1587-1590.

Theyel BB, Llano DA, Sherman SM (2010) The corticothalamocortical circuit drives higher-order cortex in the mouse. Nat Neurosci 13:84-88.

Viaene AN, Petrof I, Sherman SM (2011a) Synaptic properties of thalamic input to layers 2/3 and 4 of primary somatosensory and auditory cortices. JNeurophysiol 105:279-292.

Viaene AN, Petrof I, Sherman SM (2011b) Synaptic properties of thalamic input to the subgranular layers of primary somatosensory and auditory cortices in the mouse. JNeurosci 31:12738-12747.

Viaene AN, Petrof I, Sherman SM (2011c) Properties of the thalamic projection from the posterior medial nucleus to primary and secondary somatosensory cortices in the mouse. Proc Natl Acad Sci USA 108:18156-18161.

Zhang W, Bruno RM (2019) High-order thalamic inputs to primary somatosensory cortex are stronger and longer lasting than cortical inputs. eLife 8:e44158.

Figure 1

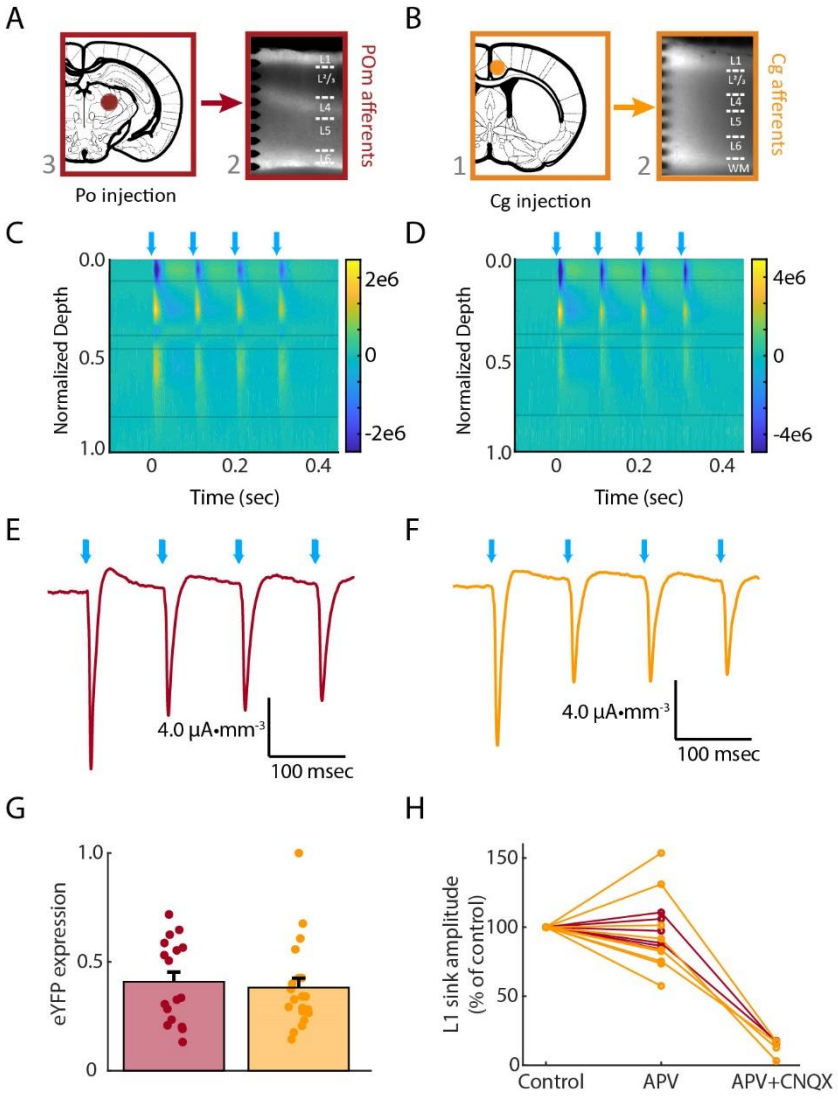

Figure 1. POm and Cg input to layer 1 of anteromedial cortex requires ionotropic glutamatergic receptors. A. Schematic demonstrating the location of unilateral viral injection into posterior medial thalamus (left), which resulted in eYFP expression in layers 1 and 4 of medial secondary visual cortex (right). B. Same as in A for viral injection in cingulate cortex (left), which resulted in eYFP expression in layer 1 (right) C. Example current source density color plot demonstrates current sinks (inward-going transmembrane current) in layer 1 (blue) evoked by activating POm afferents using 2-msec pulses of 470 nm light (blue arrows) restricted to only to layer 1. D. Same as in A for activation of Cg afferents. E,F. Current source density

signal isolated from layer 1 in C,D. G. Comparison of eYFP reporter in thalamocortical (red, n=17) and corticocortical (orange, n=20) layer 1 afferents (arbitrary units). H. NMDA receptor antagonist APV had no effect on amplitude of POm- or Cg-evoked current sinks in layer 1, but bath application of APV (20 μM) and CNQX (50 μM) together almost completely blocked layer 1 current sinks evoked by either afferent input.

Figure 2

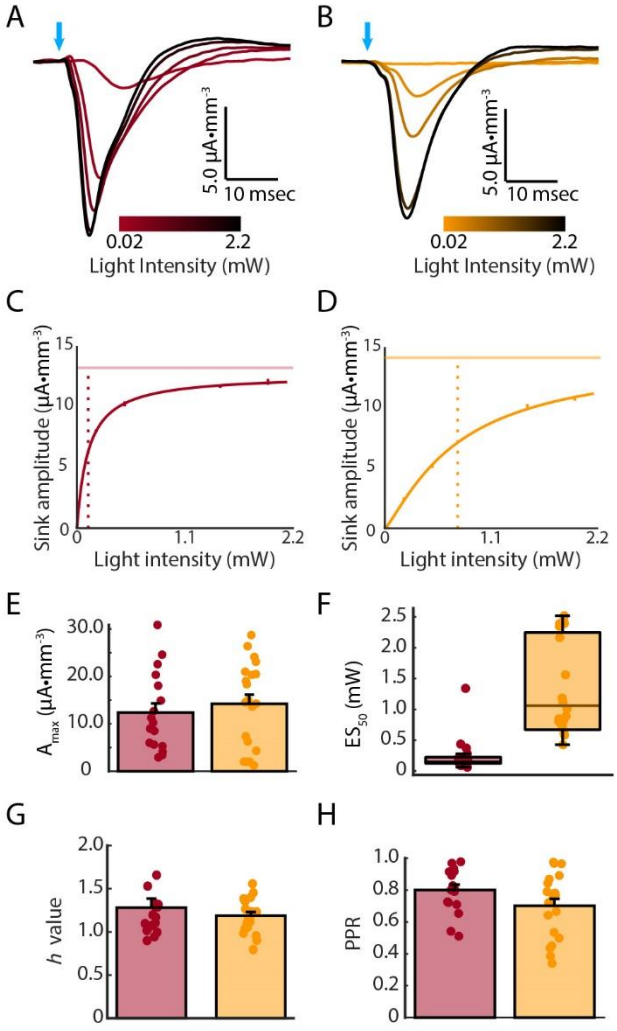

Figure 2. Evoked current sinks in layer 1 exhibit pathway-dependent properties. A. Example current source density signal isolated from layer 1 following activation of POm afferents. Negative-going current sinks represent inward-going transmembrane current. Responses from a range of stimulus intensities (0.022, 0.22, 0.56, 1.68, and 2.2 mW; red to black, respectively) reflect an all-or-none response profile with increasing light intensity. B. Same as in A, but for Cg-evoked responses. Responses exhibit a graded response profile with increasing light intensity. C. Peak sink amplitudes from A were fit to a logistic equation as a function of stimulus intensity. Fit

line (red), A_{max} (light red), and ES_{50} (dotted line) are shown. D. Same as in C, but for sink amplitudes from responses shown in B. E-G. Fit parameters are compared for POm (red) and Cg (orange) inputs for all slice experiments. E. Asymptotic maxima, A_{max}. A_{max} represents the maximum possible amplitude given unlimited light intensity. F. Effective stimulus to achieve 50% of the A_{max}, ES_{50}. ES_{50} (the light intensity at which 50% of A_{max} is reached) is used as a proxy for gradedness of response amplitude with changes in stimulus intensity. G. Coefficient *h*, which represents the degree of cooperativity among synaptic components contributing to the post-synaptic response, where deviations from hyperbolicity are represented as *h* values less than or great than 1. H. Paired pulse ratio of POm- (red) and Cg- (orange) evoked layer 1 current sinks for all slice experiments.

Figure 3

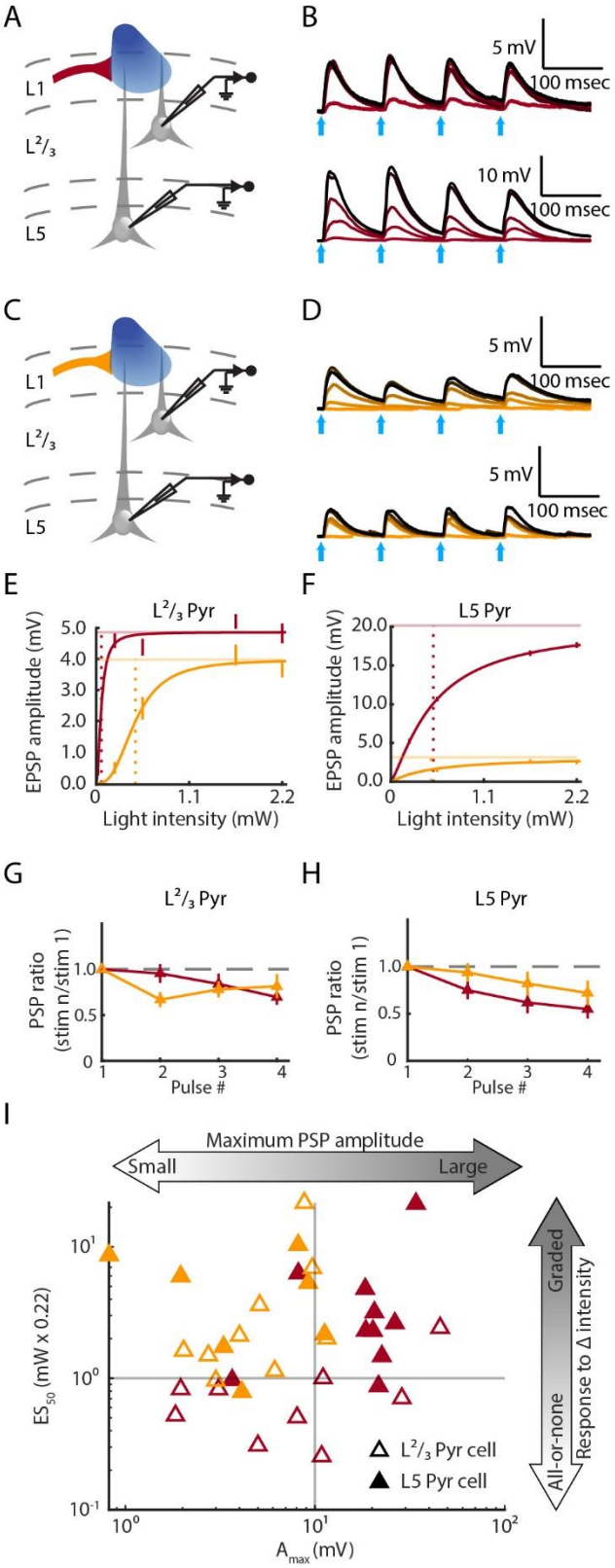
A
L1
L2/3
L5
B
5 mV
100 msec
10 mV
100 msec
C
L1
L2/3
L5
D
5 mV
100 msec
5 mV
100 msec
E
L2/3 Pyr
EPSP amplitude (mV)
Light intensity (mW)
F
L5 Pyr
EPSP amplitude (mV)
Light intensity (mW)
G
L2/3 Pyr
PSP ratio (stim n/stim 1)
Pulse #
H
L5 Pyr
PSP ratio (stim n/stim 1)
Pulse #
I
Maximum PSP amplitude
Small
Large
ES50 (mW x 0.22)
Amax (mV)
L2/3 Pyr cell
L5 Pyr cell
Graded
Response to Δ intensity
All-or-none

Figure 3. Properties of POm- and Cg-evoked post-synaptic potentials in pyramidal cells are layer- and pathway-dependent. A. Schematic demonstrating recording scheme for signals in B. POm afferents (red) were activated during whole cell patch clamp recordings from pyramidal cells in either L2/3 or L5. B. Example recordings from a L2/3 (top) and L5 (bottom) pyramidal cell during activation of POm afferents at a range of light stimulus intensities (0.022, 0.22, 0.56, 1.68, and 2.2 mW; red to black, respectively). With increasing stimulus intensity, minimal increases in amplitude were observed in L2/3 pyramidal cells (all-or-none), while L5 pyramidal cell responses were graded but typically reached a higher asymptotic maximum (A_{max}). C-D. Same as in A-B, but for Cg-evoked responses (orange). E. Peak amplitudes (first pulse only; mean ± SE shown) from L2/3 pyramidal cells in top of B (POm, red) and D (Cg, orange) were fit to a logistic equation as a function of stimulus intensity. Fit lines (solid), A_{max} (pale), and ES_{50} (dotted) are shown. F. Same as in E, but for L5 cells shown in bottom of B (POm, red) and D (Cg, orange). G. Short-term synaptic plasticity for L2/3 pyramidal cells in response to POm (red) and Cg (orange) inputs. H. Same as G, but for inputs to L5 pyramidal cells. I. Scatter plot of A_{max} versus ES_{50} values for each pyramidal cell (POm: red, Cg: orange). Empty triangles are L2/3 cells, and filled triangles are L5 pyramidal cells.

Figure 4

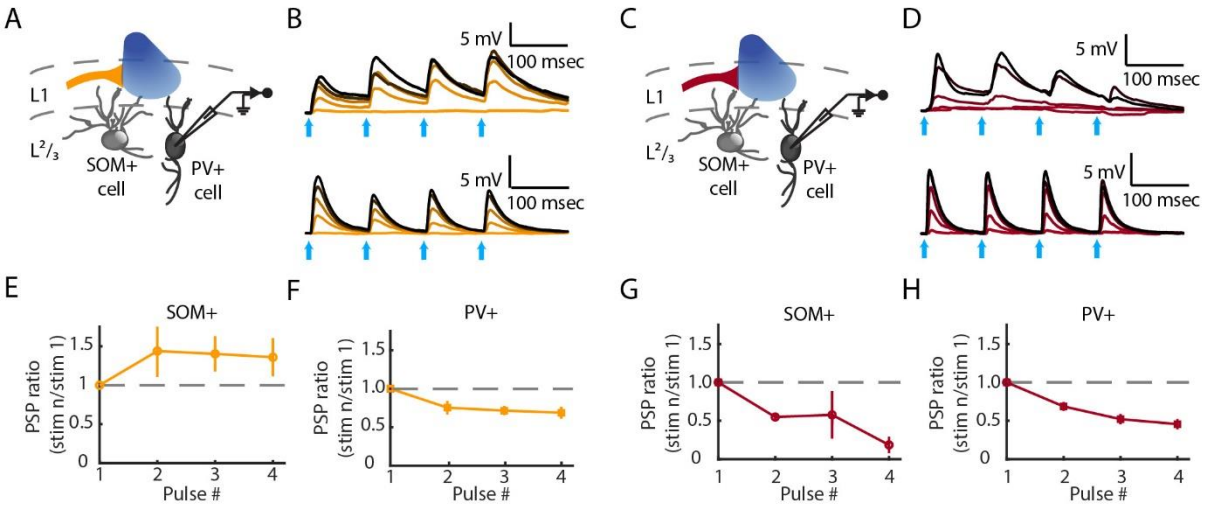

Figure 4. POm- and Cg-evoked post-synaptic potentials in PV+ and SOM+ cells are similar. A. Schematic demonstrating recording scheme for signals in B. Cg afferents (orange) were activated during whole cell patch clamp recordings from either SOM+ or PV+ interneurons. B. Example recordings from a SOM+ (top) and PV+ (bottom) interneuron during activation of POm afferents at a range of light stimulus intensities (0.022, 0.22, 0.56, 1.68, and 2.2 mW; red to black, respectively). C-D. Same as in A-B, but for POm-evoked responses (red). E. Short-term synaptic plasticity for SOM+ interneurons in response to Cg inputs. F. Short-term synaptic plasticity for PV+ interneurons in response to Cg inputs. G-H. Same as E-F, but for POm inputs to SOM+ and PV+ interneurons, respectively.

Figure 5

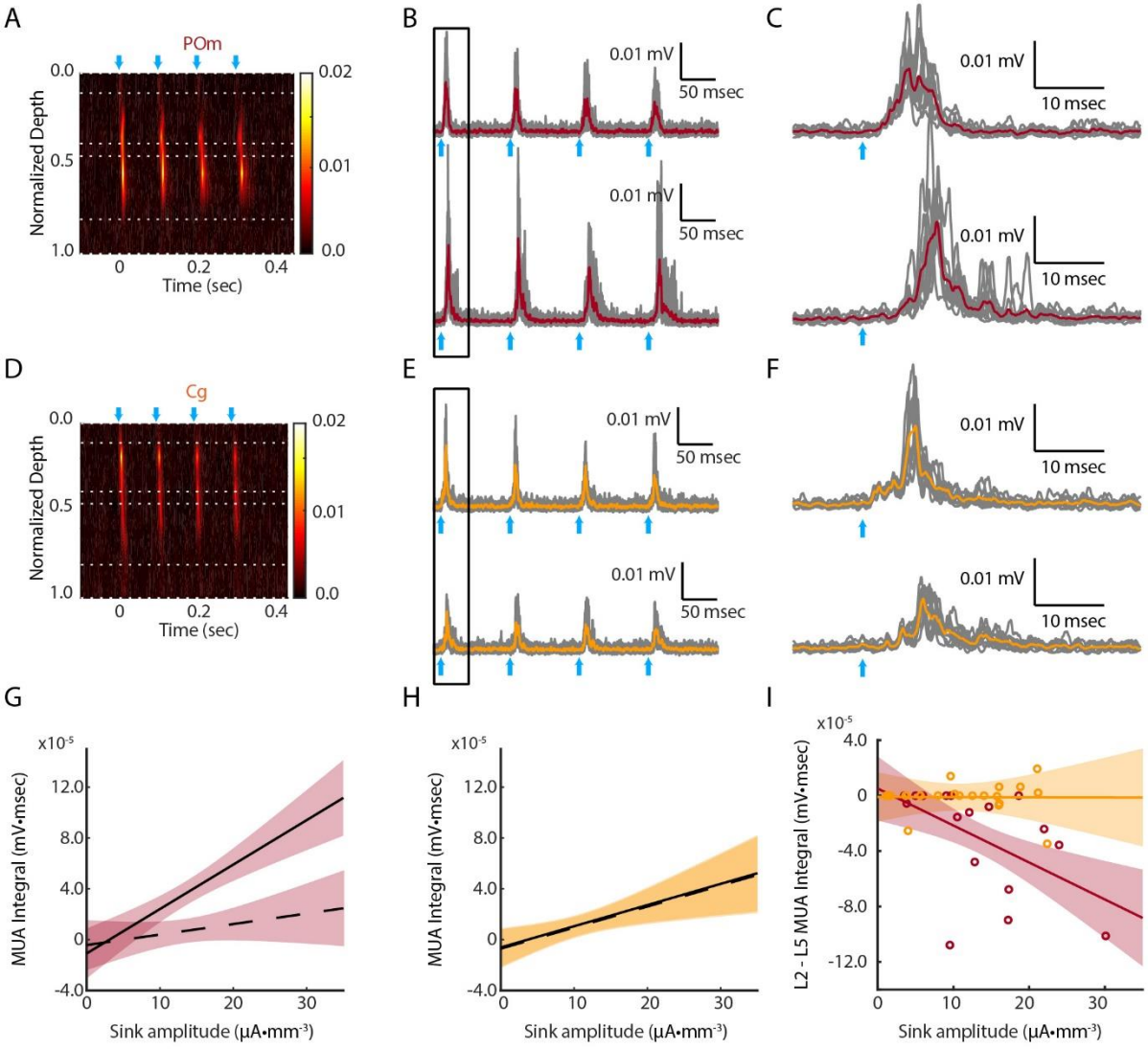

Figure 5. Multiunit activity evoked by layer 1 inputs exhibits pathway- and layer-dependent profiles within the cortical column. A. Example multiunit activity heat map evoked across the cortical column by activation of POm inputs (blue arrows). B. Multiunit activity signal isolated from L2/3 (top) and L5 (bottom) in A. C. Signals from black rectangle in B, magnified. D-F. Same as A-C, but for Cg inputs. G. For POm-evoked responses, Integral of the multiunit activity signal in L5 (solid line), but not L2/3 (dashed line), was dependent on the amplitude of inputs to layer 1. H. For Cg-evoked responses, integral of the multiunit activity signal in both L2/3 (dashed line) and L5 (solid line) was dependent on the amplitude of inputs to layer 1. Shaded

regions in G and H represent 95% confidence intervals . I. For each experiment, the difference between the integral of the multiunit activity in L2/3 minus L5 is plotted as a function of sink amplitude in layer 1. Individual experiments are shown as circles, and model fits with 95% confidence interval (shaded) are shown. With increasing layer 1 current sink amplitude, activation of POm (red) afferents evoked multiunit activity that was increasingly dominated by L5.

	Total cells from (N) slices	Early responses detected	Successful fit	Spike probability [CI]	
POm→					
$L^2/_3$ Pyr	10(6)	$^{10}/_{10}$	$^{9}/_{10}$	0.10	[-0.10 , 0.29]
L5 Pyr	12(10)	$^{11}/_{12}$	$^{10}/_{11}$	0.36	[0.16 , 0.57]
SOM+	12(5)	$^{5}/_{12}$	$^{2}/_{2}$	0.58	[0.20 , 0.96]
PV+	14(8)	$^{14}/_{14}$	$^{7}/_{8}$	0.51	[0.26 , 0.76]
Cg→					
$L^2/_3$ Pyr	16(12)	$^{14}/_{16}$	$^{10}/_{13}$	0.08	[-0.08 , 0.24]
L5 Pyr	15(11)	$^{10}/_{15}$	$^{8}/_{9}$	0.10	[-0.11 , 0.31]
SOM+	17(8)	$^{12}/_{17}$	$^{8}/_{10}$	0.45	[0.18 , 0.73]
PV+	16(8)	$^{15}/_{16}$	$^{12}/_{13}$	0.16	[-0.08 , 0.40]

Table 1. Identities of all cells for data presented. Cells were considered early responders if activation of layer 1 inputs evoked non-zero amplitudes on at least 50% of trials with a latency jitter of <1 msec. Cells that did not exhibit responses within these criteria or which exhibited latencies >10 msec were considered to be non-responders and were not used for further analysis. If cells fired spikes on every trial for one or more stimulus intensity, they were considered separately (**Supplementary Table 1**). Otherwise, amplitudes of synaptic responses (first pulse only) were fit to a three-parameter nonlinear logistic equation. The fraction of cells that were fit successfully (R>0.95) is shown here and fit parameters are compared between pathways for each cell type in Tables 2-4. Population spike probabilities (2.2 mW) are predicted from linear mixed effects model are shown with 95% confidence intervals. Comparisons of spike probabilities reflect pathway- and cell type-dependence (*P<0.05). However, no interaction between pathway and cell type was observed for spike probability ($\chi(3) = 2.482$, $P = 0.48$).

	Estimate of pathway effect (mV)	[CI] (mV)	P-value
POm – Cg			
$L^2/_3$ Pyr	9.1	[-1.3 , 19.5]	0.086
L5 Pyr	15.2	[8.4 , 22.1]	<0.0001
SOM+	0.5	[-9.8 , 10.8]	0.92
PV+	1.3	[-6.1 , 8.8]	0.72

Table 2. Size of maximum amplitude (A_{max}) is pathway-dependent. Afferent pathway had a significant effect on predicted A_{max} values ($\chi(1) = 10.6$, $P = 0.0011$), as did the interaction between pathway and cell type ($\chi(3) = 8.26$, $P = 0.040$); no effect of cell type alone was observed ($\chi(3) = 2.86$, $P = 0.41$). Estimates represent differences between A_{max} values for POm versus Cg inputs (positive values indicate larger predicted A_{max} for POm inputs) with 95% confidence intervals. Predicted A_{max} values for L5 pyramidal cells were significantly greater for POm inputs compared to Cg inputs. Population estimates of A_{max} values for each independent pathway-cell type combination are shown in **Supplementary Table 2**.

	Estimate of pathway effect	[CI]	P-value
POm – Cg			
$L^2/_3$ Pyr	-1.39	[-2.09 , -0.69]	0.0002
L5 Pyr	-0.23	[-1.10 , 0.65]	0.61
SOM+	0.98	[-0.20 , 2.17]	0.11
PV+	0.23	[-0.80 , 1.26]	0.65

Table 3. Gradedness of synaptic responses to increasing stimulus intensities is pathway-dependent. The interaction of pathway and cell type had a significant effect on ES_{50} values ($\chi(3) = 11.64$, $P = 0.008$). Estimates are presented in their exponentiated form and represent multiplicative factors in ES_{50} values between POm versus Cg inputs (positive values indicate larger predicted ES_{50} for POm inputs) with 95% confidence intervals. Predicted ES_{50} values for L2/3 pyramidal cells were significantly greater for POm inputs compared to Cg inputs. This pathway-dependent effect was significantly stronger than that in any other cell type (*P<0.05, **P<0.01). Population estimates of ES_{50} values for each independent pathway-cell type combination are shown in **Supplementary Table 3**.

	Estimate of pathway effect	[CI] (mV)	P-value
POm – Cg			
$L^2/_3$ Pyr	-0.52	[-1.11 , 0.066]	0.08
L5 Pyr	-0.26	[-0.79 , 0.28]	0.34
SOM+	-0.11	[-1.04 , 0.83]	0.82
PV+	0.29	[-0.40 , 0.97]	0.40

Table 4. Predicted *h* coefficient values are neither pathway- nor cell type-dependent. The interaction of pathway and cell type was not significant for *h* coefficients (3.31, P = 0.35). Estimates represent differences in *h* coefficient values between POm versus Cg inputs (positive values indicate larger *h* coefficient for POm inputs) with 95% confidence intervals. Population estimates of *h* coefficient values for each independent pathway-cell type combination are shown in **Supplementary Table 4**.

	Estimate of pathway effect (mV)	[CI] (mV)	P-value
POm – Cg			
$L^2/_3$ Pyr	0.22	[-0.19 , 0.63]	0.30
L5 Pyr	-0.30	[-0.71 , 0.10]	0.14
SOM+	-1.02	[-1.62 , -0.42]	0.0012
PV+	0.01	[-0.41 , 0.42]	0.98

Table 5. Paired pulse ratios are significantly higher for Cg inputs to SOM+ interneurons than they are for POm inputs. A significant interaction of pathway and cell type was observed for paired pulse ratios ($\chi(3) = 13.14$, $P = 0.0043$). Paired pulse ratios were no different between pathways for L2/3 or L5 pyramidal cells, nor for PV+ cells. However, Cg inputs to SOM+ interneurons elicited robust paired pulse facilitation compared to POm inputs. For population estimates for each distinct pathway-cell type combination, see **Supplementary Table 5.**

Supplementary Figure 1

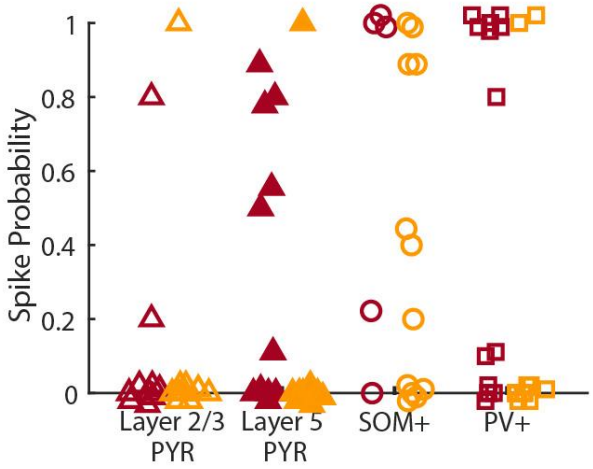

Supplementary Figure 1. Spike probabilities of individual pyramidal (empty triangles – L2/3 cells; filled triangles – L5 cells), SOM+ (circles), and PV+ (squares) cells. Responses to POm inputs are shown in red, and responses to Cg inputs are shown in orange. Population spike probabilities predicted from linear mixed effects model are shown in Table 1.

Supplementary Figure 2

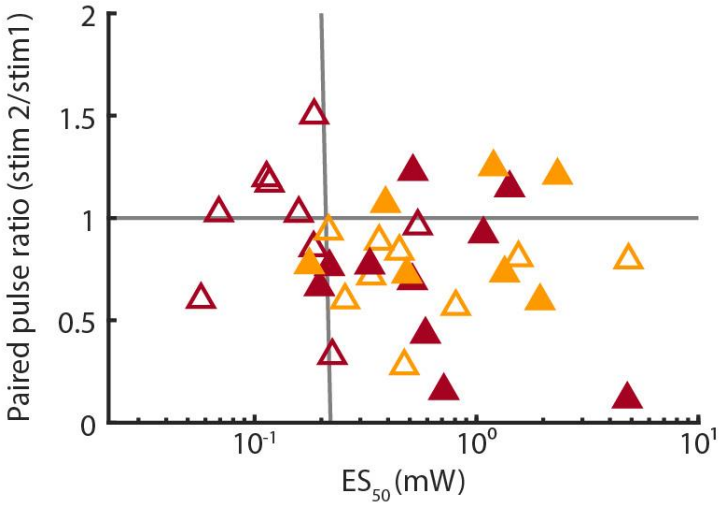

Supplementary Figure 2. Scatter plot of ES_{50} values versus paired pulse ratios for each pyramidal cell (POm: red, Cg: orange). Empty triangles are L2/3 cells, and filled triangles are L5 pyramidal cells. POm inputs to L2/3 pyramidal cells exhibited all-or-none responses with a mixture of paired pulse facilitation and paired pulse depression, while inputs to each of the other three groups mostly exhibited paired pulse depression and graded responses.

Supplementary Figure 3

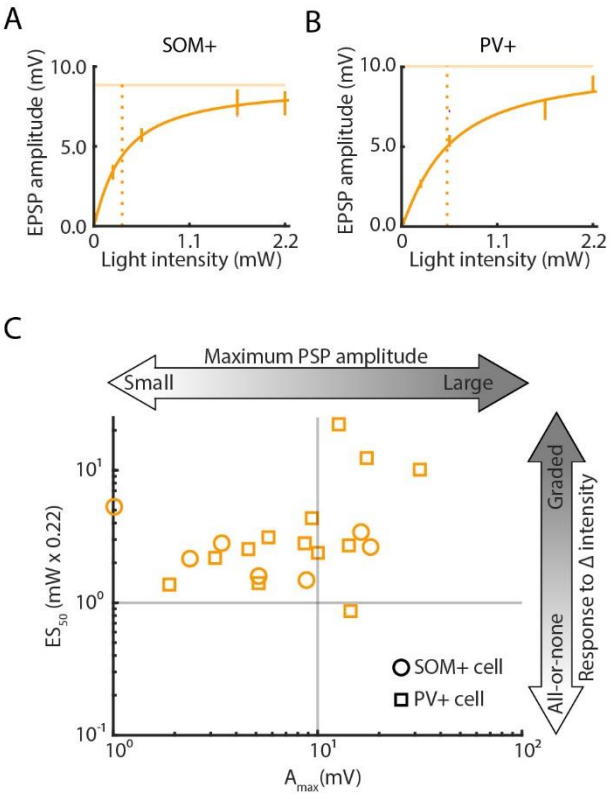

Supplementary Figure 3. A. Peak amplitudes (first pulse only; mean ± SEM shown) from responses to Cg inputs for an example SOM+ cell (same as Figure 4B, top panel) fit to a logistic equation as a function of stimulus intensity. Fit lines (solid), A_{max} (pale), and ES_{50} (dotted) are shown. B. Same as in A, but for PV+ cell in example from Figure 4B (bottom panel). C. Scatter plot of A_{max} versus ES_{50} values for each interneuron. Scale is the same as Figure 3 for comparison.

Supplementary Figure 4

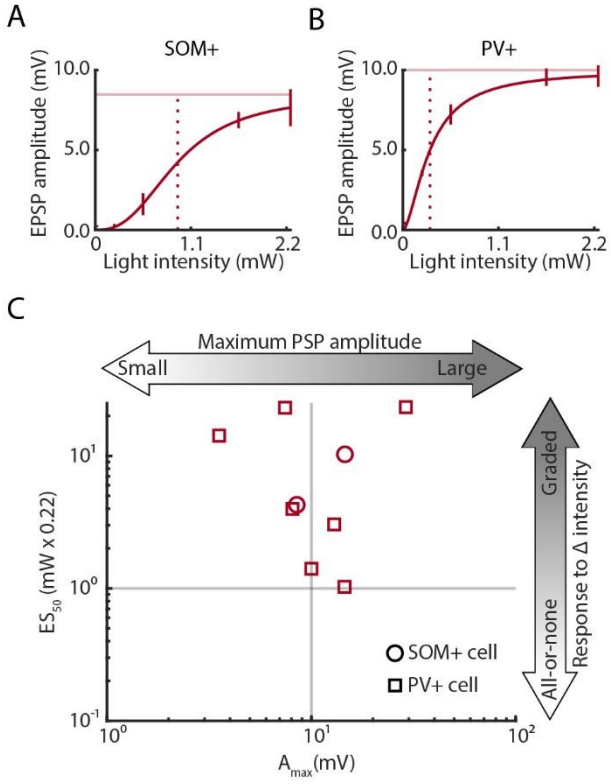

Supplementary Figure 4. A. Peak amplitudes (first pulse only; mean ± SEM shown) from responses to POm inputs for an example SOM+ cell (same as Figure 4B, top panel) fit to a logistic equation as a function of stimulus intensity. Fit lines (solid), A_{max} (pale), and ES_{50} (dotted) are shown. B. Same as in A, but for PV+ cell in example from Figure 4B (bottom panel). C. Scatter plot of A_{max} versus ES_{50} values for each interneuron. Scale is the same as Figure 3 for comparison. Note than POm inputs elicited synaptic responses in only 2 SOM+ cells.

POm→	Spikes on every trial
$L^2/_3$ Pyr	$^0/_{10}$
L5 Pyr	$^0/_{11}$
SOM+	$^3/_5$
PV+	$^6/_{14}$
Cg→	
$L^2/_3$ Pyr	$^1/_{14}$
L5 Pyr	$^1/_{10}$
SOM+	$^2/_{12}$
PV+	$^2/_{15}$

Supplementary Table 1. Fraction of cells that fired action potentials on every trial at stimulus intensity of 2.2 mW.

		A_{max} estimate [CI] (mV)		
POm→	n cells from (N) slices			
$L^2/_3$ Pyr	9(6)	16.1	[8.1 , 24.1]	
L5 Pyr	10(8)	21.0	[16.1 , 25.8]	*
SOM+	2(2)	8.2	[-1.0 , 17.3]	*
PV+	7(5)	11.3	[5.1 , 17.4]	
Cg→				
$L^2/_3$ Pyr	9(8)	7.0	[0.4 , 13.7]	
L5 Pyr	7(7)	5.7	[0.8 , 10.6]	
SOM+	7(4)	7.7	[3.0 , 12.3]	
PV+	12(6)	9.9	[5.6 , 14.2]	

Supplementary Table 2. Population estimates of A_{max} values for each independent pathway-cell type combination. Notable comparisons between cell types within pathway are shown to the right of the table. *P<0.05

		ES_{50} estimate [CI] (mW)	
POm→	n cells from (N) slices		
$L^2/_3$ Pyr	9(6)	0.15	[0.09 , 0.24]
L5 Pyr	10(8)	0.65	[0.36 , 1.16]
SOM+	2(2)	1.51	[0.53 , 4.29]
PV+	7(5)	1.08	[0.49 , 2.38]
Cg→			
$L^2/_3$ Pyr	9(8)	0.59	[0.36 , 0.97]
L5 Pyr	7(7)	0.81	[0.42 , 1.57]
SOM+	7(4)	0.56	[0.32 , 0.99]
PV+	12(6)	0.86	[0.45 , 1.65]

***
***
****

Supplementary Table 3. Population estimates of ES_{50} values for each independent pathway-cell type combination. Estimates are shown in their unexponentiated form with units of mW. Notable comparisons between cell types within pathway are shown to the right of the table. *P<0.05, **P<0.01, ***P<0.001, ****P<0.0001

		h value [CI]	
POm→	n cells from (N) slices		
$L^2/_3$ Pyr	9(6)	1.21	[0.76 , 1.65]
L5 Pyr	10(8)	1.17	[0.82 , 1.52]
SOM+	2(2)	1.77	[0.97 , 2.57]
PV+	7(5)	1.60	[1.06 , 2.15]
Cg→			
$L^2/_3$ Pyr	9(8)	1.73	[1.34 , 2.11]
L5 Pyr	7(7)	1.42	[1.02 , 1.83]
SOM+	7(4)	1.88	[1.39 , 2.36]
PV+	12(6)	1.32	[0.90 , 1.74]

Supplementary Table 4. Population estimates of *h* coefficients for each independent pathway-cell type combination. No significant effect of pathway nor cell type was observed.

		PPR	
POm→	n cells from (N) slices		
$L^2/_3$ Pyr	10(6)	0.89	[0.57 , 1.22]
L5 Pyr	11(9)	0.68	[0.40 , 0.96]
SOM+	5(4)	0.49	[-0.02 , 0.99]
PV+	14(8)	0.73	[0.43 , 1.04]
Cg→			
$L^2/_3$ Pyr	14(11)	0.67	[0.42 , 0.93]
L5 Pyr	10(9)	0.98	[0.70 , 1.27]
SOM+	12(7)	1.51	[1.17 , 1.84]
PV+	15(8)	0.73	[0.44 , 1.02]

****
*
***

Supplementary Table 5. Population estimates for paired pulse ratios for each independent pathway-cell type combination. Notable comparisons between cell types within pathway are shown to the right of the table. *P<0.05, **P<0.01, ***P<0.001, ****P<0.0001

	RMP (mV)	R_{in} (MΩ)	τ_m (msec)	Spike Threshold (mV)
$L^2/_3$ Pyr (n=24)	-71.0±5.7	116.0±45.4	15.7±10.4	-41.8±2.7
L5 Pyr (n=21)	-66.1±3.8	136.3±61.0	22.6±13.8	-43.0±3.1
SOM+ (n=17)	-57.6±7.0	274.0±112.8	39.6±40.7	-41.4±2.6
PV+ (n=29)	-63.1±4.8	156.4±52.8	9.6±3.1	-46.1±7.3

Supplementary Table 6. Intrinsic properties of each cell type assayed in this study. Measures are combined for POm-injected and Cg-injected animals, as intrinsic properties are independent of pathway. Values are mean ± standard deviation. Properties were measured ~2 minutes after achieving whole cell access. A series of 10-20 current steps (600 msec) was delivered at progressive intervals (10-40 pA), beginning with a hyperpolarizing current injection. Resting membrane potentials (RMP) were calculated by averaging membrane potentials in the 100 msec prior to onset of all current pulses. Input resistances (R_{in}) were extrapolated from relationship between current and steady state voltages. Time constants (τ_m) were estimated using the first hyperpolarizing current pulse. Spike thresholds were evaluated using the first trial to evoke an action potential, where the spike threshold was the voltage at which the second derivative exceeded twice the standard deviation of the pre-spike baseline value.

Chapter 4

Selective effects of isoflurane on cortico-cortical feedback afferent responses in murine non-primary neocortex

This chapter was published previously as:

Murphy C, Krause B, Banks M (2019). Selective effects of isoflurane on cortico-cortical feedback afferent responses in murine non-primary neocortex. British Journal of Anaesthesia. 123(4):488-496. doi: 10.1016/j.bja.2019.06.018.

C.A. Murphy[1,2], B.M. Krause[2], M.I. Banks[2]

[1]Physiology Graduate Training Program, University of Wisconsin School of Medicine and Public Health, Madison, WI 53706
[2]Department of Anesthesiology, University of Wisconsin School of Medicine and Public Health, Madison, WI 53706

Keywords: Anaesthesia, General; Anaesthetics, General; Channelrhodopsins; Isoflurane; Mice; Neocortex; Thalamus

Abstract

Background: Anaesthetics effect loss of consciousness by disrupting information-passing and integration within thalamocortical networks. Previous studies have suggested that feedback cortical connections, which carry internally-generated signals such as expectation and attention, are more sensitive to anaesthesia than feedforward signals. However, direct evidence for this effect in non-primary cortex is lacking. In addition, direct comparisons between thalamo-cortical (TC) core and matrix, and

between cortico-cortical (CC) feedforward and feedback responses have not been reported.

Methods: We investigated the disruption of synaptic responses by isoflurane of four distinct afferent pathways to non-primary neocortex. We independently activated TC core and matrix and reciprocal CC (feedforward and feedback) pathways using optogenetics and compared the relative sensitivity of synaptic responses to isoflurane.

Results: Under control conditions, activation of axon terminals of all pathways evoked post-synaptic currents (recorded extracellularly) and post-synaptic potentials in pyramidal cells. CC feedback responses were substantially more sensitive to isoflurane (0 to 0.53 mM) compared to TC core, TC matrix, or CC feedforward pathways.

Conclusion: Differential sensitivity of CC feedback synaptic responses to isoflurane in a clinically-relevant range suggests a role for disruption of these afferents in the hypnotic effects of anaesthetic agents.

Introduction

The mechanisms of anaesthetic-induced loss of consciousness (LOC) have profound clinical relevance and are relevant as well for expanding and unifying basic theories of consciousness (Alkire, 2008; Mashour, 2013). Central to these theories is the sharing of information between nodes in the cortico-thalamic network (Llinas et al., 1998; Crick and Koch, 2003; Koch et al., 2016) carried by thalamo-cortical (TC) and cortico-cortical (CC) feedback and feedforward pathways (Friston, 2005; Dehaene and Changeux, 2011). Studies examining the effects of anaesthetics on the contents of consciousness have focused on this information exchange in particular (Mashour and Hudetz, 2017). However, the degree to which anaesthetics selectively modulate these pathways,

especially in non-primary cortical areas that are critical for consciousness and particularly sensitive to anaesthetics (Liu et al., 2012; Nourski et al., 2018), remains unclear.

Previous noninvasive studies suggest that CC connectivity (especially feedback connectivity) is suppressed by anaesthetics (Ferrarelli et al., 2010; Ku et al., 2011; Schrouff et al., 2011; Lee et al., 2013). Similarly, we showed previously in slices that synaptic responses in primary auditory cortex (A1) to intracortical stimulation were suppressed to a greater extent than were responses to stimulation of TC afferents from primary auditory thalamus (Raz et al., 2014). Less is known about anaesthetic effects on projections of non-primary thalamic nuclei, which are the source of both modulatory ('matrix') and information-bearing ('core') efferents (Jones, 2001) to non-primary cortex. These nuclei receive little direct sensory input but facilitate information transfer between cortical areas via recurrent cortico-thalamocortical loops and may contribute to maintaining awareness (Guillery and Sherman, 2002; Saalmann, 2014; Neske, 2015). Also unknown is whether cortico-cortical feedforward afferents, which connect directly different levels of the cortical hierarchy, are as robust to anaesthetic effects as primary thalamic feedforward afferents. Here, we activate four distinct afferent thalamocortical and corticocortical pathways and compare the effects of isoflurane on synaptic responses of each in non-primary cortex.

Methods

Expression of channelrhodopsin and brain slice preparation

Synaptic pathways were activated optogenetically after expressing excitatory opsins in nerve terminals of specific afferent fibers (Figure 1A, see Supplementary Methods for additional details). To obtain ChR2 expression in both TC matrix and core projections to non-primary cortex, injections were made in posterior thalamus (Po; Figure 1B, top), a non-primary thalamic nucleus that contains a combination of matrix and core cells, distinguished here by the laminar distribution of their axon terminals in layers 1 and 4 (L1 and L4; Figure 1C, top), respectively (Jones, 2001); following injections in Po, brain slice recordings were made in the medial parietal association area (mPtA). To examine reciprocal CC connections, injections were made in either a secondary visual area (V2MM) to label feedforward afferents (Figure 1B, middle row) or anterior cingulate cortex (Cg) to label feedback afferents (Figure 1B, bottom row), and recordings made in Cg (Figure 1C, middle row) or V2MM (Figure 1C, bottom row), respectively. Acute coronal brain slices (500 µm thick) were prepared from mPtA, Cg, or V2MM, ipsilateral to viral injections (see Supplementary Materials for additional details). Responses to afferent stimulation were recorded using a multichannel electrode that spanned the cortical column under control, isoflurane (0-0.53 mM; 1-2 different concentrations, delivered in aqueous phase), and recovery conditions, as described previously (Hentschke et al., 2017). In a subset of slices, intracellular recordings were made from cortical pyramidal cells using whole-cell patch clamp to compare excitatory postsynaptic potentials (EPSPs) with extracellular responses, as described previously (Krause et al., 2017).

Optogenetic stimulation of afferent axon terminals

Synaptic responses were evoked using light stimulation of TC or CC axon terminals expressing ChR2, restricted to the cortical layer with the highest expression of YFP. Brief (0.5-2.0 msec) light pulses were delivered at a range of 1-10 different light intensities (1.5-15 mW) randomly interleaved with an inter-stimulus interval between 20 seconds and 2 minutes, directed over the cortical column containing the recording array. Synaptic responses were evoked using light stimulation of axon terminals expressing ChR2 via a fiberoptic cable (250 µm diameter; ThorLabs, Newton, NJ) coupled to a TTL-triggered LED (473 nm; Luxeon Star, Lethbridge, Alberta) or a patterned illumination device (Polygon400; Mightex, Pleasanton, CA). For animals injected in non-primary thalamus, the light was positioned in mPtA over either L1 (to activate TC matrix afferents) or L4 (to activate TC core afferents). For animals injected in Cg, the light was positioned in V2MM over L1 to activate feedback CC terminals. For animals injected in V2MM, the light was positioned in Cg over L2/3 to activate feedforward CC terminals.

Data analysis

Local field potentials (LFPs) were isolated by applying a bandpass filter at 1-300Hz (expanded to 1-1000Hz for latency calculations to avoid signal distortion) and averaged across trials of the same light stimulus intensity. The current source density (CSD; (Mitzdorf, 1985)) was calculated using the spline inverse CSD method (Pettersen et al., 2006) applied to the LFPs across 16 channels, such that negative values represent current sinks (i.e., inward transmembrane currents). Using the channel with the earliest

current sink onset, percent block was calculated by dividing the difference in sink amplitude between control and isoflurane conditions by the control sink amplitude. Experiments in which at least partial recovery was not observed were excluded. Intracellular recordings were bandpass filtered at 0.1-2000Hz and averaged across trials. Latency, amplitude, and half-widths were calculated for both CSD and intracellular recordings for comparison.

Linear Mixed-Effects Model

To evaluate the effect of isoflurane on sink magnitude in each of four afferent pathways, data were fit to a linear mixed-effects model.(Kristensen and Hansen, 2004) The use of a linear mixed effects model allows for principled analysis of hierarchical data by including both random and fixed effects in statistical models, such that non-independence among or within samples and experimental groups is considered. Our model included the response variable 'percent block by isoflurane', fixed effects of afferent pathway (TC core, TC matrix, CC feedforward, or CC feedback) and isoflurane concentration (0 to 0.53 mM), and random effect of slice (experiment) with random slope. To exclude the possibility that the effects we observe were simply due to degradation of responses over time, we included several 'sham' experiments (0 mM isoflurane) for each pathway and allowed for random intercepts in the model. A likelihood ratio test was used to compare a model with an interaction term between fixed effects of afferent pathway and concentration of isoflurane to a model with no such interaction; the model was significantly improved by including the interaction ($\chi^2(3) = 12.21$, $p = 0.0067$). After choosing this model, coefficient estimates were generated for

comparison of slopes between afferent pathways using t-tests with Satterthwaite's method for degrees of freedom.

Results

Synaptic responses under control conditions

For each afferent pathway, synaptic responses were elicited by directing light over the cortical layer with the highest density of YFP-labelled axon terminals (Figure 1C). We distinguished TC core versus matrix projections by activating thalamic terminals in cortical L4 and L1, respectively (Figure 1C, top row). CC feedforward projections terminated in the superficial layers, with heaviest labeling in L2/3 (Figure 1C, middle row). CC feedback projections terminated in all layers, though labeling density was highest in L1 (Figure 1C, bottom row), as observed previously (Oh et al., 2014; Zhang et al., 2014). For all afferent pathways, stimuli elicited short-latency (Table 1), putatively monosynaptic current sinks and EPSPs (Figure 2). The shortest latency current sinks were in L1 and L4 for TC matrix and core projections, respectively, and in L2/3 and L1 for CC feedforward and feedback projections, respectively. Durations of CC feedback synaptic responses were significantly longer than CC feedforward responses, and TC matrix longer than TC core (Table 1), consistent with the postulated modulatory roles of the former. Similar to previous results (Sherman and Guillery, 1998), TC core afferents, but not CC feedforward or feedback afferents, exhibited short-term synaptic depression (Figure 2B, Table 1). Short-term synaptic depression was also observed in TC matrix responses (Figure 2B, Table 1), as has been found in non-primary thalamic inputs to L1

of prefrontal cortex (Cruikshank et al., 2012) and L4 of secondary somatosensory cortex (Viaene et al., 2011).

We also recorded intracellular correlates of synaptic responses under control conditions to ensure that extracellular recordings were associated with EPSPs of typical latency and shape. For each stimulus pathway, intracellular recordings from L2/3 and L5 pyramidal cells showed a monosynaptic EPSPs following each of four light pulses delivered at 10Hz (Figure 2C). Latencies from intracellular recordings were comparable to corresponding parameters from CSD traces. Half-widths of EPSPs were notably longer than those of CSD current sinks (Table 1), as expected from the effect of membrane capacitance on the voltage signal.

Effect of isoflurane on monosynaptic current sink amplitude is pathway-specific

We investigated the anaesthetic sensitivity of the four synaptic pathways by applying isoflurane to brain slices, as described previously.(Hentschke et al., 2017) After eliciting synaptic responses to light stimulation under control conditions, isoflurane was applied at 0.0 to 0.53 mM, followed by recovery in regular artificial cerebrospinal fluid (CSF). Sink amplitudes were compared across drug conditions. We observed a striking difference in the sensitivity of CC feedback responses compared to the other three pathways (Figure 3). Current sinks elicited by activation of feedback CC terminals were substantially smaller in the presence of isoflurane compared to control and recovery periods, while the amplitudes of CC feedforward and both TC matrix and core

responses were largely unaffected. No significant effect of isoflurane on half-widths or latencies was observed for any pathway (Table 1).

The effect of isoflurane on sink magnitude was compared across slices, pathways, and isoflurane concentrations using a linear mixed-effects model (Figure 4). Responses from all pathways were blocked to some extent by isoflurane, but CC feedback responses were blocked to the greatest extent (Table 2). Pairwise comparisons of effects on all afferent pathways showed a significantly greater effect of isoflurane on CC feedback synaptic responses compared to TC matrix and CC feedforward pathways (Table 2), where CC feedback responses were suppressed by 14.9% (SD=2.5%) per 0.1 mM isoflurane ($p = 8.1e-8$). There was no significant difference in the effect of isoflurane between the TC matrix and TC core pathways ($p=0.41$).

Discussion

We show that CC feedback synaptic responses in non-primary cortex were suppressed by isoflurane more than TC matrix, TC core, and CC feedforward responses, complementing our previous study in primary auditory cortex(Raz et al., 2014) and indirect evidence from noninvasive electrophysiology and imaging studies (Ferrarelli et al., 2010; Schrouff et al., 2011; Lee et al., 2013). In predictive processing theories of brain function, feedback signals carry internally generated predictions about sensory observations, and feedforward signals carry information about mismatches between those predictions and observations. Conscious perception is the process of adjusting generative model parameters to explain away the sensory signals (Friston, 2005;

Dehaene and Changeux, 2011). It is within this context that anaesthetic suppression of CC feedback signals could act to disrupt awareness (Mashour and Hudetz, 2017).

The molecular mechanisms underlying differential sensitivity to isoflurane are of considerable practical interest. Anaesthetics have been shown to suppress synaptic transmission presynaptically via altering calcium influx, synaptic machinery, and vesicle release (Herring et al., 2009; Xie et al., 2013; Baumgart et al., 2015), and previous studies have demonstrated greater sensitivity of glutamatergic compared to GABAergic synapses (Westphalen and Hemmings, 2006; Westphalen et al., 2013). CC and TC synapses differ at the molecular and ultrastuctural level (Fremeau et al., 2004), which may contribute to their differential sensitivity to anaesthetics. Future experiments could test the sensitivity of these protein components to isoflurane in isolation.

The relative insensitivity of TC matrix responses to isoflurane observed here (Table 2, Figure 4) is surprising. TC matrix afferents overlap with CC feedback terminal fields (Oh et al., 2014), and may facilitate conscious sensory processing (Larkum, 2013; Castejon and Nunez, 2016). Indeed, activity in TC matrix cells is high during wakefulness and low during non-REM sleep, and activation of matrix thalamic nuclei during sleep promotes rapid awakening in mice and during anaesthesia promotes EEG desynchronization (Honjoh et al., 2018), suggesting a role for these cells in recovery of consciousness following sleep and anaesthesia (Saalmann, 2014; Crunelli et al., 2015). Our findings are incongruent with conclusions drawn by Liu and colleagues (Liu et al., 2013) regarding the effects of propofol anaesthesia on functional TC connectivity in human volunteers, which found that functional connectivity between nonspecific (i.e., non-primary) thalamic nuclei and a number of non-primary cortical areas is more

sensitive to propofol anaesthesia compared to specific thalamic connectivity. However, though useful for identifying distinct effects on correlated activity among brain areas, functional connectivity measures cannot distinguish directionality or indirect effects. Indeed, it is possible that the effects of propofol on TC connectivity observed by Liu's study reflect a decrease in synaptic efficacy at cortico-thalamic synapses or indirect effects on connectivity among cortical areas, rather than direct effects on thalamocortical connections we investigate here.

Raz and colleagues (Raz et al., 2014) showed that in primary auditory cortex, synaptic responses to electrical stimulation of either L1 or of feedback projections from V2 were preferentially suppressed by isoflurane compared to stimulation of core TC afferents. Because of their overlapping terminal fields, stimulation of L1 could engage both CC feedback and TC matrix afferents simultaneously, while activation of V2→A1 projections alone would be exclusively CC feedback; still, the authors found that isoflurane suppressed L1 and V2→A1 responses comparably. In this study, we use optogenetics to activate each afferent pathway independently. We note that the block by isoflurane of L1 or V2→A1 responses found by Raz and colleagues is comparable to the block of CC feedback responses alone that we find here: 13.5% decrease in sink amplitude/0.1mM isoflurane found previously compared to 14.9% decrease in sink amplitude/0.1mM isoflurane here, raising the possibility that sensitivity or density of TC matrix afferents may vary with cortical region. Thus, the functional roles of TC matrix inputs may also vary at different levels of the cortical hierarchy, taking on a modulatory role in primary sensory cortex, but acting as driving inputs in higher order areas (Viaene et al., 2011; Cruikshank et al., 2012).

The work presented here clearly and directly demonstrates the sensitivity of CC feedback connectivity to anaesthetics, and the relative insensitivity of thalamic and cortical feedforward connectivity. However, we note that although brain slice preparations are ideally suited to answer specific questions about pharmacological sensitivity of specific groups of synapses, these preparations have several limitations that are relevant to investigation of mechanisms of anesthesia and features of conscious sensory perception. For example, spontaneous cortical activity is very sensitive to anesthetic agents (Nourski et al., 2018), but spontaneous activity is already suppressed in brain slice preparations even under control conditions, likely due to the absence of neuromodulators and long-range excitatory connections (Stepanyants et al., 2009). These limitations motivate future experiments *in vivo* to determine the extent to neuromodulators and long-range connections and suppression of ongoing activity contribute to loss of consciousness under anesthesia.

The results we present here precipitate an intriguing question. Why is activity in higher order cortical areas especially sensitive to anaesthetics (Liu et al., 2012; Nourski et al., 2018) even though synaptic responses of their driving inputs, non-primary TC and feedforward CC afferents, are insensitive (Figure 4)? This question may relate to two distinguishing features of the dynamic brain: *activity* and *connectivity*. Our experimental approach of optogenetically activating synaptic terminals in cortical target areas directly tests the effect of isoflurane on *connectivity* by eliminating the prerequisite for *activity* of afferent pathways. However, these two features of neural networks are not entirely dissociable. For example, most anaesthetics (other than ketamine) suppress spiking activity and raise spike thresholds (Zurita et al., 1994; Antkowiak and Helfrichforster,

1998; Ries and Puil, 1999; Gaese and Ostwald, 2001; Hentschke et al., 2005; Hudetz et al., 2009), and changes in excitability will also contribute to changes in connectivity (Friston, 2011). Likewise, Hentschke and colleagues(Hentschke et al., 2017) showed that despite the preservation of early TC responses, evoked recurrent activity in brain slices was not sustained in the presence of isoflurane. The distinction between activity and connectivity may also help explain the diversity of results among EEG studies of changes in connectivity under anesthesia. For example, while some investigations have shown preferential suppression of long-range intracortical connectivity (Ferrarelli et al., 2010; Ku et al., 2011; Lee et al., 2013), others have shown increases (Murphy et al., 2011; Lee et al., 2017). It is possible that the latter scenario arises in spite of decreases in synaptic strength when activity becomes synchronized and thus strongly coordinated between regions.

Questions remain as well regarding the relevance of CC feedback connections to consciousness. Studies of the neural basis of consciousness, as well as investigations of mechanisms of loss of consciousness under anaesthesia such as this study, are correlative in nature. Feedback connections are relevant for sensory processing and are particularly sensitive to anaesthetics, but it is unlikely that suppression of feedback inputs alone is responsible for loss of consciousness. Demonstrating the contribution of differential sensitivity of feedback connections to anaesthetic LOC will require causal manipulations *in vivo* that can explicitly link activity and connectivity within cortico-thalamic networks to distinct features of consciousness. How sensitivity of distinct synaptic inputs, as we observe here, synergistically interacts with intrinsic and network-level changes observed during anaesthesia in the intact brain will help elucidate the

spatiotemporal relationships within thalamocortical networks that subserve consciousness.

Conflict of Interest: The authors declare no competing financial interests.

Funding: *Supported by National Institutes of Health (R01 GM109086 to M. I. Banks), and the Department of Anesthesiology, School of Medicine and Public Health, University of Wisconsin, Madison, WI.*

Acknowledgements: *The authors thank Donata Oertel for comments on the manuscript, and Sean M. Grady for technical assistance.*

Contributions of Authors

C.M.: Study design, data collection, data analysis, manuscript preparation

B.K.: Data analysis, manuscript preparation

M.B.: Study design, data analysis, manuscript preparation

References

Alkire MT (2008) Loss of effective connectivity during general anesthesia. IntAnesthesiolClin 46:55-73.

Antkowiak B, Helfrichforster C (1998) Effects of small concentrations of volatile anesthetics on action potential firing of neocortical neurons in vitro. Anesthesiology 88:1592-1605.

Baumgart JP, Zhou ZY, Hara M, Cook DC, Hoppa MB, Ryan TA, Hemmings HC, Jr. (2015) Isoflurane inhibits synaptic vesicle exocytosis through reduced Ca2+ influx, not Ca2+-exocytosis coupling. Proc Natl Acad Sci U S A 112:11959-11964.

Castejon C, Nunez A (2016) Cortical Neural Computation by Discrete Results Hypothesis. Front Neural Circuits 10:81.

Crick F, Koch C (2003) A framework for consciousness. Nat Neurosci 6:119-126.

Cruikshank SJ, Ahmed OJ, Stevens TR, Patrick SL, Gonzalez AN, Elmaleh M, Connors BW (2012) Thalamic Control of Layer 1 Circuits in Prefrontal Cortex. The Journal of Neuroscience 32:17813-17823.

Crunelli V, David F, Lőrincz ML, Hughes SW (2015) The thalamocortical network as a single slow wave-generating unit. Current Opinion in Neurobiology 31:72-80.

Dehaene S, Changeux JP (2011) Experimental and theoretical approaches to conscious processing. Neuron 70:200-227.

Ferrarelli F, Massimini M, Sarasso S, Casali A, Riedner BA, Angelini G, Tononi G, Pearce RA (2010) Breakdown in cortical effective connectivity during midazolam-induced loss of consciousness. Proc Natl Acad Sci USA 107:2681-2686.

Fremeau RT, Voglmaier S, Seal RP, Edwards RH (2004) VGLUTs define subsets of excitatory neurons and suggest novel roles for glutamate. Trends in Neurosciences 27:98-103.

Friston K (2005) A theory of cortical responses. Philos Trans R Soc Lond B Biol Sci 360:815-836.

Friston KJ (2011) Functional and Effective Connectivity: A Review. Brain Connectivity 1:13-36.

Gaese BH, Ostwald J (2001) Anesthesia changes frequency tuning of neurons in the rat primary auditory cortex. J Neurophysiol 86:1062-1066.

Guillery RW, Sherman SM (2002) Thalamic Relay Functions and Their Role in Corticocortical Communication: Generalizations from the Visual System. Neuron 33:163-175.

Hentschke H, Schwarz C, Antkowiak B (2005) Neocortex is the major target of sedative concentrations of volatile anaesthetics: strong depression of firing rates and increase of GABAA receptor-mediated inhibition. Eur J Neurosci 21:93-102.

Hentschke H, Raz A, Krause BM, Murphy CA, Banks MI (2017) Disruption of cortical network activity by the general anesthetic isoflurane. Br J Anaesth 119:685-696.

Herring BE, Xie Z, Marks J, Fox AP (2009) Isoflurane inhibits the neurotransmitter release machinery. J Neurophysiol 102:1265-1273.

Honjoh S, Sasai S, Schiereck SS, Nagai H, Tononi G, Cirelli C (2018) Regulation of cortical activity and arousal by the matrix cells of the ventromedial thalamic nucleus. Nature Communications 9:2100.

Hudetz AG, Vizuete JA, Imas OA (2009) Desflurane selectively suppresses long-latency cortical neuronal response to flash in the rat. Anesthesiology 111:231-239.

Jones EG (2001) The thalamic matrix and thalamocortical synchrony. Trends in neurosciences 24:595-601.

Koch C, Massimini M, Boly M, Tononi G (2016) Neural correlates of consciousness: progress and problems. Nat Rev Neurosci 17:307-321.

Krause BM, Murphy CA, Uhlrich DJ, Banks MI (2017) PV+ Cells Enhance Temporal Population Codes but not Stimulus-Related Timing in Auditory Cortex. Cereb Cortex.

Kristensen M, Hansen T (2004) Statistical analyses of repeated measures in physiological research: a tutorial.

Ku SW, Lee U, Noh GJ, Jun IG, Mashour GA (2011) Preferential inhibition of frontal-to-parietal feedback connectivity is a neurophysiologic correlate of general anesthesia in surgical patients. PLoSOne 6:e25155.

Larkum M (2013) A cellular mechanism for cortical associations: an organizing principle for the cerebral cortex. Trends Neurosci 36:141-151.

Lee M, Sanders RD, Yeom S-K, Won D-O, Seo K-S, Kim HJ, Tononi G, Lee S-W (2017) Network Properties in Transitions of Consciousness during Propofol-induced Sedation. Scientific Reports 7:16791.

Lee U, Ku S, Noh G, Baek S, Choi B, Mashour GA (2013) Disruption of frontal-parietal communication by ketamine, propofol, and sevoflurane. Anesthesiology 118:1264-1275.

Liu X, Lauer KK, Ward BD, Li SJ, Hudetz AG (2013) Differential effects of deep sedation with propofol on the specific and nonspecific thalamocortical systems: a functional magnetic resonance imaging study. Anesthesiology 118:59-69.

Liu X, Lauer KK, Ward BD, Rao SM, Li SJ, Hudetz AG (2012) Propofol disrupts functional interactions between sensory and high-order processing of auditory verbal memory. Hum Brain Mapp 33:2487-2498.

Llinas R, Ribary U, Contreras D, Pedroarena C (1998) The neuronal basis for consciousness. Philos Trans R Soc Lond B Biol Sci 353:1841-1849.

Mashour GA (2013) Cognitive unbinding: a neuroscientific paradigm of general anesthesia and related states of unconsciousness. Neurosci Biobehav Rev 37:2751-2759.

Mashour GA, Hudetz AG (2017) Bottom-Up and Top-Down Mechanisms of General Anesthetics Modulate Different Dimensions of Consciousness. Front Neural Circuits 11:44.

Mitzdorf U (1985) Current source-density method and application in cat cerebral cortex: investigation of evoked potentials and EEG phenomena. Physiol Rev 65:37-100.

Murphy M, Bruno MA, Riedner BA, Boveroux P, Noirhomme Q, Landsness EC, Brichant JF, Phillips C, Massimini M, Laureys S, Tononi G, Boly M (2011) Propofol anesthesia and sleep: a high-density EEG study. Sleep 34:283-291A.

Neske GT (2015) The Slow Oscillation in Cortical and Thalamic Networks: Mechanisms and Functions. Front Neural Circuits 9:88.

Nourski KV, Steinschneider M, Rhone AE, Kawasaki H, Howard MA, 3rd, Banks MI (2018) Auditory Predictive Coding across Awareness States under Anesthesia: An Intracranial Electrophysiology Study. J Neurosci 38:8441-8452.

Oh SW et al. (2014) A mesoscale connectome of the mouse brain. Nature 508:207-214.

Paxinos G, Franklin KBJ (2003) The Mouse Brain in Stereotaxic Coordinates, 2 Edition. San Diego, CA: Academic Press.

Pettersen KH, Devor A, Ulbert I, Dale AM, Einevoll GT (2006) Current-source density estimation based on inversion of electrostatic forward solution: effects of finite extent of neuronal activity and conductivity discontinuities. JNeurosciMethods 154:116-133.

Raz A, Grady SM, Krause BM, Uhlrich DJ, Manning KA, Banks MI (2014) Preferential effect of isoflurane on top-down versus bottom-up pathways in sensory cortex. Front Syst Neurosci 8.

Ries CR, Puil E (1999) Mechanism of anesthesia revealed by shunting actions of isoflurane on thalamocortical neurons. J Neurophysiol 81:1795-1801.

Saalmann YB (2014) Intralaminar and medial thalamic influence on cortical synchrony, information transmission and cognition. Front Syst Neurosci 8:83.

Schrouff J, Perlbarg V, Boly M, Marrelec G, Boveroux P, Vanhaudenhuyse A, Bruno MA, Laureys S, Phillips C, Pelegrini-Issac M, Maquet P, Benali H (2011) Brain functional integration decreases during propofol-induced loss of consciousness. Neuroimage 57:198-205.

Sherman SM, Guillery RW (1998) On the actions that one nerve cell can have on another: distinguishing "drivers" from "modulators". Proc Natl Acad Sci USA 95:7121-7126.

Stepanyants A, Martinez LM, Ferecsko AS, Kisvarday ZF (2009) The fractions of short- and long-range connections in the visual cortex. Proc Natl Acad Sci U S A 106:3555-3560.

Viaene AN, Petrof I, Sherman SM (2011) Properties of the thalamic projection from the posterior medial nucleus to primary and secondary somatosensory cortices in the mouse. Proc Natl Acad Sci USA 108:18156-18161.

Westphalen RI, Hemmings HC, Jr. (2006) Volatile anesthetic effects on glutamate versus GABA release from isolated rat cortical nerve terminals: 4-aminopyridine-evoked release. JPharmacolExpTher 316:216-223.

Westphalen RI, Desai KM, Hemmings HC, Jr. (2013) Presynaptic inhibition of the release of multiple major central nervous system neurotransmitter types by the inhaled anaesthetic isoflurane. Br J Anaesth 110:592-599.

Xie Z, McMillan K, Pike CM, Cahill AL, Herring BE, Wang Q, Fox AP (2013) Interaction of anesthetics with neurotransmitter release machinery proteins. Journal of neurophysiology 109:758-767.

Zhang S, Xu M, Kamigaki T, Hoang Do JP, Chang WC, Jenvay S, Miyamichi K, Luo L, Dan Y (2014) Long-range and local circuits for top-down modulation of visual cortex processing. Science 345:660-665.

Zurita P, Villa AEP, Deribaupierre Y, Deribaupierre F, Rouiller EM (1994) Changes of Single-Unit Activity in the Cats Auditory Thalamus and Cortex Associated to Different Anesthetic Conditions. Neurosci Res 19:303-316.

Supplementary Methods

Injection of viral vector and expression of channelrhodopsin

All experiments were performed using male B6CBAF1/J mice (F1 hybrid of C57/B6 and CBA/J; The Jackson Laboratory, Bar Harbor, ME). Several weeks (7.4 ± 2.6) before tissue was harvested for brain slices, viral constructs containing genes for channelrhodopsin and the fluorescent reporter protein YFP (AAV2-hSyn-hChR2(H134R)-eYFP; provided by K. Deisseroth, Stanford University via University of North Carolina Vector Core) were injected unilaterally into 3- to 5-week-old mice. Injections were made in posterior thalamus (AP: -2.25 mm, ML: 1.25 mm, DV: -3.35 mm; vol: □1□l), anterior cingulate cortex (AP: 0.2 mm, ML: 0.3 mm, DV: 0.9 mm; □0.8□l), and a secondary visual area (AP: -2.7, ML: 1.5, DV: 0.7; □0.8□l) to independently test TC, CC feedback, and CC feedforward pathways, respectively.

Slices and solutions

To prepare acute brain slices, mice were anesthetized using isoflurane and decapitated, and slices were collected at 0-4°C in 'cutting' artificial CSF consisting of (in mM) 111 NaCl, 35 $NaHCO_3$, 20 HEPES, 1.8 KCl, 1.05 $CaCl_2$, 2.8 $MgSO_4$, 1.2 KH_2PO_4, and 10 glucose, saturated with 95% O_2/5% CO_2. Slices were immediately placed in warm cutting artificial CSF (34°C) and gradually cooled to room temperature. After a one-hour equilibration period, one slice was transferred to the recording chamber and perfused at 6-8 mL/min with warm (30-32°C) regular artificial CSF consisting of (in mM) 111 NaCl, 35 $NaHCO_3$, 20 HEPES, 1.8 KCl, 2.1 $CaCl_2$, 1.4 $MgSO_4$, 1.2 KH_2PO_4, and 10 glucose,

saturated with 95% O_2/5% CO_2. Slices were allowed to recover for at least one hour in the recording chamber before commencing data collection.

Anesthetic application

During each experiment, extracellular responses were recorded under control, isoflurane (0-0.53 mM; 1-2 different concentrations per experiment), and recovery conditions, each separated by a 20-minute wash-in period. To apply isoflurane to slices in the aqueous phase, gaseous isoflurane was dissolved into artificial CSF. The partition coefficient of isoflurane ($\lambda = 1.2$) was used to determine the pre-equilibrium gas concentration of isoflurane.[52] Sealed Teflon bags (cat. No. 10-923-5; Fisher Scientific, Hampton, NH) were filled in a 1:1 gas-to-liquid ratio with regular artificial CSF (saturated with 95% O_2/5% CO_2) and a gas mixture of isoflurane and 95% O_2/5% CO_2. Bags were shaken for at least 1 hour to allow isoflurane phase equilibration (The Belly Dancer; Stovall Life Science Inc., NC). Equilibrated isoflurane concentrations were confirmed by measuring the gas phase concentration (Poet II Anesthesia Monitor; Criticare Systems, Waukesha, WI). Equivalent millimolar concentrations of isoflurane were calculated from gas phase concentrations, where C_{aq} (mM) = 0.44614 ·α·P(% atm)(%), where α=1.08 at 25°C.[53] Physiological effects of volatile anesthetics are particularly sensitive to temperature;[53, 54] loss of righting reflex, which occurs at ~0.9% in mice *in vivo*,[55] would occur (hypothetically) at approximately 0.4% isoflurane at 25°C.[53] Thus, the approximated corresponding concentration for loss of righting reflex in our experiments is 0.19 mM isoflurane.

Electrophysiological recordings

Cortical responses to afferent stimulation (see below) were recorded using a 16x1 multichannel silicon electrode array (A16x1-2mm-100-177-A16; Neuronexus Technologies, Ann Arbor, MI) inserted orthogonally to the white matter, such that the recording sites spanned a single cortical column (see Figure 1C, top right and bottom right). Extracellular signals were amplified (2000x), filtered (0.1-10 kHz; Lynx-8; Neuralynx, Bozeman, MT), and digitized at 40 kHz (Digidata 1440A; Molecular Devices, Sunnyvale, CA). In a subset of slices, whole-cell current-clamp recordings were obtained from somata of cortical cells to compare excitatory postsynaptic potentials (EPSPs) with extracellular responses. Layer 2/3 (L2/3) and layer 5 (L5) pyramidal cells were visualized using infrared differential interference contrast microscopy and targeted based on morphology. Glass patch-clamp pipettes (KG-33, 1.7 mm OD, 1.1 mm ID; King Precision Glass, Claremont, CA) were pulled to impedances of 3-5 MΩ and filled with intracellular solution (in mM: 140 K-gluconate, 10 NaCl, 10 HEPES, 0.1 EGTA, 4 MgATP, and 0.3 NaGTP; pH 7.2). Following gigaseal formation, whole-cell configuration was achieved, and pyramidal cell identity was assumed based on characteristic spiking responses to depolarizing current pulses. Intracellular voltage signals were low-pass filtered at 4 kHz and digitized at 40 kHz.

Data analysis

After filtering and averaging the data as described in the Methods, the latency and half-width of each signals were calculated for CSD and intracellular data. For CSD, the latency to the onset of the synaptic response was defined as the first crossing of a

threshold 2.5 times the standard deviation of the mean of a 20-msec pre-stimulus baseline of the CSD signal. Half-width was calculated as the time between two crossings of half the maximum amplitude of the current sink. Using the channel with the earliest current sink onset, response magnitude was defined as the peak in the CSD trace within 30 msec following current onset. Percent block was calculated by dividing the difference in sink amplitude between control and isoflurane conditions by the control sink amplitude. A standard one-way ANOVA was used to compare latencies and half-widths of synaptic responses among pathways (Table 1).

Intracellular recordings were bandpass filtered at 0.1-2000Hz and averaged across trials. The latency to the onset of EPSPs was defined as the time for the voltage signal to exceed five times the standard deviation of the mean of a 20-msec pre-stimulus baseline of the derivative voltage signal. Half-widths were calculated in a similar fashion to CSD recordings.

Figure 1

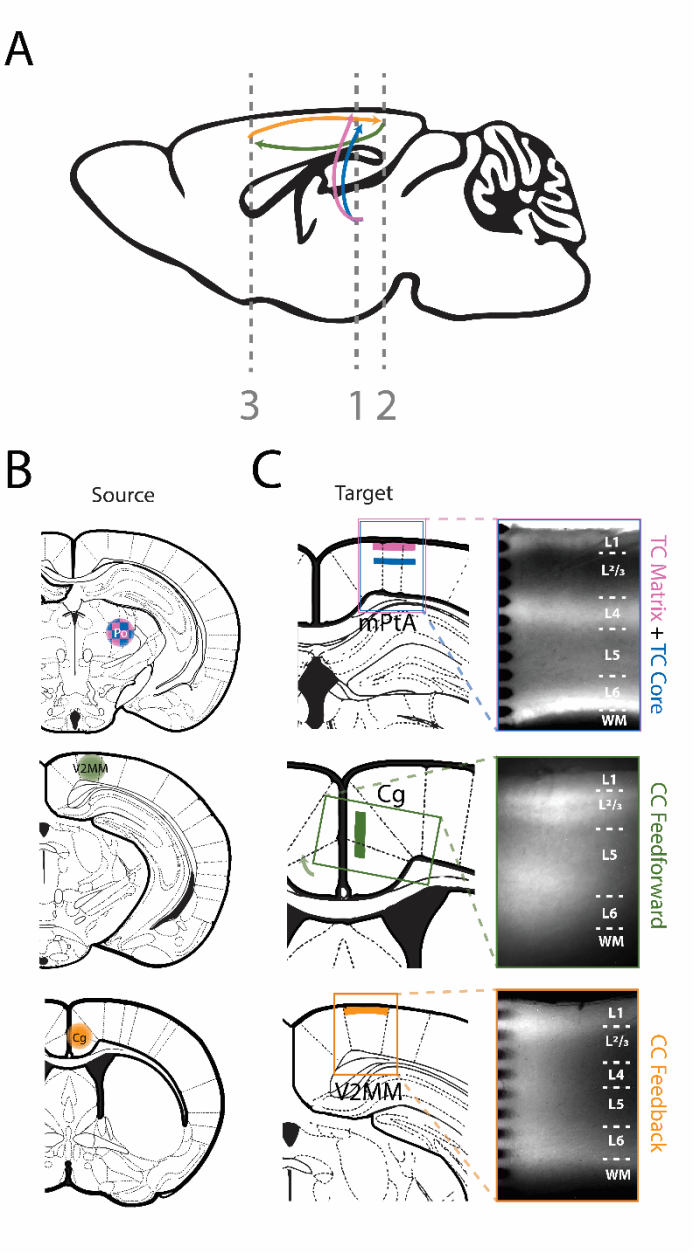

Figure 1. *Optogenetic activation of four independent afferent pathways in neocortex.* (A) A schematic showing projection patterns of four distinct afferent pathways: TC matrix (pink), TC core (blue), CC feedforward (green), and CC feedback (gold). Vertical dashed lines show coronal planes of section for brain slices in C. (B) A viral vector containing ChR2 and YFP reporter was injected into the Po (top), V2MM (V2MM; middle), or Cg (bottom). Color scheme of injection is representative of

pathway shown in A. Note that TC core (blue) and TC matrix (pink) cells are interspersed in Po, as reflected by the checkered pattern in the schematic. (C) Atlas (left) and fluorescence (right) images of recording area. Shaded colored regions in atlas images represent ChR2 and YFP reporter expressed in axon terminals following injections shown in B, in mPtA (top), Cg (middle), and V2MM (bottom). Only the terminal regions optically stimulated in this report are shaded. Colored boxes in the atlas images represent the approximate recording area shown in fluorescence images. Layer boundaries are delineated with dotted lines in fluorescence images. The tips of the multichannel recording array are visible on the left-hand side of the fluorescence images in the top and bottom panels. Abbreviations: TC = thalamocortical; CC = corticocortical; Po = posterior thalamus; V2MM = secondary visual area; Cg = anterior cingulate cortex; mPtA = medial parietal association area; WM = white matter.(Paxinos and Franklin, 2003)

Figure 2

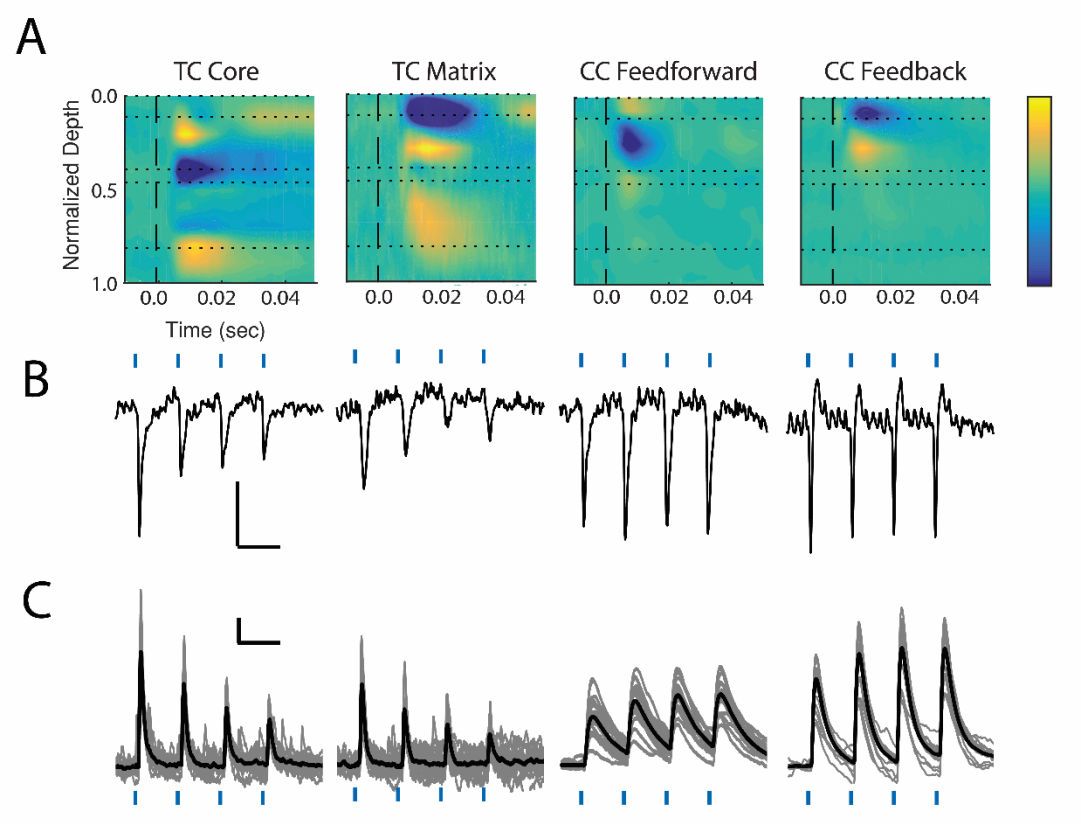

Figure 2. *Synaptic responses evoked under control conditions. (*A) Representative examples of responses following a single light pulse (473 nm, black dashed line) used to activate ChR2-expressing axon terminals of four afferent pathways to cortex (left to right): TC core, TC matrix, CC feedforward, and CC feedback. CSD color plots are shown, where current sinks (inward-going transmembrane current) are blue (scale: -2.0 to 2.0 µA mm^{-3} for TC matrix and CC feedforward, -1.0 to 1.0 µA mm^{-3} for TC core and CC feedback) and layer boundaries are shown with horizontal dotted lines. (B) CSD signals evoked as in A, but with a train of four light pulses (blue tick marks) delivered at 10 Hz. Signals shown were isolated from the channel exhibiting the earliest current sink in A. Horizontal scale bars: 100 msec. Vertical scale bar represents 1.0 µA mm^{-3} for TC matrix and CC feedforward traces, and 2.0 µA mm^{-3} for TC core and CC feedback traces. (C) Whole-cell current-clamp recordings from four cortical pyramidal cells demonstrating intracellular analogs of CSDs shown in B (not

necessarily from same experiment); excitatory postsynaptic potentials were evoked by a train of four light pulses at 10 Hz. Horizontal scale bar: 100 msec. Vertical scale bar represents 0.5 mV for TC matrix, TC core, and CC feedforward traces, and 2.0 mV for CC feedback traces.

Figure 3

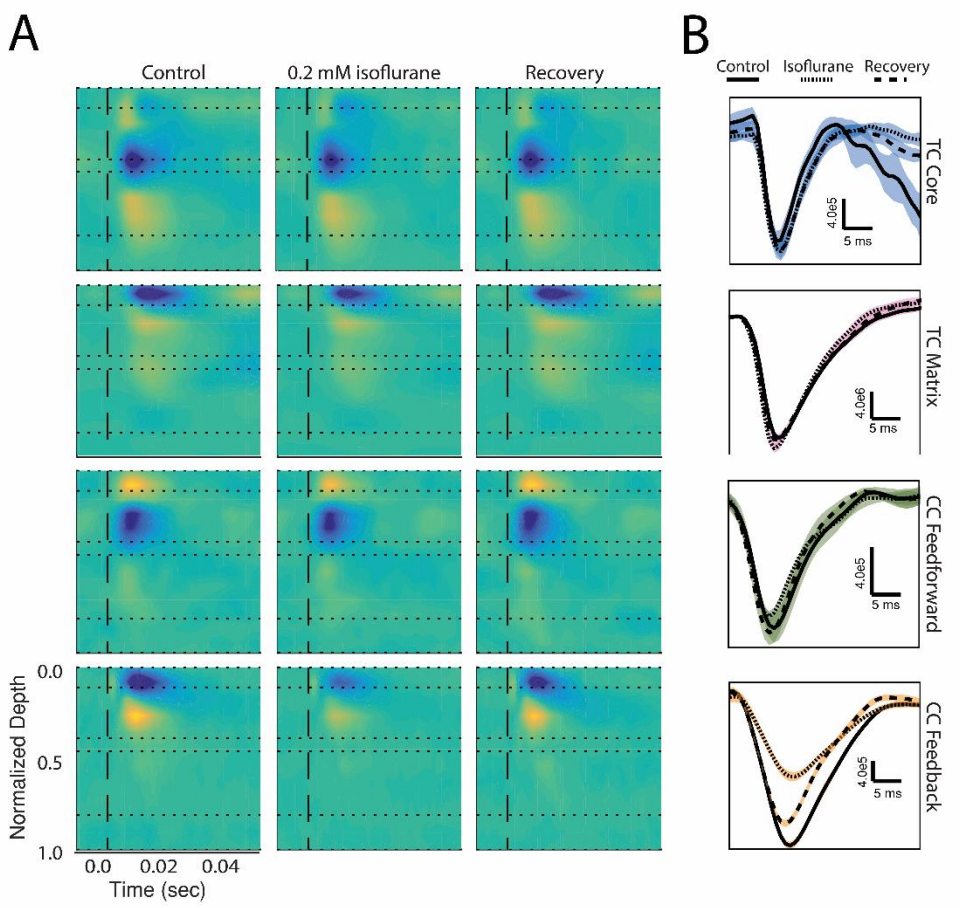

Figure 3. *Current sinks evoked in each of four afferent pathways across control, isoflurane, and recovery.* (A) CSD color plots comparing evoked synaptic responses across control (A, left column), 0.2 mM isoflurane (A, middle column), and recovery (A, right column) for representative examples of each of four afferent pathways to cortex, from top to bottom row: TC core, TC matrix, CC feedforward, and CC feedback; color scale: -2.0 to 2.0 µA mm^{-3} for TC core and CC feedback, -1.0 to 1.0 µA mm^{-3} for CC feedforward, and -5.0 to 5.0 µA mm^{-3} for TC matrix. (B) Signal from the channel with the earliest sink were used to compare synaptic effects across control (solid), 0.2 mM isoflurane (dotted), and recovery (dashed). Shaded regions, which are colored using color scheme in Figure 1, indicate ± 1 SD among trials.

Figure 4

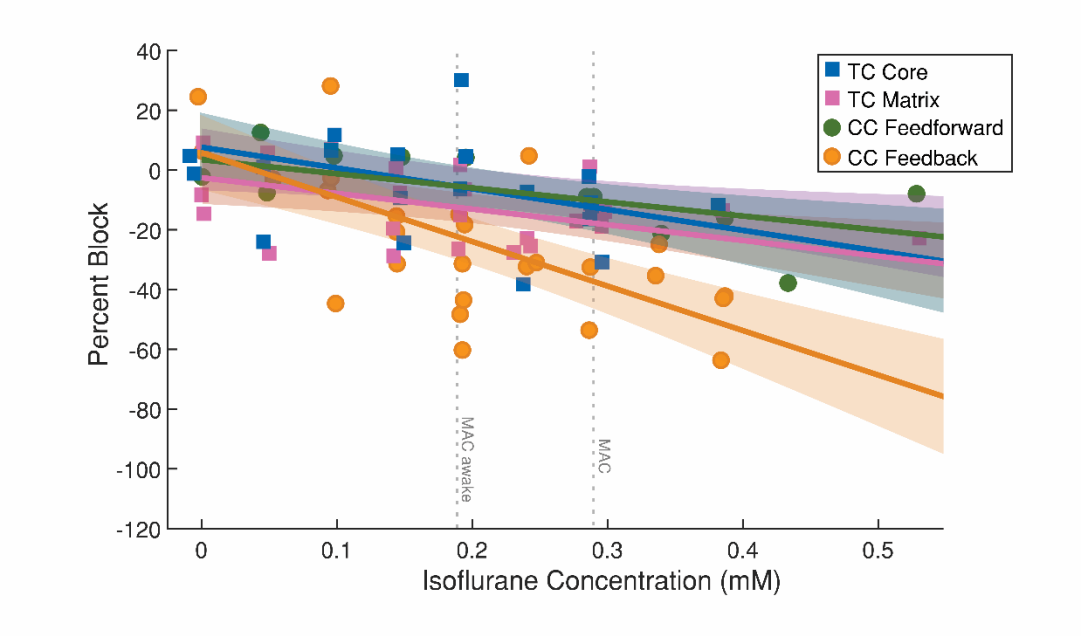

Figure 4. *CC feedback cortical afferents are preferentially suppressed under isoflurane.* Results from individual experiments (individual markers) and model fits (i.e. percent block as a function of concentration of isoflurane; solid lines) with 95% confidence interval (shaded) are shown. Responses evoked by stimulation of CC feedback afferents to cortical layer 1 (gold) are suppressed to a greater extent under isoflurane than CC feedforward (green) and both TC matrix (pink) and core (blue) pathways, especially at and above a concentration corresponding to □0.9% isoflurane, the concentration at which loss of consciousness occurs in mice.

Table 1

		Latency (msec)	Half-width (msec)	Paired pulse ratio
TC Core	CSD (n=16)	4.67 (1.85)	8.27 (3.06)*	0.64 (0.23)
	Intracellular (n=7)	3.57 (1.01)	30.00 (15.90)	0.62 (0.22)
TC Matrix	CSD (n=23)	5.11 (1.69)	12.13 (2.62)*	0.72 (0.19)
	Intracellular (n=10)	4.63 (1.87)	26.10 (14.27)	0.61 (0.16)
CC Feedforward	CSD (n=8)	3.02 (1.01)	7.81 (1.31)†	1.17 (0.37)
	Intracellular (n=4)	3.63 (0.78)	32.75 (16.46)	1.04 (0.13)
CC Feedback	CSD (n=21)	4.15 (1.97)	9.42 (1.77)†	0.90 (0.31)
	Intracellular (n=4)	3.69 (2.29)	27.49 (14.31)	1.04 (0.22)

Table 1. Properties of post-synaptic responses. Values are presented as mean (SD). Parameters from extracellular data were calculated using the CSD signal from the channel that showed the earliest onset of the inward-going current following the light stimulus. Half-widths are width of current sink or EPSP signal at half the maximum amplitude. Comparisons of half-widths of the CSD signal were made within TC* and within CC† groups using a standard one-way ANOVA; TC matrix responses were longer than TC core responses (*$F(1\ 41) = 19.82$, $P < 0.0001$) and CC feedback half-widths were longer than CC feedforward (†$F(1\ 34) = 7.70$, $P = 0.009$).

Table 2

Effect on distinct pathways (% block per 0.1 mM isoflurane)			
Pathway	**Estimate**	**95% CI**	***P*-value**
TC core	-7.03	[-12.2, -2.25]	0.0059
CC feedforward	-4.17	[-9.89, 0.91]	0.14
TC matrix	-5.65	[-9.88,-1.18]	0.0076
CC feedback	-14.9	[-20.0, -10.1]	3.09e-8

Pairwise comparison of slopes			
Comparison	**Estimate**	**95% CI**	***P*-value**
CC feedback – TC core	-7.90	[-14.9,-1.35]	0.023
CC feedback – CC feedforward	-10.8	[-17.4,-3.49]	0.0045
CC feedback – TC matrix	-9.29	[-15.9,-3.42]	0.0040
TC core – TC matrix	-1.38	[-7.67,4.71]	0.64
TC core – CC feedforward	-2.85	[-11.4,4.42]	0.45
CC feedforward – TC matrix	1.47	[-5.69,8.27]	0.67

Table 2. Comparison of effect of isoflurane on synaptic responses of four distinct afferent pathways to cortex. Slopes of the effect of isoflurane on each pathway with reference to no slope (shown as % block per 0.1 mM isoflurane) are shown, followed by pairwise comparison of effects slopes between any two pathways, represented as the difference between individual slopes. Note that the effect isoflurane on CC feedback responses is significantly greater than CC feedforward and both TC core and matrix responses.

Chapter 5

Cell type-specific effects of isoflurane on two distinct afferent inputs to cortical layer 1.

This chapter will be submitted for publication as:

Murphy CM, [], Banks MI (2020). Cell type-specific effects of isoflurane on two distinct afferent inputs to cortical layer 1.

Abstract

While their behavioral effects are well-characterized, the mechanisms by which anesthetics induce loss of consciousness are largely unknown. Anesthetics may disrupt integration and propagation of information in thalamocortical networks. Recent studies have shown that isoflurane diminishes synaptic responses of thalamocortical (TC) and corticocortical (CC) afferents in a pathway-specific manner. However, whether the synaptic effects of isoflurane observed in extracellular recordings persist at the cellular level has yet to be explored. Here, we activate TC and CC layer 1 inputs in non-primary mouse neocortex in ex vivo brain slices and explore the degree to which isoflurane modulates synaptic responses in pyramidal cells and in two inhibitory cell populations, somatostatin-positive (SOM+) and parvalbumin-positive (PV+) interneurons. We show that the effects of isoflurane on synaptic responses and intrinsic properties of these cells varies among cell type and by cortical layer. Layer 1 afferents inputs to L4 pyramidal

cells were suppressed by isoflurane at both TC and CC synapses, while those to L2/3 pyramidal cells and PV+ interneurons were not. TC inputs to SOM+ cells were rarely observed at all, while CC inputs to SOM+ interneurons were robustly suppressed by isoflurane, These results suggest a mechanism by which isoflurane disrupts integration and propagation of incoming cortical signals.

Introduction

Anesthetics may ultimately influence both the level and contents of consciousness via actions on corticothalamic circuits, disrupting integration of information throughout the cortical hierarchy (Crick and Koch, 2003; Dehaene and Changeux, 2011; Koch et al., 2016). Activity in higher order cortical areas is particularly sensitive to anesthetics(Nourski et al., 2017; Nourski et al., 2018), as is corticocortical feedback connectivity (Ferrarelli et al., 2010; Boly et al., 2012; Liu et al., 2012; Raz et al., 2014; Mashour and Hudetz, 2017; Murphy et al., 2019). In addition to cortical effects, higher order thalamocortical connectivity is suppressed during both sleep(Picchioni et al., 2014) and anesthesia(Langsjo et al., 2012; Liu et al., 2013; Akeju et al., 2014). Activation of non-specific thalamic nuclei during anesthetic-induced unconsciousness(Redinbaugh et al., 2020) and non-REM sleep(Honjoh et al., 2018) promotes behavioral arousal, implicating higher order thalamic centers as enablers of consciousness.

Recent studies from our lab have shown that in ex vivo slices, isoflurane diminishes synaptic responses in a pathway-specific manner (Raz et al., 2014; Murphy et al., 2019). Despite overlapping terminal fields in layer 1, corticocortical feedback

afferents to higher order cortex were preferentially suppressed by isoflurane compared to non-primary thalamocortical inputs. However, extracellular recordings used in these investigations capture summed effects across all synapses, leaving open questions as to whether observed effects are consistent across post-synaptic targets. For example, differential effects on inhibitory interneurons compared to excitatory cells may shift the balance of excitation and inhibition(Haider et al., 2013; Xue et al., 2014), disrupting integration of inputs in pyramidal cell dendrites or constraining the output of the cortical column. Moreover, superficial and deep layers may operate within functionally separate domains, where cells in superficial layers primarily carry out corticocortical interactions, and those in deep layers facilitate interactions with lower cortical and subcortical targets in the feedback direction (Douglas et al., 1989; Douglas and Martin, 2004; Douglas and Martin, 2007; Binzegger et al., 2009). As such, differential effects of anesthetics on cells residing in different layers may provide further insight into the functional roles of discrete cortical networks and the mechanisms that subserve the breakdown of connectivity observed during anesthesia.

Here, we investigate the effect of isoflurane on independently activated higher order thalamocortical and corticocortical inputs to layer 1 of non-primary neocortex in brain slices. We evaluate the pathway- and cell type-specific effects of isoflurane on synaptic responses recorded in pyramidal cells in layers 2-5 and in two subpopulations of inhibitory cells, SOM+ and PV+ interneurons.

Methods

Intracellular whole cell patch clamp recordings were conducted in current clamp mode from pyramidal cells in layers 2-5, parvalbumin-positive interneurons, or somatostatin-positive interneurons; extracellular multichannel recordings were collected concurrently. Cell types were identified either by Cre-dependent expression of td-Tomato reporter (for parvalbumin-positive and somatostatin-positive interneurons) or by morphology (pyramidal cells). To further guide identification of cell types, each cell's response to 600 msec current steps was evaluated as previously described (Krause et al., 2017). All signals were low-pass filtered at 10 kHz and digitized at 40 kHz.

To activate either POm or Cg afferents, blue light was delivered exclusively to layer 1 (150 µm diameter, 470 nm; Polygon400, Mightex Systems, Toronto, Ontario). For each trial, synaptic responses were evoked using four brief pulses of light (2 msec; 10 Hz) at one of at least five light intensities randomly selected from a range of intensities (0.022-2.2 mW). Each trial was separated by ten seconds, and at least eight trials were conducted for each light intensity, randomly interleaved.

Signals from each of 16 extracellular channels were filtered (bandpass filter, 1-300Hz) to yield local field potentials used to calculate the current source density (CSD; (Mitzdorf, 1985)) with the spline inverse method(Pettersen et al., 2006). The signal in layer 1 with the shortest latency current sink (inward transmembrane current) was used for further analysis. Intracellular signals were filtered (bandpass filter, 0.1-1000 Hz). Responses were averaged across trials of the same stimulus intensity. Responses to a single stimulus intensity were selected for detailed analysis. This intensity was the minimum light intensity for which at least 50% of trials (8-10 trials per intensity) evoked a response with <1 msec latency jitter.

Response amplitude was defined as the peak of the signal within 50 msec of the stimulus (first pulse only). Paired pulse ratio was computed for intracellular recordings, calculated by dividing the PSP amplitude of second pulse by the PSP amplitude of first pulse. POm- and Cg-evoked responses were compared across control, isoflurane (0.24-0.29 mM), and recovery conditions. To exclude the possibility that effects of isoflurane were due to response degradation over time, the average of control and recovery measures were used as a baseline for comparison to isoflurane.

A linear mixed effects model was used to evaluate the pathway- and cell type-dependent effects of isoflurane on a variety of intrinsic and evoked response properties of individual cells. Fixed effects were cell type (L2/3 Pyr, L4 Pyr, L5 Pyr, SOM+, or PV+) and drug condition (baseline or isoflurane), as well as afferent pathway (POm or Cg) for evoked responses. Interaction terms between isoflurane and each of the other fixed effects were also included, as well as a three-way interaction term representing interactions between cell type and pathway of drug effects; random effects were slice experiment and cell with random slopes for drug condition. For amplitude and input resistance measures, heteroscedasticity was corrected by log transforming response variables. To allow for direct comparison among cell types and pathways, all isoflurane effects are reported relative to baseline.

Results

Activation of TC and CC inputs to layer 1 elicit short-latency synaptic responses

Synaptic responses from TC and CC afferents were elicited by activating channelrhodopsin in afferent axon terminals in layer 1. Brief pulses of light evoked short

latency current sinks in layer 1 (Table 1). No effect of afferent pathway was observed for baseline amplitude ($t(29) = 0.41$, $p=0.69$) or latency ($t(29) = 0.26$, $P = 0.80$) of layer 1 current sinks. Evoked currents in layer 1 precipitated post-synaptic potentials in pyramidal cells in layers 2-5 (Table 2; Figure 2B,D), and in two subpopulations of inhibitory interneurons, SOM+ and PV+ cells (Table 2; Figure 4B,D,F). Main effects of afferent pathway and cell type on baseline amplitudes at the lowest stimulus intensity required to elicit a response were tested. A 2-way ANOVA was not significant for effects of pathway ($F(1,47) = 0.07$, $P=0.79$) nor target cell population ($F(4,47) = 1.68$, $P=0.17$), suggesting no differences in baseline (i.e., in the absence of isoflurane) amplitudes among recorded cells. Similarly, no significant effect on latency was observed for main effects of pathway ($F(1,47) = 1.00$, $P=0.32$) nor cell type ($F(4,47) =1.68$, $P=0.17$).

Isoflurane suppresses layer 1 current sinks elicited by CC inputs, but not TC inputs

Despite their overlapping terminal fields and similar synaptic dynamics under control conditions, TC and CC inputs to layer 1 were differentially affected by isoflurane (Figure 1; Table 1), consistent with previous results from our lab(Murphy et al., 2019). Amplitudes of layer 1 current sinks were suppressed by isoflurane by 21.8% for CC inputs, while current sinks evoked by TC inputs were relatively resistant to isoflurane (Figure 1).

Isoflurane differentially affects synaptic responses in a cell type-dependent manner

Current sinks isolated from current source densities represent averages of inward-going transmembrane currents across all synapses. However, evidence suggests that the

synaptic properties – and therefore potential functional roles – of thalamocortical versus corticocortical inputs to layer 1 may be cell type- and layer-dependent(Cruikshank et al., 2012) (see Chapter 3). Therefore, we sought to investigate whether the effects of isoflurane on layer 1 current sinks were uniform for all post-synaptic targets of each afferent pathway, or whether certain cell populations were differentially sensitive to isoflurane.

We evaluated the degree to which isoflurane modulated the amplitudes of post-synaptic potentials elicited by layer 1 afferents in $L^2/_3$, L4, and L5 pyramidal cells (Figure 2) as well as SOM+ and PV+ cells (Figure 4). Independent of any interactions of cell type or afferent pathway, isoflurane significantly suppressed evoked post-synaptic potentials of target cells ($\chi(1) = 16.6$, $P<0.0001$). Contrary to our findings for extracellularly recorded layer 1 current sinks, we found no significant interaction of pathway on the effect of isoflurane ($\chi(1) = 2.00$, $P=0.16$). However, the effect of isoflurane was significantly dependent on cell type ($\chi(4) = 17.862$, $P=0.0013$). The interaction between cell type and pathway was not significant ($\chi(1) = 6.52$, $P=0.16$). In other words, the effect of isoflurane is cell type-dependent, and within each cell type, no significant differences were observed between afferent pathways.

Amplitudes of synaptic responses in $L^2/_3$ cells were not significantly affected by isoflurane for either TC or CC inputs (Figure 2B,D; Figure 3; Table 3). Conversely, amplitudes of synaptic responses in L4 cells were significantly suppressed by isoflurane for both TC and CC inputs, to approximately the same degree (Figure 2B,D; Figure 3; Table 3). Isoflurane also suppressed CC inputs, but not TC inputs, to L5 pyramidal cells

(Figure 2D; Figure 3; Table 3), though this effect was not significantly different between pathways (P=0.19).

In addition to providing input to pyramidal cells, long-range TC and CC projections also target inhibitory interneurons. Thus, we were also interested in the effect of isoflurane on evoked responses in two subpopulations of inhibitory cells, SOM+ and PV+ interneurons, and whether these effects were different than those observed for pyramidal cell populations. Consistent with previous studies(Beierlein et al., 2003; Cruikshank et al., 2010; Audette et al., 2018) and the results described in Chapter 3 of this thesis, TC inputs rarely elicited synaptic responses in SOM+ cells (n=2 cells); as such, isoflurane effects on TC inputs to SOM+ cells are not reported. Activation of CC afferents, however, reliably elicited synaptic responses in SOM+ cells (Figure 4). These synapses were particularly sensitive to isoflurane; amplitudes of synaptic responses for CC inputs to SOM+ cells were suppressed 35.8% during isoflurane compared to baseline (Table 3). Conversely, no effect of isoflurane on amplitudes of responses in PV+ cells was detected for either afferent pathway (Table 3). Thus, even among subpopulations of GABAergic interneurons, the effect of isoflurane on CC responses was significantly different (-35.8% for SOM+ cells versus -10.0% for PV+ cells, P=0.014; Figure 5), suggesting distinct roles of each cell type during anesthesia.

Effects of isoflurane on intrinsic cellular properties are cell type-dependent

A multitude of cellular and synaptic dynamics may underlie changes in neural activity observed during anesthesia. For example, effects of isoflurane on synaptic responses as we describe here may manifest as a result of pre-synaptic effects of isoflurane (e.g.,

effects on calcium influx or vesicle release), on discrete intrinsic properties of post-synaptic cells that give rise to changes in their excitability, or a combination of pre- and post-synaptic effects. Although we cannot ascribe the contributions of specific synaptic or intrinsic effects of isoflurane to observed effects on evoked responses, characterizing isoflurane-induced changes in synaptic plasticity or intrinsic properties of post-synaptic cells may provide insight into the complicated interactions of network components during anesthesia. To this end, we evaluated the extent to which isoflurane modulated paired pulse ratios and intrinsic membrane properties (resting membrane potential, input resistance, membrane time constant, and spike threshold) of each cell. Baseline values are displayed in Table 2 (PPR) and Table 4 (intrinsic membrane properties); effects of isoflurane are described below and in figures and tables as changes relative to baseline.

Isoflurane significantly enhanced the paired pulse ratio of CC inputs to SOM+ cells, but had no effect on paired pulse ratios for other pathway-cell type combinations (Figure 6; Table 5). Intrinsic membrane properties of L4 pyramidal cells were especially sensitive to isoflurane. In L4 pyramidal cells, input resistance was 13.5% lower and membrane time constants 27.8% shorter during isoflurane relative to baseline; isoflurane did not affect input resistance nor time constants of any other cell type (Figure 7). Isoflurane also reduced resting membrane potential in L4 and L5 pyramidal cells (Figure 7). Effects of isoflurane observed in L4 pyramidal cells were accompanied by a decrease in spike threshold (Figure 7).

Discussion

In these experiments, we describe the effects of isoflurane on synaptic responses and intrinsic membrane properties of pyramidal cells in layers 2-5, as well as in SOM+ and PV+ interneurons. Previous investigations of the effects of isoflurane on synaptic responses have suggested that feedback corticocortical inputs are suppressed to a greater extent than both thalamocortical and feedforward corticocortical inputs(Raz et al., 2014; Murphy et al., 2019). Here, we show that suppression of extracellular synaptic responses is pathway-dependent, recapitulating previous findings using a similar experimental paradigm Raz, 2014 #7659;Murphy, 2019 #8516}. We also demonstrate that the suppression of synaptic responses by isoflurane is cell type- and layer-dependent, providing insight into the mesocircuit-level mechanisms underlying the mechanisms of anesthesia.

Resistance of PV+ interneurons suggests shift in E/I balance during isoflurane

We show that synaptic responses of PV+ interneurons to both TC and CC inputs were resistant to suppression during isoflurane. TC input to PV+ cells provides stimulus-locked fast feedforward-inhibition to pyramidal cells, restricting the window of opportunity for generating spikes and improving spike timing among populations of pyramidal cells(Pouille and Scanziani, 2001; Krause et al., 2017). We propose that the relative insensitivity of fast-spiking PV+ neurons we observe here may underlie previous observations from our lab and others that early responses of the cortical network to TC inputs are relatively preserved during isoflurane, while recurrent, propagating network activity is highly sensitive(Hentschke et al., 2017; Murphy et al., 2017). Although we report activity of single cells only in our study, the relative preservation of PV+ cell

responses is likely to shift the E/I balance in the network toward inhibition. PV+ cells are known to be important for mediating E/I balance within cortical networks(Dichter and Ayala, 1987; Ferguson and Gao, 2018). Pyramidal cells in L2/3, for example, receive PV+ cell-mediated inhibitory input proportional to their excitation under normal conditions, and changes in input to pyramidal cells – as we observe in L4 cells in our experiments – without commensurate changes in PV+ cells disrupts this E/I balance(Xue et al., 2014). If these cell type-specific effects of isoflurane occur in multiple cortical areas, shifts in local E/I balance may contribute to progressively greater suppression in the ascending cortical hierarchy.

Suppression of L4 pyramidal cells during isoflurane may disrupt feedforward processing

We show that synaptic responses of L4 pyramidal cells are suppressed during isoflurane for responses evoked by both TC and CC inputs. That TC inputs to any cell type would be affected by isoflurane is somewhat surprising, and that this effect would be exclusively observed in L4 pyramidal cells is even more unexpected. L4 pyramidal cells are typically considered mediators for propagating feedforward information, receiving sensory-specific information from thalamus and lower areas(Cruikshank et al., 2010; Covic and Sherman, 2011; De Pasquale and Sherman, 2011; Viaene et al., 2011a; Viaene et al., 2011b) and targeting L2/3 for output to higher areas(Xu et al., 2016; Meyer et al., 2018). Feedforward circuits are relatively resistant to anesthetics(Lee et al., 2013; Raz et al., 2014; Murphy et al., 2019) (though, see (Maksimow et al., 2014; Sanders et al., 2018)), and we show here that extracellular recordings of current sinks evoked by activation of TC afferents were not affected by

isoflurane (Figure 1). Yet, interestingly, our results show that inputs to L4 cells are preferentially suppressed by isoflurane, suggesting that suppression of TC and CC inputs together may disrupt feedforward signaling.

While pre-synaptic mechanisms of isoflurane have been well-described (Herring et al., 2009; Xie et al., 2013; Baumgart et al., 2015), our observations suggest that the mechanisms underlying isoflurane effects in L4 pyramidal cells were not limited to pre-synaptic effects. No changes in short-term synaptic plasticity were observed at these synapses (Figure 6), and TC and CC inputs to L4 pyramidal cells were suppressed to a similar extent (Figure 3). However, L4 pyramidal cells were significantly leakier during isoflurane, as evidenced by lower input resistances and shorter membrane time constants relative to baseline (Figure 7). Not only might these effects dampen voltage changes evoked by synaptic currents, but they are likely to also contribute to the overall excitability of L4 cells, thereby attenuating their contributions to processing of cortical signals.

Evidence for disruption of predictive coding schemes during anesthesia

In the present study, we find that isoflurane suppresses CC feedback afferents to L4 and L5 pyramidal cells (Figure 3) as well as those to dendrite-targeting SOM+ interneurons (Figure 5), consistent with previous studies showing sensitivity of feedback connections during anesthesia(Boly et al., 2012; Liu et al., 2012; Raz et al., 2014; Mashour and Hudetz, 2017; Murphy et al., 2019). Feedback activation of the cortical column is mediated largely by intracortical afferents to layer 1 that target distal dendrites of pyramidal cells. Dendritic calcium currents activated by these inputs increase the gain

of the input/output relationship of cortical pyramidal cells and are highly correlated with sensory perception (Manita et al., 2015; Takahashi et al., 2016). This process is tightly regulated by powerful disynaptic inhibition from SOM+ interneurons(Murayama et al., 2009). Our observation that inputs to both SOM+ cells and infragranular pyramidal cells are preferentially suppressed notably intersects with these previous findings in the context of sensory coding. Suppression of intracortical feedback inputs to two key players in this integration process may therefore disrupt the typical input/output function of pyramidal cells.

Disruption of integration of inputs to L5 pyramidal cells is also consistent with what might be expected under anesthesia in the context of current theoretical models. The predictive coding hypothesis, for example, has often been used as a framework for understanding consciousness and sensory processing(Friston, 2005; Bastos et al., 2012; Clark, 2013). Under the predictive coding hypothesis, feedback signals must activate inhibition to offset incoming excitatory signals and prevent propagation of the excitatory, ascending error signal. Discrepancies between internally generated predictions and sensory input from external sources are propagated as excitatory “error signals”. Our data provide further evidence that multiple components of the predictive coding architecture may be disrupted by anesthesia. First, integration of predictions carried by feedback afferents may be perturbed, as feedback inputs to both SOM+ cells and L5 pyramidal cells – key mediators of feedback modulation of sensory responses – are altered by isoflurane. Second, propagation of error signals in the feedforward direction may be disrupted, as both TC and CC inputs to L4 cells – which mediate intracortical feedforward signals – are suppressed by isoflurane. Our data may

demonstrate physiological correlates of components of the predictive coding model, and provide insight into the disruption of sensory processing during anesthesia.

Future Directions

In these experiments, we investigate the effect of isoflurane on discrete components of a higher order cortical circuit. Investigating the pathway-, cell type-, and layer-specific effects of isoflurane is imperative for understanding the larger systems in which these components operate. Our findings will inform future investigations of sensory processing and changes in consciousness during anesthesia. Although here we activated inputs to layer 1 independently, future experiments *in vivo* will provide insight into how overlapping inputs to layer 1 affect arousal and sensory processing. It is reasonable to expect that the combined effects of isoflurane on TC and CC inputs, for example, may engender supralinear effects on underlying circuit components, synergistically contributing to disruption of sensory processing. Moreover, *in vivo* investigations, such as those that involve artificially manipulating activity in different cell types during anesthesia, may allow for causal, detailed descriptions of the pathway- and cell type-specific components that are necessary and/or sufficient for consciousness. Lastly, a recent study by Suzuki and Larkum (2020) suggests that anesthetics may prevent integration of feedback signals by targeting signal amplification in apical dendrites of pyramidal cells, and implies that this process may be mediated by metabotropic glutamate and cholinergic receptors(Suzuki and Larkum, 2020). Future investigations should probe the extent to which distinct inputs to layer 1 engage metabotropic

glutamate or cholinergic systems, and how the synaptic effects of anesthetics on layer 1 contributes to disruption of input-output computations by anesthetics.

Acknowledgements

The authors would like to thank Bryan Krause for insight provided for the statistical analyses conducted in this study, and Sean Grady for technical support.

References

Akeju O, Loggia ML, Catana C, Pavone KJ, Vazquez R, Rhee J, Contreras Ramirez V, Chonde DB, Izquierdo-Garcia D, Arabasz G, Hsu S, Habeeb K, Hooker JM, Napadow V, Brown EN, Purdon PL (2014) Disruption of thalamic functional connectivity is a neural correlate of dexmedetomidine-induced unconsciousness. Elife 3:e04499.

Audette NJ, Urban-Ciecko J, Matsushita M, Barth AL (2018) POm Thalamocortical Input Drives Layer-Specific Microcircuits in Somatosensory Cortex. Cereb Cortex 28:1312-1328.

Bastos AM, Usrey WM, Adams RA, Mangun GR, Fries P, Friston KJ (2012) Canonical microcircuits for predictive coding. Neuron 76:695-711.

Baumgart JP, Zhou ZY, Hara M, Cook DC, Hoppa MB, Ryan TA, Hemmings HC, Jr. (2015) Isoflurane inhibits synaptic vesicle exocytosis through reduced Ca2+ influx, not Ca2+-exocytosis coupling. Proc Natl Acad Sci U S A 112:11959-11964.

Beierlein M, Gibson JR, Connors BW (2003) Two dynamically distinct inhibitory networks in layer 4 of the neocortex. Journal of Neurophysiology 90:2987-3000.

Binzegger T, Douglas RJ, Martin KA (2009) Topology and dynamics of the canonical circuit of cat V1. Neural Netw 22:1071-1078.

Boly M, Moran R, Murphy M, Boveroux P, Bruno MA, Noirhomme Q, Ledoux D, Bonhomme V, Brichant JF, Tononi G, Laureys S, Friston K (2012) Connectivity changes underlying spectral EEG changes during propofol-induced loss of consciousness. J Neurosci 32:7082-7090.

Clark A (2013) Whatever next? Predictive brains, situated agents, and the future of cognitive science. Behav Brain Sci 36:181-204.

Covic EN, Sherman SM (2011) Synaptic properties of connections between the primary and secondary auditory cortices in mice. CerebCortex 21:2425-2441.

Crick F, Koch C (2003) A framework for consciousness. Nat Neurosci 6:119-126.

Cruikshank SJ, Urabe H, Nurmikko AV, Connors BW (2010) Pathway-Specific Feedforward Circuits between Thalamus and Neocortex Revealed by Selective Optical Stimulation of Axons. Neuron 65:230-245.

Cruikshank SJ, Ahmed OJ, Stevens TR, Patrick SL, Gonzalez AN, Elmaleh M, Connors BW (2012) Thalamic Control of Layer 1 Circuits in Prefrontal Cortex. The Journal of Neuroscience 32:17813-17823.

De Pasquale R, Sherman SM (2011) Synaptic properties of corticocortical connections between the primary and secondary visual cortical areas in the mouse. JNeurosci 31:16494-16506.

Dehaene S, Changeux JP (2011) Experimental and theoretical approaches to conscious processing. Neuron 70:200-227.

Dichter MA, Ayala GF (1987) Cellular mechanisms of epilepsy: a status report. Science 237:157-164.

Douglas RJ, Martin KA (2004) Neuronal circuits of the neocortex. AnnuRevNeurosci 27:419-451.

Douglas RJ, Martin KAC (2007) Recurrent neuronal circuits in the neocortex. Current Biology 17:R496-R500.

Douglas RJ, Martin KAC, Whitteridge D (1989) A canonical microcircuit for neocortex. Neural Computation 1:480-488.

Ferguson BR, Gao W-J (2018) PV Interneurons: Critical Regulators of E/I Balance for Prefrontal Cortex-Dependent Behavior and Psychiatric Disorders. Frontiers in Neural Circuits 12.

Ferrarelli F, Massimini M, Sarasso S, Casali A, Riedner BA, Angelini G, Tononi G, Pearce RA (2010) Breakdown in cortical effective connectivity during midazolam-induced loss of consciousness. Proc Natl Acad Sci USA 107:2681-2686.

Friston K (2005) A theory of cortical responses. Philos Trans R Soc Lond B Biol Sci 360:815-836.

Haider B, Häusser M, Carandini M (2013) Inhibition dominates sensory responses in the awake cortex. Nature 493:97-100.

Hentschke H, Raz A, Krause BM, Murphy CA, Banks MI (2017) Disruption of cortical network activity by the general anesthetic isoflurane. Br J Anaesth 119:685-696.

Herring BE, Xie Z, Marks J, Fox AP (2009) Isoflurane inhibits the neurotransmitter release machinery. J Neurophysiol 102:1265-1273.

Honjoh S, Sasai S, Schiereck SS, Nagai H, Tononi G, Cirelli C (2018) Regulation of cortical activity and arousal by the matrix cells of the ventromedial thalamic nucleus. Nature Communications 9:2100.

Koch C, Massimini M, Boly M, Tononi G (2016) Neural correlates of consciousness: progress and problems. Nat Rev Neurosci 17:307-321.

Krause BM, Murphy CA, Uhlrich DJ, Banks MI (2017) PV+ Cells Enhance Temporal Population Codes but not Stimulus-Related Timing in Auditory Cortex. Cereb Cortex.

Langsjo JW, Alkire MT, Kaskinoro K, Hayama H, Maksimow A, Kaisti KK, Aalto S, Aantaa R, Jaaskelainen SK, Revonsuo A, Scheinin H (2012) Returning from oblivion: imaging the neural core of consciousness. J Neurosci 32:4935-4943.

Lee U, Ku S, Noh G, Baek S, Choi B, Mashour GA (2013) Disruption of frontal-parietal communication by ketamine, propofol, and sevoflurane. Anesthesiology 118:1264-1275.

Liu X, Lauer KK, Ward BD, Li SJ, Hudetz AG (2013) Differential effects of deep sedation with propofol on the specific and nonspecific thalamocortical systems: a functional magnetic resonance imaging study. Anesthesiology 118:59-69.

Liu X, Lauer KK, Ward BD, Rao SM, Li SJ, Hudetz AG (2012) Propofol disrupts functional interactions between sensory and high-order processing of auditory verbal memory. Hum Brain Mapp 33:2487-2498.

Maksimow A, Silfverhuth M, Langsjo J, Kaskinoro K, Georgiadis S, Jaaskelainen S, Scheinin H (2014) Directional connectivity between frontal and posterior brain regions is altered with increasing concentrations of propofol. PLoS One 9:e113616.

Manita S, Suzuki T, Homma C, Matsumoto T, Odagawa M, Yamada K, Ota K, Matsubara C, Inutsuka A, Sato M, Ohkura M, Yamanaka A, Yanagawa Y, Nakai J, Hayashi Y, Larkum ME, Murayama M (2015) A Top-Down Cortical Circuit for Accurate Sensory Perception. Neuron 86:1304-1316.

Mashour GA, Hudetz AG (2017) Bottom-Up and Top-Down Mechanisms of General Anesthetics Modulate Different Dimensions of Consciousness. Front Neural Circuits 11:44.

Meyer JF, Golshani P, Smirnakis SM (2018) The Effect of Single Pyramidal Neuron Firing Within Layer 2/3 and Layer 4 in Mouse V1. Front Neural Circuits 12:29.

Mitzdorf U (1985) Current source-density method and application in cat cerebral cortex: investigation of evoked potentials and EEG phenomena. Physiol Rev 65:37-100.

Murayama M, Pérez-Garci E, Nevian T, Bock T, Senn W, Larkum ME (2009) Dendritic encoding of sensory stimuli controlled by deep cortical interneurons. Nature 457:1137-1141.

Murphy C, Krause B, Banks M (2019) Selective effects of isoflurane on cortico-cortical feedback afferent responses in murine non-primary neocortex. Br J Anaesth 123:488-496.

Murphy CA, Krause BM, Grady SM, Banks MI (2017) Effect of isoflurane on selectively activated afferent pathways in neocortex. In: Society for Neuroscience Annual Meeting. Washington D.C., USA.

Nourski KV, Steinschneider M, Rhone AE, Kawasaki H, Howard MA, 3rd, Banks MI (2018) Auditory Predictive Coding across Awareness States under Anesthesia: An Intracranial Electrophysiology Study. J Neurosci 38:8441-8452.

Nourski KV, Banks MI, Steinschneider M, Rhone AE, Kawasaki H, Mueller RN, Todd MM, Howard MA, 3rd (2017) Electrocorticographic delineation of human auditory cortical fields based on effects of propofol anesthesia. Neuroimage 152:78-93.

Pettersen KH, Devor A, Ulbert I, Dale AM, Einevoll GT (2006) Current-source density estimation based on inversion of electrostatic forward solution: effects of finite extent of neuronal activity and conductivity discontinuities. JNeurosciMethods 154:116-133.

Picchioni D, Pixa ML, Fukunaga M, Carr WS, Horovitz SG, Braun AR, Duyn JH (2014) Decreased connectivity between the thalamus and the neocortex during human nonrapid eye movement sleep. Sleep 37:387-397.

Pouille F, Scanziani M (2001) Enforcement of temporal fidelity in pyramidal cells by somatic feed- forward inhibition. Science 293:1159-1163.

Raz A, Grady SM, Krause BM, Uhlrich DJ, Manning KA, Banks MI (2014) Preferential effect of isoflurane on top-down versus bottom-up pathways in sensory cortex. Front Syst Neurosci 8.

Redinbaugh MJ, Phillips JM, Kambi NA, Mohanta S, Andryk S, Dooley G, Afrasiabi M, Raz A, Saalmann Y (2020) Thalamus Modulates Consciousness Via Layer-Specific Control of Cortex. Neuron 105.

Sanders RD, Banks MI, Darracq M, Moran R, Sleigh J, Gosseries O, Bonhomme V, Brichant JF, Rosanova M, Raz A, Tononi G, Massimini M, Laureys S, Boly M (2018) Propofol-induced unresponsiveness is associated with impaired feedforward connectivity in cortical hierarchy. Br J Anaesth 121:1084-1096.

Suzuki M, Larkum ME (2020) General Anesthesia Decouples Cortical Pyramidal Neurons. Cell 180:666-676.e613.

Takahashi N, Oertner TG, Hegemann P, Larkum ME (2016) Active cortical dendrites modulate perception. Science 354:1587-1590.

Viaene AN, Petrof I, Sherman SM (2011a) Synaptic properties of thalamic input to layers 2/3 and 4 of primary somatosensory and auditory cortices. JNeurophysiol 105:279-292.

Viaene AN, Petrof I, Sherman SM (2011b) Properties of the thalamic projection from the posterior medial nucleus to primary and secondary somatosensory cortices in the mouse. Proc Natl Acad Sci USA 108:18156-18161.

Xie Z, McMillan K, Pike CM, Cahill AL, Herring BE, Wang Q, Fox AP (2013) Interaction of anesthetics with neurotransmitter release machinery proteins. Journal of neurophysiology 109:758-767.

Xu X, Olivas ND, Ikrar T, Peng T, Holmes TC, Nie Q, Shi Y (2016) Primary visual cortex shows laminar-specific and balanced circuit organization of excitatory and inhibitory synaptic connectivity. Journal of Physiology 594:1891-1910.

Xue M, Atallah BV, Scanziani M (2014) Equalizing excitation–inhibition ratios across visual cortical neurons. Nature 511:596.

Figure 1

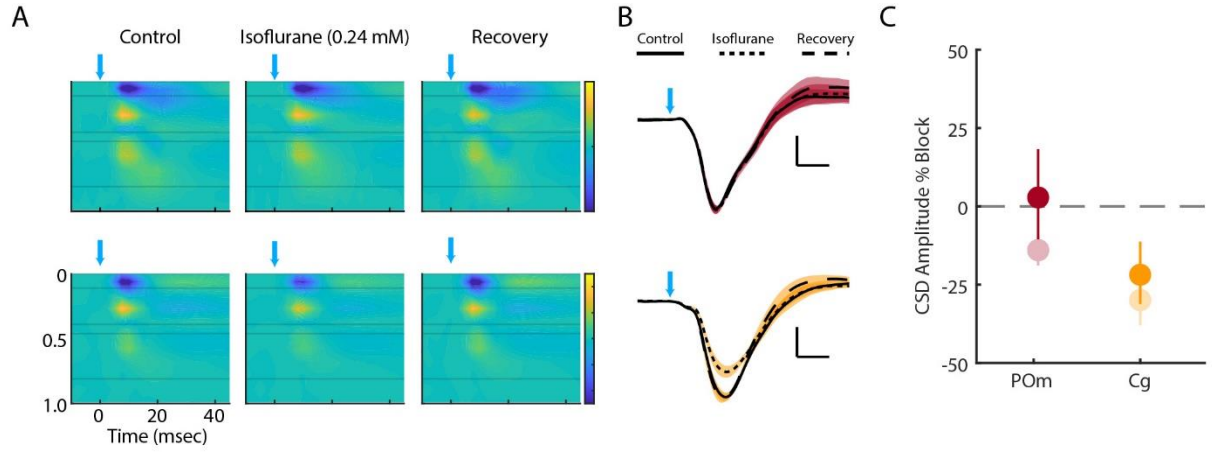

Figure 1. Effects of isoflurane on optogenetically evoked current sinks in layer 1 are pathway-specific. (A) CSD color plots comparing evoked synaptic responses to a 2 msec light pulse (blue arrows) across control (A, left column), 0.24 mM isoflurane (A, middle column), and recovery (A, right column) for representative examples for thalamocortical (top row) and corticocortical (bottom row) afferents; color scale: -5.0 to 5.0 µA mm^{-3}. (B) Signals from channel 1 were used to compare synaptic effects across control (solid), 0.24 mM isoflurane (dotted), and recovery (dashed). Shaded regions indicate ± 1 SD among trials. C. Model fits of percent block of layer 1 sink by isoflurane with 95% confidence interval (vertical line). Responses evoked by stimulation of CC feedback afferents to cortical layer 1 (orange) are suppressed to a greater extent under isoflurane than TC inputs (red). Pale markers reflect estimates of block by isoflurane at 0.24 mM based on results from Murphy et al., 2019. Raw values for control conditions are shown in **Table 1.**

Figure 2

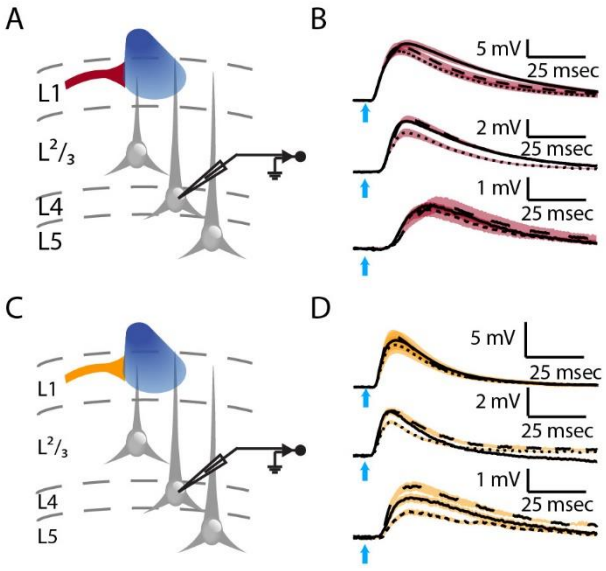

Figure 2. Example recordings from cortical pyramidal cells in response to activation of two distinct layer 1 afferents. A. Schematic demonstrating recordings conducted for panel B. Afferents originating in POm were optogenetically activated while whole cell patch clamp recordings were conducted in pyramidal cells in L2/3, L4, or L5. B. Example recordings of POm-evoked responses from L2/3 (top), L4 (middle), or and L5 (bottom) cells during control (solid), 0.24 mM isoflurane (dotted), and recovery (dashed) conditions. Shaded regions indicate ± 1 SD among trials. C-D. Same as A-B for responses to Cg inputs. Population results of isoflurane effects are shown in **Figure 3.** Raw values for control conditions are shown in **Table 2.**

Figure 3

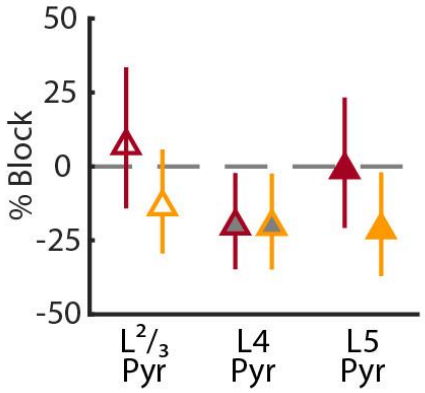

Figure 3. Suppression of post-synaptic responses by isoflurane is cell type-specific. Model estimates of the percent block by isoflurane of post-synaptic responses evoked by TC (red) or CC (orange) inputs to L2/3, L4, and L5 cell populations. Estimates are represented by triangles; vertical lines span 95% confidence intervals for isoflurane effects for each pathway-cell type combination, where confidence intervals overlapping 0% block are not significant (P>0.05). Both TC and CC inputs to L4 pyramidal cells were suppressed by isoflurane, as were CC inputs to L5 pyramidal cells. Effects are also quantified in **Table 3.**

Figure 4

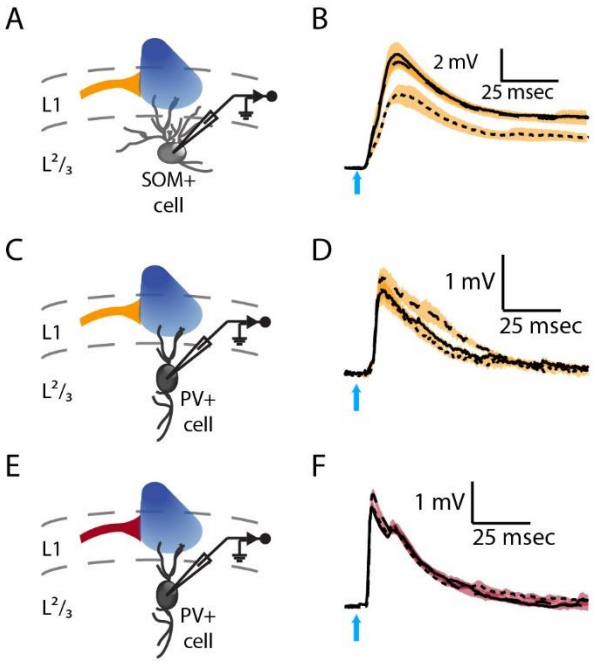

Figure 4. Example recordings from SOM+ and PV+ interneurons in response to activation of distinct layer 1 afferents. A. Schematic demonstrating recordings conducted for panel B. CC afferents to layer 1 were optogenetically activated while whole cell patch clamp recordings were conducted in SOM+ interneurons. B. Example recordings from CC-evoked responses in a SOM+ cell during control (solid), 0.24 mM isoflurane (dotted), and recovery (dashed) conditions. Shaded regions indicate ± 1 SD among trials. C-D. Same as A-B for CC inputs to PV+ cells. E-F. Same as A-B for TC inputs to PV+ cells. Note that examples of TC inputs to SOM+ cells are not shown, as TC inputs failed to evoke synaptic responses in SOM+ cells, Population results of isoflurane effects are shown in **Figure 5.** Raw values for control conditions are shown in **Table 2.**

Figure 5

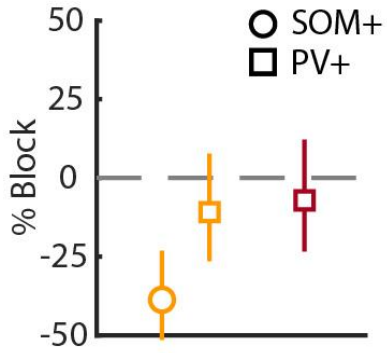

Figure 5. CC feedback inputs to SOM+ interneurons are suppressed by isoflurane, while TC and CC inupts to PV+ interneurons are not. Model estimates of the percent block by isoflurane of post-synaptic responses evoked by TC (red) or CC (orange) inputs to SOM+ and PV+ interneuron populations. Estimates are represented by circles (SOM+) or squares (PV+); vertical lines span 95% confidence intervals for isoflurane effects for each pathway-cell type combination, where confidence intervals overlapping 0% block are not significant (P>0.05). CC inputs to SOM+ cells were suppressed by isoflurane, but no effect of isoflurane was detected in TC nor CC inputs to PV+ cells. Effects are also quantified in **Table 3.**

Figure 6.

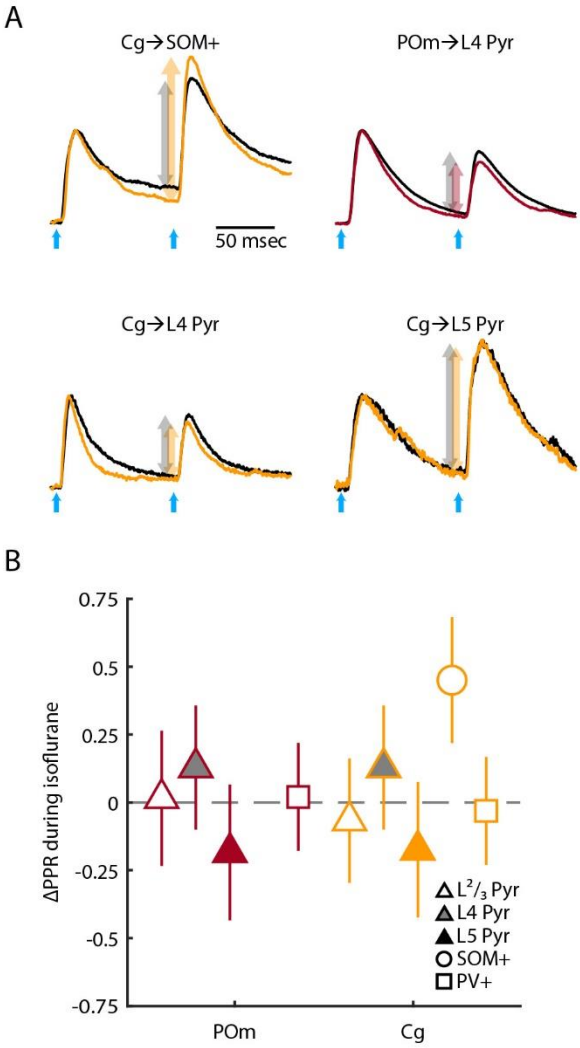

Figure 6. Isoflurane increases paired pulse ratios for CC inputs to SOM+ cells, suggest pre-synaptic mechanisms. A. Examples recordings from the four different pathway-cell type pairs that demonstrated suppression of synaptic responses by isoflurane. Responses for control (black) and isoflurane (either orange (CC) or red (TC)) conditions are normalized to the amplitude of the first pulse under control conditions to demonstrate paired pulse effects. Arrows show comparison of paired pulse effects between control (black) and isoflurane (either orange or red) conditions. B. Model estimates of the changes to paired pulse ratio during isoflurane, where positive values represent higher paired pulse ratios during isoflurane. Estimates of isoflurane effects on paired pulse ratios for responses evoked by TC (red) or CC

(orange) inputs to all recorded populations are shown. Estimates are represented by shapes; vertical lines span 95% confidence intervals for isoflurane effects for each pathway-cell type combination, where confidence intervals overlapping 0 are not significant (P>0.05). Paired pulse ratios for CC inputs to SOM+ cells were enhanced by isoflurane, suggesting isoflurane blocks synaptic responses to SOM+ cells through pre-synaptic mechanisms. Raw values for control conditions are shown in **Table 2**, and isoflurane effects are quantified in **Table 5.**

Figure 7.

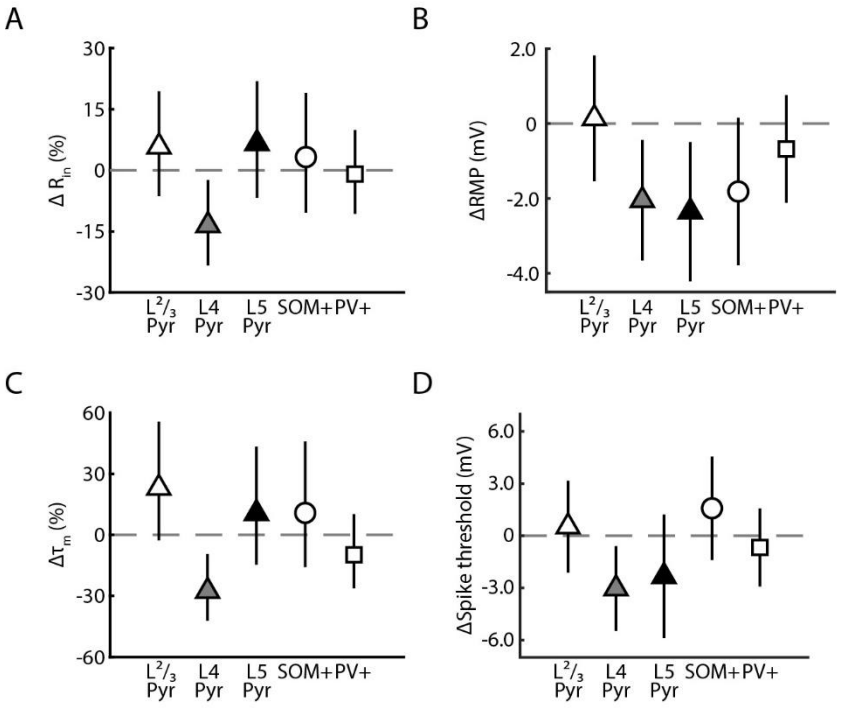

Figure 7. Isoflurane alters intrinsic membrane properties of L4 pyramidal cells, suggesting a shared mechanism by which TC and CC inputs are blocked. A. Model estimates of percent change of input resistance during isoflurane, where negative values represent decreases in input resistance (i.e., increased conductance). B. Model estimates of shifts of resting membrane potential during isoflurane, where negative values represent hyperpolarization of membrane potentials during isoflurane compared to baseline values. C. Same as in A for percent changes in membrane time constants. D. Same as in B for spike thresholds. L4 pyramidal cells became leakier (i.e., lower input resistances and shorter time constants) during isoflurane relative to baseline. Raw values for control conditions are shown in **Table 4.**

Table 1

	Latency (msec)	L1 sink amplitude ($\mu A \cdot mm^{-3}$)	% Block by isoflurane [95% CI]	P-value
POm	3.81±0.52	6.18±1.64	+2.9 [-10.6 18.3]	0.69
Cg	3.61±0.56	5.33±1.35	-21.8 [-31.1 -11.3]	0.00026

Table 1. Activation of cortical afferents evokes short latency current sinks in layer 1 that are sensitive to isoflurane in a pathway-dependent manner. Layer 1 current sink amplitudes evoked by activation of Cg inputs were suppressed by isoflurane, while those evoked by POm inputs were not. Estimates are based on predicted values from linear mixed effects model (see Methods).

Table 2

	PSP amplitude	PSP latency	PPR
POm→			
$L^2/_3$ Pyr (n=5)	2.4±1.8	5.9±2.3	0.86±0.33
L4 Pyr (n=6)	4.1±2.3	5.6±1.6	0.64±0.23
L5 Pyr (n=5)	8.3±5.7	5.4±1.8	0.77±0.29
SOM+ (n=2)	5.1±4.5	3.0±0.5	0.61±0.04
PV+ (n=8)	6.4±2.3	4.1±0.7	0.68±0.25
Cg→			
$L^2/_3$ Pyr (n=6)	2.0±1.4	4.6±1.2	0.57±0.30
L4 Pyr (n=6)	4.6±4.6	4.8±1.2	0.79±0.27
L5 Pyr (n=5)	2.6±1.7	6.5±1.8	1.05±0.34
SOM+ (n=6)	6.5±5.0	4.6±0.7	0.74±0.45
PV+ (n=8)	4.3±4.8	4.9±1.2	0.78±0.32

Table 2. Properties of evoked responses in whole cell patch clamp recordings conducted during control conditions in pyramidal cells and interneurons. Values shown are mean ± standard deviation. Latency was calculated relative to onset of 2 msec light pulse. Paired pulse ratios were calculated as the amplitude of the 2nd post-synaptic potential (relative to the pre-response baseline) divided by the baseline subtracted amplitude of the 1st post-synaptic potential.

Table 3.

	% Block	95% CI	P-value
POm→			
$L^2/_3$ Pyr	7.0	[-14.2 33.5]	0.54
L4 Pyr	-20.1	[-34.7 -2.3]	0.029
L5 Pyr	-1.1	[-20.7 23.3]	0.92
PV+	-6.6	[-21.6 11.3]	0.44
Cg→			
$L^2/_3$ Pyr	-13.6	[29.4 5.7]	0.15
L4 Pyr	-20.3	[-34.8 -2.4]	0.028
L5 Pyr	-21.5	[-37.0 -2.0]	0.033
SOM+	-35.8	[-47.5 -21.4]	<0.0001
PV+	-10.0	[-24.5 7.2]	0.23

Table 3. Isoflurane affects synaptic responses in a cell type-dependent manner. Estimates are based on predicted values from linear mixed effects model (see Methods). Values represent the percent change in the amplitude of post-synaptic responses during isoflurane relative to baseline conditions. Negative values represent suppression of synaptic responses by isoflurane.

Table 4.

	RMP (mV)	R_{in} (MΩ)	τ_m (msec)	Spike Threshold (mV)
$L^2/_3$ Pyr (n=11)	-71.5±3.6	114.2±45.9	14.1±10.7	-43.1±4.0
L4 Pyr (n=12)	-68.9±5.3	183.2±103.8	19.0±13.2	-41.9±6.1
L5 Pyr (n=10)	-65.1±3.7	135.77±85.9	18.0±9.8	-41.8±5.3
SOM+ (n=8)	-60.3±6.2	317.3±138.8	38.2±38.0	-42.2±3.9
PV+ (n=16)	-63.5±4.0	166.8±47.1	9.6±2.5	-46.3±7.9

Table 4. Intrinsic properties of recorded cell types during control conditions. Values are mean ± standard deviation. Properties were measured ~2 minutes after achieving whole cell access. A series of 10-20 current steps (600 msec) was delivered at progressive intervals (10-40 pA), beginning with a hyperpolarizing current injection. Resting membrane potentials (RMP) were calculated by averaging membrane potentials in the 100 msec prior to onset of all current pulses. Input resistances (Rin) were extrapolated from relationship between current and steady state voltages. Time constants (τm) were estimated using the first hyperpolarizing current pulse. Spike thresholds were evaluated using the first trial to evoke an action potential, where the spike threshold was the voltage at which the second derivative exceeded twice the standard deviation of the pre-spike baseline value.

Table 5.

	ΔPPR	95% CI	P-value
POm→			
$L^2/_3$ Pyr	+0.02	[-0.32 0.26]	0.90
L4 Pyr	+0.13	[-0.10 0.36]	0.27
L5 Pyr	-0.18	[-0.43 0.07]	0.15
PV+	+0.02	[-0.18 0.22]	0.84
Cg→			
$L^2/_3$ Pyr	-0.07	[-0.30 0.16]	0.56
L4 Pyr	+0.13	[-0.10 0.36]	0.27
L5 Pyr	-0.18	[-0.42 0.08]	0.17
SOM+	+0.45	[0.22 0.68]	0.0002
PV+	-0.03	[-0.23 0.17]	0.76

Table 5. Isoflurane alters short-term synaptic plasticity for Cg inputs to SOM+ interneurons. Estimates are based on predicted values from linear mixed effects model (see Methods) and represent the change in PPR (in mV) relative to baseline PPR. Negative values represent decreases in PPR (e.g., stronger paired pulse depression) during isoflurane.

Chapter 6

Summary and future directions

Summary

In the previous four chapters of this thesis, I describe a series of experiments that provide insight into the synaptic properties and potential functional roles of discrete components of a higher order thalamocortical mesocircuit. In Chapter 2, I outline a protocol for probing synaptic and network responses to optogenetic activation of afferent fibers in brain slices, and I describe how the properties of volatile anesthetics may be utilized for testing the effects of isoflurane on components of cortical networks. I use this protocol to conduct the remainder of experiments in Chapters 3-5. In Chapter 3, I show that thalamocortical and corticocortical afferents to layer 1 target specific populations of excitatory and inhibitory cells. The response properties of evoked responses are cell type- and pathway-specific. Thalamocortical afferents activate large amplitude post-synaptic responses and action potentials in L5 pyramidal cells, while corticocortical afferents strongly activate somatostatin-positive interneurons and elicit only small amplitude responses in pyramidal cells. The differences observed from intracellular recordings are also represented in the input-output relationship of the cortical column, where thalamocortical afferents evoke robust input-dependent activity in L5 and outputs evoked by corticocortical afferents are relatively small even with lots of input to layer 1. In Chapter 4, I show that each of these inputs to layer 1, as well as

thalamocortical and corticocortical feedforward inputs, is blocked by isoflurane in a concentration-dependent manner. Importantly, this effect is significantly more pronounced for corticocortical feedback inputs to layer 1. Yet, the experiments in Chapter 4 do not provide information about whether specific afferent inputs are affected by isoflurane differently depending on their post-synaptic targets. In Chapter 5, I show that the pathway-dependent effects of isoflurane on synaptic responses are cell type-specific. I provide evidence that isoflurane may disrupt both integration of feedback signals as well as propagation of information through feedforward circuits.

These experiments and the conclusions I draw from them are additions to a growing body of literature that together provide insight into the neurobiological underpinnings of consciousness, as well as potential mechanisms by anesthetics induce loss of consciousness. In the sections below, I pose and elaborate upon scientific questions to guide future lines of inquiry.

Future directions

A brief note about semantics as our understanding of cortical circuits evolves

The distinction between “inputs to layer X” and “inputs targeting layer X cells” is relevant. In our experiments, the afferent axons we activate make synaptic connections *within* layer 1, but we record only from cells *outside* layer 1. Conversely, interneurons with cell bodies *within* layer 1 receive inputs from and send outputs to cells whose cell bodies are both *within and outside* layer 1. If the functional input/output relationship of cells can be entirely independent of the layer in which their cell body resides, what is the purpose of the nomenclature designating cells to certain layers? Of course, the answer

is likely mostly historical. We record from cell bodies, therefore categorize them accordingly. But, as others have proposed (Larkum et al., 2018), this somato-centric perspective is limiting, as it doesn't consider the multiple input and output "compartments" that may contribute to the behavior of a single neuron. As our understanding of cortical circuits evolves, I expect that perspectives regarding intra- and interlaminar (as well as intra- and inter-areal) influences may be expanded by these semantic considerations.

What role do inhibitory interneurons with cell bodies in layer 1 play in sensory processing and unconsciousness during anesthesia?

Layer 1 is characterized by a paucity of cell bodies compared to the cortical layers below. The only cell bodies that reside in cortical layer 1 are those of a select population of inhibitory interneurons, 93% of which express the 5HT3a serotonin receptor (Rudy et al., 2011). These layer 1 interneurons can be further broken down into three non-overlapping populations with variable molecular, electrophysiological, and morphological properties (Schuman et al., 2019). For example, the axons of layer 1 interneurons expressing vasointestinal peptide branch very little and target the deep cortical layers. Alternatively, approximately 70% of layer 1 interneurons are neurogliaform cells, which have extensive axonal arborizations – often spanning multiple cortical columns – that are contained almost exclusively within layer 1 (Kubota, 2014; Tremblay et al., 2016; Schuman et al., 2019).

The connectivity of layer 1 interneurons highly complex and sophisticated, as layer 1 interneuron populations are involved in feedforward inhibition of excitatory cells, disinhibition of local interneurons, and extrasynaptic regulation via tonic GABA release

(Wozny and Williams, 2011; Cruikshank et al., 2012; Schuman et al., 2019). Via these networks, interneurons with cell bodies in layer 1 are positioned to regulate swaths of pyramidal cell dendrites (Oláh et al., 2009) or other interconnected interneuron circuits (Jiang et al., 2013), often from a distance, though the specifics of these interactions are beyond the scope of this thesis.

Still, the functional roles of layer 1 interneurons remain relatively unexplored. Layer 1 interneurons receive direct input from thalamocortical and corticocortical targets; given their connectedness with local circuits, they are therefore likely to play a role in mediating and/or modulating intracortical and thalamocortical inputs. Future studies, especially those *in vivo*, should manipulate activity in layer 1 interneurons, and explore the extent to which they play a role in sensory processing or in anesthetic-induced loss of consciousness.

How does isoflurane affect intracortical connections within the cortical column?
Processing of sensory signals is an iterative process that involves message passing *between* cortical areas, but information is also coded in spiking patterns generated in local recurrent interlaminar connections. For example, work from our lab and others has shown that activation of thalamocortical afferents can evoke robust spiking activity in L5 that may include the superficial layers with a sufficient stimulus (Sakata and Harris, 2009; Constantinople and Bruno, 2013; Krause et al., 2014). This recurrent network activity propagates by way of intra- and inter-laminar connections, an “internally-generated non-linear amplification process” that has implications for the state-dependence of perception and the coding of sensory information. Our lab has shown

that these network events are highly sensitive to isoflurane, despite early responses being relatively unaffected(Hentschke et al., 2017; Murphy et al., 2017).

In Chapter 3, I demonstrate that afferents to layer 1 target the apical dendrites of pyramidal cells and interneurons in a pathway-dependent manner, and I suggest that the input-output relationship of the cortical column is likely predicated upon the interactions among underlying cell populations. In Chapter 5, I provide evidence that integration and propagation of both feedback and feedforward signals may be disrupted by isoflurane. Inputs to layer 4 cells, which play a key role in mediating feedforward responses, were suppressed by isoflurane; corticocortical feedback inputs to layer 5 pyramidal cells and somatostatin-positive interneurons were also suppressed, presenting a possible mechanism by which feedback-mediated information integration is perturbed during anesthesia.

Together with results from previous studies, these conclusions suggest that both inputs and outputs of the column are impacted by isoflurane. Yet, it is unclear by what mechanisms the input/output relationship is disrupted. Thus, further investigations should explore the effects of isoflurane on connected cell *within* a cortical column. For example, if connections between L5 pyramidal cells are suppressed by isoflurane, their failure to participate in generating and propagating network activity is likely to be compounded.

How do synaptic effects of isoflurane interact with effects on signaling in dendritic compartments?

Because inputs to layer 1 target only interneurons and the distal dendrites of excitatory cells, their influence over cortical output is ostensibly limited. However, activation of

distal dendrites of pyramidal cells can activate calcium-dependent potentials in the apical dendrite (Larkum et al., 2004; Murayama et al., 2009; Larkum, 2013 ; Takahashi et al., 2016), amplifying the relative influence of layer 1 inputs. A recent set of experiments by Mototaka Suzuki and Matthew Larkum showed that isoflurane, ketamine/xylazine, and urethane each independently decoupled signaling in the apical dendrites of layer 5 pyramidal cells (Suzuki and Larkum, 2020), thereby disrupting the intrinsic input/output function of these cells. During control conditions, direct activation of channelrhodopsin expressed in the distal dendrites resulted in spike output at the cell body, which was suppressed during anesthesia even upon controlling for input amplitudes. The authors provide evidence that that this decoupling of inputs from outputs may be mediated by anesthetic effects on muscarinic acetylcholine receptors and metabotropic glutamate receptors.

In the experiments described in this thesis, synaptic effects of isoflurane were examined by optogenetically activating pre-synaptic cells. The experiments described by Suzuki and Larkum circumvent the pre-synaptic effects of isoflurane by directly eliciting depolarizing potentials in the distal dendrites of pyramidal cells. Synaptic transmission is affected by anesthetics in a pathway-dependent manner (Chapters 4 and 5); dendritic integration is affected independent of afferent pathway. Further investigation of the interplay between these results should explore whether the synaptic and dendritic effects of anesthetics are distinct and possibly cooperative. Such studies may unify theories implicating thalamus and cortex in the neural correlates of consciousness.

In what ways will in vivo manipulations substantiate and build upon the findings in these chapters?

Ex vivo brain slices facilitate the study of individual components that operate simultaneously in the brain. However, while reduced preparations confer certain benefits, it is difficult to draw sweeping conclusions about cortical circuits or to make causal inferences without further study in *in vivo* systems. The act of harvesting tissue itself is traumatic and maintaining the appropriate conditions for the duration of data collection can be difficult. Because long-range projections tend to be excitatory, slices may have excitation/inhibition ratios that do not represent those found *in vivo* (Stepanyants et al., 2009). Moreover, slice preparations lack state-dependent neuromodulatory input that modulates typical physiological activity (Gil et al., 1997; Lam and Sherman, 2018); especially because anesthetics may influence the actions of neuromodulatory input (Suzuki and Larkum, 2020), conclusions drawn from *ex vivo* preparations should always be interpreted with these caveats.

First, the data and the conclusions I draw from it in this thesis should be substantiated *in vivo*. Does activation of intracortical feedback versus higher order thalamocortical afferents differentially activate populations of post-synaptic cells? Are these synaptic responses preferentially attenuated during isoflurane anesthesia? Next, manipulations of distinct projections or cell types may provide insight into the roles of each. How do synaptic and network responses change if distinct layer 1 afferents or activity of underlying cell types are disabled? Does this affect sensory perception? Consciousness? Can the behavioral phenotypes of anesthetics be recapitulated by disrupting discrete components of cortical circuits? Chemogenetic and optogenetic manipulations may be targeted to specific cell types for select activation or inactivation

of independent cell populations to further validate the conclusions draw in these chapters. For example, to explore the influence of the relative resistance of PV+ interneurons to isoflurane, investigators might selectively suppress only PV+ interneurons in an anesthetized animal. And lastly, causal roles may be elucidated by reinstating the activity of specifically affected components of the cortical mesocircuit during anesthesia (Redinbaugh et al., 2020). For example, can an animal be aroused from anesthesia if the synaptic effects of anesthetics are rescued, or if the cell type-specific effects of anesthetics are reversed? These causal investigations not only help us understand and improve clinical practices, but will contribute to our understanding of consciousness itself.

What advances in optogenetic technology would improve the conclusions draw in these chapters?

Prior investigations of layer 1 afferents used electrical stimuli to elicit post-synaptic responses (Larkum et al., 1999; Raz et al., 2014; Hentschke et al., 2017). As both intracortical and thalamocortical axons traverse layer 1, electrical activation of cortical layer 1 does not discriminate between afferents with distinct origins. Moreover, the probability of activation of local neurons is dependent upon their unique axonal arborization patterns and myelination profiles, suggesting that direct electrical activation of layer 1 may inappropriately engage certain local cell populations over others (Komarov et al., 2019). With the development of optogenetic constructs, however, afferent pathways may be independently activated by expressing viral constructs in specific projections and not others.

The experiments described in this thesis are the first to compare synaptic responses to two distinct afferent pathways overlapping in cortical layer 1. However, due to the limitations of the opsins that are currently available, channelrhodopsin was expressed in a single area (either thalamus or cortex) only. As such, response properties could not be compared within a single slice experiment, nor simultaneously activated. As optogenetic technology advances, the results I present in Chapter 3 should be examined using paired samples by expressing two different opsins with non-overlapping excitation spectra and similar kinetics, to compare thalamocortical and corticocortical inputs within a single cell recording. Additionally, responses to simultaneous activation of thalamocortical and corticocortical inputs should be assayed.

Evidence suggests that responses evoked by concurrent activation of afferent pathways may greater than the sum of responses evoked by each pathway independently (Banks et al., 2011; Hentschke et al., 2017). Coincident activation of pyramidal cells by thalamocortical and corticocortical inputs has been proposed as a cellular mechanism by which ascending and descending processing streams are integrated during sensory processing (Larkum, 2013; Suzuki and Larkum, 2020). By expressing unique opsins in distinct areas, independent afferent pathways may be isolated in the same slice. This will allow independent or concurrent activation of afferents and will provide insight into how thalamocortical and corticocortical inputs (including overlapping inputs to layer 1) may contribute to information processing.

References

Banks MI, Uhlrich DJ, Smith PH, Krause BM, Manning KA (2011) Descending projections from extrastriate visual cortex modulate responses of cells in primary auditory cortex. CerebCortex 21:2620-2638.

Constantinople CM, Bruno RM (2013) Deep cortical layers are activated directly by thalamus. Science 340:1591-1594.

Cruikshank SJ, Ahmed OJ, Stevens TR, Patrick SL, Gonzalez AN, Elmaleh M, Connors BW (2012) Thalamic Control of Layer 1 Circuits in Prefrontal Cortex. The Journal of Neuroscience 32:17813-17823.

Gil Z, Connors BW, Amitai Y (1997) Differential regulation of neocortical synapses by neuromodulators and activity. Neuron 19:679-686.

Hentschke H, Raz A, Krause BM, Murphy CA, Banks MI (2017) Disruption of cortical network activity by the general anesthetic isoflurane. Br J Anaesth 119:685-696.

Jiang X, Wang G, Lee AJ, Stornetta RL, Zhu JJ (2013) The organization of two new cortical interneuronal circuits. NatNeurosci 16:210-218.

Komarov M, Malerba P, Golden R, Nunez P, Halgren E, Bazhenov M (2019) Selective recruitment of cortical neurons by electrical stimulation. PLOS Computational Biology 15:e1007277.

Krause BM, Raz A, Uhlrich DJ, Smith PH, Banks MI (2014) Spiking in auditory cortex following thalamic stimulation is dominated by cortical network activity. Front Syst Neurosci 8:170.

Kubota Y (2014) Untangling GABAergic wiring in the cortical microcircuit. Current opinion in neurobiology 26:7-14.

Lam Y-W, Sherman SM (2018) Convergent synaptic inputs to layer 1 cells of mouse cortex. European Journal of Neuroscience 49:1388-1399.

Larkum M (2013) A cellular mechanism for cortical associations: an organizing principle for the cerebral cortex. Trends Neurosci 36:141-151.

Larkum ME, Zhu JJ, Sakmann B (1999) A new cellular mechanism for coupling inputs arriving at different cortical layers. Nature 398:338-341.

Larkum ME, Senn W, Luscher HR (2004) Top-down Dendritic Input Increases the Gain of Layer 5 Pyramidal Neurons. Cerebral Cortex 14:1059-1070.

Larkum ME, Petro LS, Sachdev RNS, Muckli L (2018) A Perspective on Cortical Layering and Layer-Spanning Neuronal Elements. Frontiers in Neuroanatomy 12.

Murayama M, Pérez-Garci E, Nevian T, Bock T, Senn W, Larkum ME (2009) Dendritic encoding of sensory stimuli controlled by deep cortical interneurons. Nature 457:1137-1141.

Murphy CA, Krause BM, Grady SM, Banks MI (2017) Effect of isoflurane on selectively activated afferent pathways in neocortex. In: Society for Neuroscience Annual Meeting. Washington D.C., USA.

Oláh S, Füle M, Komlósi G, Varga C, Báldi R, Barzó P, Tamás G (2009) Regulation of cortical microcircuits by unitary GABA-mediated volume transmission. Nature 461:1278-1281.

Raz A, Grady SM, Krause BM, Uhlrich DJ, Manning KA, Banks MI (2014) Preferential effect of isoflurane on top-down versus bottom-up pathways in sensory cortex. Front Syst Neurosci 8.

Redinbaugh MJ, Phillips JM, Kambi NA, Mohanta S, Andryk S, Dooley G, Afrasiabi M, Raz A, Saalmann Y (2020) Thalamus Modulates Consciousness Via Layer-Specific Control of Cortex. Neuron 105.

Rudy B, Fishell G, Lee S, Hjerling-Leffler J (2011) Three groups of interneurons account for nearly 100% of neocortical GABAergic neurons. Developmental neurobiology 71:45-61.

Sakata S, Harris KD (2009) Laminar structure of spontaneous and sensory-evoked population activity in auditory cortex. Neuron 64:404-418.

Schuman B, Machold RP, Hashikawa Y, Fuzik J, Fishell GJ, Rudy B (2019) Four Unique Interneuron Populations Reside in Neocortical Layer 1. The Journal of Neuroscience 39:125.

Stepanyants A, Martinez LM, Ferecsko AS, Kisvarday ZF (2009) The fractions of short- and long-range connections in the visual cortex. Proc Natl Acad Sci U S A 106:3555-3560.

Suzuki M, Larkum ME (2020) General Anesthesia Decouples Cortical Pyramidal Neurons. Cell 180:666-676.e613.

Takahashi N, Oertner TG, Hegemann P, Larkum ME (2016) Active cortical dendrites modulate perception. Science 354:1587-1590.

Tremblay R, Lee S, Rudy B (2016) GABAergic Interneurons in the Neocortex: From Cellular Properties to Circuits. Neuron 91:260-292.

Wozny C, Williams SR (2011) Specificity of synaptic connectivity between layer 1 inhibitory interneurons and layer 2/3 pyramidal neurons in the rat neocortex. CerebCortex 21:1818-1826.